# Ultrasensitive force field sensors based on suspended nanowires: Novel explorations in cavity nano-optomechanics, proximity forces and hybrid spin qubit nanomechanics

O Arcizet

**Université Grenoble Alpes**

# Ultrasensitive force field sensors based on suspended nanowires:

## Novel explorations in cavity nano-optomechanics, proximity forces and hybrid spin qubit nanomechanics

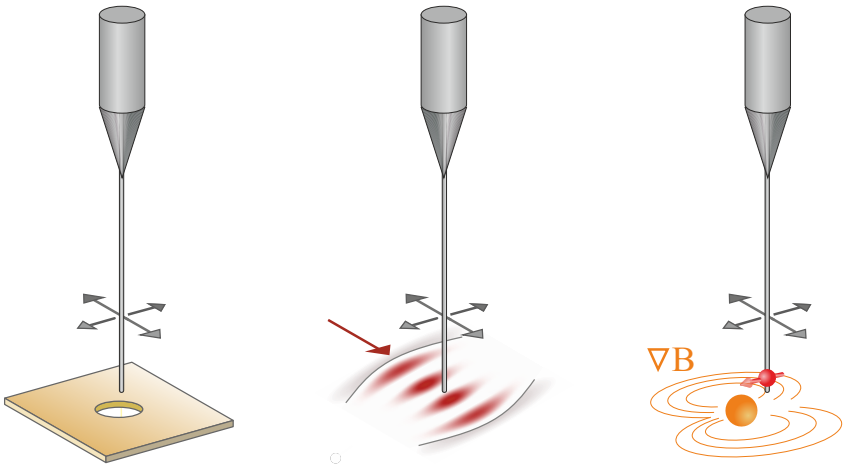


**Olivier Arcizet**

**Institut Néel - CNRS**

**Habilitation à diriger des recherches**

présentée le 31 Janvier 2022 devant un jury composé de

| | | | |
|---|---|---|---|
| Mr | **Franck Balestro** | Institut Néel | Président du jury |
| Mr | **Cyriaque Genet** | Institut de science et d'ingénierie supramoléculaires | Rapporteur |
| Mr | **Fabio Pistolesi** | Laboratoire Ondes et Matière d'Aquitaine | Examinateur |
| Mme | **Isabelle Philip** | Laboratoire Charles Coulomb | Examinatrice |
| Mr | **Jean-François Roch** | Laboratoire Lumière Matière et Interfaces | Rapporteur |
| Mr | **Philipp Treutlein** | Basel University | Rapporteur |

# Contents

# Chapter 1

# Context and evolutions of the research topics

This short chapter provides a brief overview of the progression of the conducted research activities, and their evolution since my arrival in Grenoble at Institut Néel in December 2009.

After my PhD thesis realized at the Laboratoire Kastler Brossel in the group of Antoine Heidmann in the field of Cavity Optomechanics and defended in December 2006, I went to work as a postdoc at the Max Planck Institute for Quantum Optics in Garching, in the group of Tobias Kippenberg. There I worked on high-Q toroidal optical microcavities with applications in the fields of frequency comb generation (with Pascal Del'Haye), biophysics (with Bastian Shroeter and Jens Dobrindt) but also in cavity optomechanics at low phonon numbers (with Albert Schliesser, Rémi Rivière, Xiaoquing Zhou and Stefan Weis). In the low temperature experiments, realized in a Helium 3 cryostat, we investigated the interaction of the phononic excitations in the vibrational mode of interest, a radial breathing mode of the micro-toroïd, to the amorphous material defects, which can be modelled by an assembly of two level states (TLS) - often attributed to the different conformations between which the atoms forming the glassy material can transit under the action of an external perturbation - featuring a large distribution in energy and coupling strength. At large temperatures, typically above 10 K, this interaction is essentially dissipative, the mechanical modes of interest for optomechanics being coupled to an assembly of TLS with very different energies, thus causing an irreversible loss of energy for the phonon mode. However at lower temperatures, the thermally activated processes become progressively inefficient and the dissipation is now dominated by tunnel-mediated transitions between the different conformations. At even lower temperatures (approx. ¡500 mK)) the phonon-TLS interaction becomes dominated by the TLS whose energy splitting is quasi-resonant with the phonon mode [1]. This resonant coherent interaction, which is analog to a coherent laser-atom interaction, was largely investigated in bulk amorphous materials. Some experiments realized at very low temperatures investigated the acoustic echoes which originate from this coherent interaction, and the notions of pi-pulses, Rabi precessions, which I only learned in atomic physics and RMN courses suddenly jumped into the physics of the system I worked on. I found fascinating to see that it could be possible to reproduce and explore this Jaynes Cummings like physics with macroscopic mechanical oscillators. Furthermore, such a coherent interaction to a TLS could be exploited to generate non-classical states of the oscillator position, which was one of the main objectives for the community after reaching the ground state cooling.
We spent a non negligible amount of time in the lab with Rémi Rivière trying to observe some typical signatures of this resonant interaction in the micro-cavities, such as the saturation of the mechanical dissipation as a function of the oscillation amplitude, but the experimental margin was pretty narrow in our temperature/frequency parameter range. If we believe we were able to see a trend [2], the experiments were pretty blind in the sense that we did not know the characteristics of the defects involved (number, coupling strength...) and furthermore had no

possibility of measuring or manipulating the TLS involved. These attempts however motivated me to further develop this research direction, aiming at investigating the coherent coupling between a mechanical oscillator and a qubit-like system, and became one of the central objective of my CNRS research project. The proposition of I. Wilson Rae and colleagues [3] to manipulate a nanomechanical oscillator by optical addressing of a quantum dot via strain coupling, even if at that time it was very far from experimental reach, was certainly very appealing in the sense that it suggested exploiting a TLS which could be independently readout and manipulated.

A more accessible experimental platform emerged after having met Alessandro Siria and Vincent Jacques. In particular at a physics school in Les Houches, we discussed the idea of combining Nitrogen Vacancy (NV) defects and Silicon Carbide (SiC) nanowires to operate both with a very light oscillator and a robust spin qubit. After my installation in Grenoble as a CNRS researcher, in December 2009, this became my first experimental objective. By dipping a silicon carbide nanowire in a solution containing diamond nano-crystals, it was possible to functionalize the nanowire with a single NV defect, thus forming a hybrid spin-mechanical system. The interaction between both components was realized by inserting the system in a very strong magnetic field gradient, enabled by a position-dependent Zeeman effect, which renders the spin energy dependent on the oscillator position. Such a parametric interaction reproduces a Stern-and-Gerlach-like interaction (the silver atoms being differently deviated by a magnetic field gradient depending on their spin state) and since the spin energy depends on the oscillator position, it also permits to generate a spin-dependent force, the key ingredient to generate non-classical states of motion. A first experiment [4] demonstrated the feasibility of the approach and allowed to characterize the interaction strength, by measuring how the spin qubit energy was affected by the mechanical vibrations. This experiment was a good illustration of the experimental strength found in the Institute: we used micro-magnets produced in the group of Nora Dempsey, benefitted from the local expertise in microwaves, low noise electronics, micro- and macro- fabrications platforms, and through the collaboration with our colleagues (P. Poncharal, P. Vincent) from the LPMCN in Lyon on the Silicon Carbide nanowires.

After this proof-of-principle experiment, two PhD students started a PhD thesis in the group, with the goal of pursuing this research direction. Following the advice of Jean-François Roch, Sven Rohr contacted us and finally started working on the hybrid experiment in 2011 [5], and with Benjamin Pigeau, who joined the group initially as a postdoc in 2012, we could investigate the dynamical side of the parametric hybrid interaction, and in particular the regime where one drives the oscillator at resonance, while simultaneously generating a Rabi precession of the spin qubit at a similar frequency. We could observe a synchronization [6, 7] of the spin precession on the mechanical tone, which we termed "phononic Mollow triplet regime" in view of the analogy one can build with the QED phenomenon: the fluorescence of an atom, when resonantly pumped with an intense laser, presents some sidebands separated by the Rabi frequency, and are thus proportional to the laser field strength. This experiment allowed us to further investigate the hybrid interaction and convinced us that it was possible to observe the reversed side of the interaction which consists in measuring the impact of the spin qubit on the mechanical oscillator. This rather elegant objective, which literally consists in measuring mechanically the spin state through its action on the macroscopic mechanical oscillator, is however rather demanding. For a magnetic field gradient strength of $10^6\,\mathrm{T/m}$, the spin dependent force is about 20 aN. This value is extremely small, but is well within the theoretical force sensitivity of the silicon carbide nanowires (of a few $\mathrm{aN/Hz^{1/2}}$ at room temperature). To do so, it was necessary to efficiently probe the vibrations of the nanowires, in order to measure the faint displacements caused by the spin-dependent force.

This was the first objective of the internship of Arnaud Gloppe, who joined the group in 2011.

We developed an optical readout, by focussing a visible laser field on the vibrating extremity of the nanowire using a high-NA microscope objective and exploiting low noise photodetectors developed in the Institute with the help of Daniel Lepoittevin. The method was simple but efficient, and we could rapidly observe the thermal noise of the nanowires at room pressure despite the large acoustic damping which limited the mechanical quality factor to almost unity in air. We could also investigate their response to an electrostatic force. Arnaud started his PhD in the group [8], and one of the first step consisted in lowering the acoustic dissipation by realizing the experiment in a vacuum chamber, which was designed with the help of Laurent Del'Rey. I remember standing in front of the spectrum analyzer, impressed by the astonishing SNRs we could observe at low pressure, which were approaching 60 dB even for the modest quality factors obtained (few thousands), and the simplicity of the thermal noise spectra we observed. This definitively convinced me of the interest of operating with these light and simple nanomechanical oscillators.
This operation at low pressure also allowed us to spectrally identify the 2 transverse modes, which present a typical relative frequency splitting around 1%. Those two modes oscillate along perpendicular directions in the transverse plane, which granted a vectorial force sensing capacity to the nanowires. We rapidly observed that at large optical powers, on the side of the optical beam, the nanowire became instable following a peculiar transition towards the instability: when increasing the optical power, their frequency splitting was reduced, and the instability emerged after reaching the degeneracy point. This phenomenology was rather new, and we spent some time investigating its origin and rapidly suspected the peculiar structure of the optical force field in the waist area to be responsible for it. To verify this hypothesis, we developed a methodology that allowed us to map the optical force field in the waist area, using pump-probe techniques. Our measurements could be confronted to the numerical simulations realized by G. Bachelier. This mapping allowed us to verify that the 2D optical force gradients were responsible for the perturbation of the mechanical properties of the nanowire, and in particular that the rotational structure of the force field lead to the frequency merging and instability observed. Those observations first highlighted the role of the non-conservative optical force field, and also lead us to analyze the impact of the 2D force field gradients on the nanowire properties [9].

Such vectorial measurements of the optical force experienced by the nanowire were possible because we could modulate the light intensity at frequencies close to the mechanical resonances of the nanowire, and thus determine the projection of the force vector on both eigenmodes. This method can thus only be implemented for measuring forces which can be externally controlled and modulated, such as optical or electrostatic forces. This is not the case for proximity forces, such as Casimir or Van der Waals, and more generally when the origin of a force field under investigation is not yet understood. During the PhD of Laure Mercier de Lépinay [10], we then developed a universal methodology which allows to map the 2D force field gradients experienced by the nanowire. The method is based on the analysis of the perturbation of the nanowire eigenmodes caused by the 2D force field gradients, which can lead to frequency shifts and eigenmode rotations. To implement it, it was necessary to realize a complete 2D readout of the nanowire deformations in the transverse plane, and we made use of a 2 channels refined version of the photodiode amplifiers realized by Daniel Lepoittevin. We demonstrated that by measuring the induced mechanical perturbations, it was possible to completely reconstruct the local force field gradients experienced by the nanowire. The method was validated on the case of a tunable electrostatic force field, produced by a sharp metallic tip approached in the vicinity of the nanowire extremity [11].

Among the 2D force fields $\mathbf{F}(\mathbf{r})$, the rotational ones, for which $\mathrm{rot}\mathbf{F} \neq \mathbf{0}$, have a fundamental status. We already described that they can lead to a topological instability and we came back on their analysis during the PhD of Laure. We measured how they impact the spectro-angular

structure of the thermal noise of the nanowires. We demonstrated [12] that they were responsible for an eigenmode orthogonality breaking, that they bring the nanowire in an out-of-equilibrium state, and that they can lead to an excess of noise violating the fluctuation dissipation relation. In a second time, we also investigated the nanowire trajectories in the position and speed spaces, and observed that they are also responsible for a noise reduction in a direction perpendicular to the one towards which the eigenmodes orientations are commonly converging. This noise reduction was first anticipated in numerical simulations, and subsequently verified on experimental traces. Philip Heringlake spent part of his PhD thesis [13] to develop artificial force fields, which are produced by applying a force on the nanowire, along a given direction, proportional to the displacement along another orientation. This technique was implemented using a FPGA architecture he completely re-designed with the help of Julien Minet from the electronic department. When the measurement and feedback vectors are perpendicular, it allows to produce pure shearing force fields, of the type $\delta\mathbf{F} = g\,(\delta\mathbf{r}\cdot\mathbf{e_x})\,\mathbf{e_z}$. Such a synthetic force field is also rotational, and when oriented along the eigenmodes, does not generate frequency shifts, which allows to operate with large feedback gains without suffering from the topological instability. It allowed to further explore the impact of the rotational force fields on the nanowire dynamics, and in particular to evidence the apparition of a circulation in the trajectories, in the sense that the orthoradial speed $v_\theta$ acquires a non-zero local mean value which becomes oriented in the direction of the force rotational. Furthermore, we observed that the mean orthoradial speed also monotonously increases with the distance $r$ towards the rest position of the nanowire. Thanks to a fruitful input from Fabio Pistolesi, we could solve the Fokker Planck equation describing the thermal noise trajectories of the nanowire in the position and speed spaces, which was then satisfyingly confronted to our experimental results. Another peculiar observation concerned the possibility to squeeze/antisqueeze the noise distribution not only in the $\{x, z\}$ position space, but also in the $\{v_x, v_z\}$ speed space along quasi identical directions. Such an observation was puzzling since we observed that the thermal noise could be reduced up to 3 dB in a given direction, simultaneously in the position and speed space. Since the dressing mechanism of the nanowire by an external non-reciprocal force field can in principle identically be transposed to a 2D ultra-cold oscillator cooled in its ground state of motion, we were puzzled by what could have been an apparent violation of the Heisenberg limit. However the non-conservative nature of the rotational force field leads to an impossibility to define a potential energy from which it derives, out of which we could have developed a Hamiltonian approach. Fortunately, we found an analysis by Michael Berry [14] of the dynamics of a particle in a similar "circulating" force field, in which he introduced an effective Hamiltonian making use of an anisotropic kinetic mass (of the type $P_x^2/2M_x + P_z^2/2M_z$ with $M_x \neq M_z$). Such an approach let us compute a conjugate quantity for the position of the nanowire, which was combining the speed along both perpendicular orientations. All those puzzling effects hint towards the fundamental nature of the radiation pressure force, an impulsion flow which provides a unique implementation of a circulating force field. One can believe this is not the end of the story, in particular for what concerns the analysis of the orthoradial speed circulation, which presents noticeable similarities with the orthoradial speed anomaly of stars observed inside the galaxies.

Most of the above mentioned force sensing experiments were realized by deducing the mechanical properties of the nanowires through the analysis of the spectro-angular structure of their thermal noise, and the perturbation caused by the force field gradients under investigation. Working on the thermal noise is however a rather slow acquisition principle: recording a useful thermal noise trajectory requires averaging over several inverse mechanical damping rates, meaning over tens of seconds in our case and to realize a subsequent noise analysis, which can also be time consuming. To accelerate the measurement process, Philip Heringlake developed during his PhD several protocols based on resonantly driven trajectories instead of random Brownian trajectories: by simultaneously driving the nanowires at the resonance of their 2 fun-

damental transverse eigenmodes, using a phase lock loop to track the frequency shifts induced by the force field under investigation, it is possible to determine the eigenmodes orientations by measuring their projection on both measurement channels. Realizing a proper measurement thus only requires to wait for the nanowire to reach its steady state and this typically takes $\sim 100\,\mathrm{ms}$. Furthermore the deduction of the mechanical properties of the nanowire eigenmodes orientation can be directly calculated from the raw measurement signals, and can thus be displayed and recorded in quasi real-time. This acceleration of the measurement process allowed us to realize a significant jump in term of experimental reliability, and allowed the nanowire to approach surfaces at a closer distances so that we could safely explore the proximity forces experienced by the nanowire.

Armed with the advanced force sensing protocols he developed, Philip first investigated electrostatic forces above nano-structures [15] such as tips or trenches and holes drilled in metallic surfaces, which were realized at the NanoFab facility in the Institute (thanks to the focused ion beam (FIB) skills of Jean-François Motte and Gwénaëlle Julie). The electrostatic forces can be estimated by integrated the Maxwell stress tensor on the nanowire surface and are thus quadratic in the electric field found around the nanowire. To discriminate between the electric fields generated by the surface geometry ($E_V$) from residual electric fields ($E_{\mathrm{res}}$), a common methodology consists in measuring the force gradients for varying bias sample voltages (while the nanowire tip support serves as an electric ground). The nanowire, a dielectric, is attracted towards locations of large electric field, and such a force is quadratic in the bias voltage ($\propto E_V^2$), as in a capacitor, so that the nanowire detects force gradient with a parabolic dependence on the bias voltage. When scanning the nanowire above a nano-structure, the parabola curvature gives us information on the capacitor like electrostatic force. We mapped the trapping (tip, disks) or anti-trapping (holes) electrostatic force field above the nano-structures down to lateral dimensions smaller than 50 nm.

In most samples, there exists residual electric fields $E_{\mathrm{res}}$, which do not depend on the bias voltage, due to trapped electronic charges, patches on the metallic surface or contaminants for example. Through the quadratic electric field dependence of the Maxwell stress tensor, they are responsible for a linear contribution with the bias voltage in the force gradient ($\propto E_{\mathrm{res}} E_V$), which shifts and displaces the force parabolas, as well as a residual background, which do not depends on the bias voltage ($\propto E_{\mathrm{res}}^2$). The measurement of the parabola shifts permits to estimate and image their impact in the force fields involved but this remains a qualitative estimation for the moment.

The next sample generations, which are currently studied in the PhD of Hugo Weltz, were designed to incorporate a set of 4 external electrodes located on each sides of the sample area, to generate a tunable homogeneous electric field aiming at compensating the local residual electric fields experienced by the nanowire. They were realized by Bruno Fernandez from the NanoFab team using oxidized silicon wafers covered with the metallic electrodes, while the nano-structures were subsequently milled using the FIB. Operating with such a sample architecture will allow to compensate the residual electric field at any position above the nanostructure, and this is a key ingredient to achieve a quantitative estimation of the Casimir forces. These forces are also called "quantum vacuum forces", they originate from the fact that the electromagnetic quantum vacuum is constituted of electromagnetic fluctuations $\delta E_{\mathrm{vac}}$, which oscillate around zero ($\delta \bar{E}_{\mathrm{vac}} = 0$), with a non-zero rms value ($\delta \bar{E}^2_{\mathrm{vac}} \neq 0$). As such, the vacuum fluctuations can create forces via their quadratic contribution in the Maxwell stress tensor if there exists an imbalance of vacuum fluctuations around the nanowire. This appears when approaching nano-structures. While most of the existing experiments were realized in the quasi 1D geometry, there exists theoretical predictions that the Casimir forces could become repulsive in the proximity of nano-structures [16]. Philip obtained convincing qualitative measurements in his PhD demon-

strating the existence of laterally repulsive residual forces, whose quantitative assessment should be within reach through the use of those external control electrodes. When investigating those topics, we largely benefitted from the theoretical and conceptual assistance of Serge Reynaud and Romain Guérout from the Laboratoire Kastler Brossel, and from the numerical simulation cluster maintained by Patrick Belmain at the Institute.

All the experiments described above were realized at room temperature. Lowering the temperature of the nanomechanical force probes is a straight-forward method to improve their force sensitivity, by reducing their thermal motion and their mechanical damping rates and furthermore opens new possibilities to realize force sensing experiments above samples at low temperatures. We had the chance to benefit from the incredible in-house expertise in cryogeny, and decided to develop a specific cryostat to operate the already ultrasensitive force probe at dilution temperatures. Engaging discussions with Wolfgang Wernsdorfer, Eric Eyraud and Laetitia Marty, we developed a table-top dilution fridge based on the "sionludi" architecture that has been continuously optimized by Eric and Woflgang over the last decade. The first cool down was realized in September 2015, and with the help of Benjamin Besga we developed a first version of the optical head, which aimed at probing the mechanical optical and thermal properties of the nanowires at dilution temperatures. This became the first topic of the PhD thesis of Francesco Fogliano [17]. We first spent a year and a half in the building D of the Institute, in the "cryogenic maturation room", where with the constant help of Wolfgang and Eric, as well as many others (N. Roch, F. Balestro, C. Winkelmann, J. Renard), we progressively got to learn how to operate the cryostat, and where we developed several key ingredients such as optical interferometric objectives (heroically machined by Julien Jarreau), soft thermalization links, and a readout method operating in the photon counting regime. We spent hours investigating the noise temperature of the nanowires, which was rapidly found to rise very quickly with the probe power due to the very low heat conduction of the nanowire at sub-1K temperatures. After this "learning period", we moved the experiment in the low noise Z building of the Institute, where in the mean time we had prepared the suspended optical table and the cryogenic gas handling system, aiming at benefiting from this very quiet environment: there we were not obliged to suspend the cryostat to the room 's ceiling in order not to suffer from the acoustic noise caused by the close-by air-conditioning system. We could then rapidly identify the pertinent sources of artificial noise, which were of electrical and vibrational origin. While the first one was rapidly mitigated, we identified the internal vibrations of the cryostat due to the fluid circulation (probably in the still area) as the dominant source of noise. We developed a suspension stage, realized by Julien in less than a week, so that in three weeks in June 2019, we could lower the noise temperature of the nanowire from the 400 mK range down to 30 mK. To reach such a low vibrational temperature, we had to operate with ultra-low optical powers, with less than a pW injected in the probe fibers, a power at which all standard detectors are insensitive. The readout technique based on single photon detectors, allowed to reach a signal to background ratio close to but larger than unity on the nanowire thermal noise readout, providing record force sensitivities, around $40\,\mathrm{zN/Hz^{1/2}}$ for a scanning force sensor [18]. Those measurements allowed us to investigate the optical heating properties of the nanowire, reaching a regime where the heat conduction is likely to be dominated by the ballistic heat transport (compared to the diffusive regime observed at higher temperatures). This subject, and more generally the prolongation of the experiments at dilution temperatures is part of the current PhD thesis of Clément Gouriou. He investigates in particular how a thermal wave, generated by an intensity modulated laser can propagate along the nanowire and generate either a deformation or a reflectivity change. Those measurements allow in principle to measure heat conduction properties without physically contacting the nanowire. The developments realized in the cryostat, will allow and have already allowed to investigates different samples realized by other colleagues in the lab and elsewhere, such as silicon nitride nanowires or membranes, graphene and other 2D

resonators metallic drums, and have more generally allowed us to share the knowledge acquired in nano-optics at dilution temperatures.

The second (part of the) PhD thesis of Francesco Fogliano was dedicated to the integration of the nanowires in a cavity nano-optomechanical experiment. We already had investigated part of the physical richness of the vectorial optomechanical interaction in a cavity-free configuration, which underlined the apparition of the non-reciprocal rotational structure in the 2D optomechanical coupling landscape. We were also convinced that the simple optomechanical interaction to a focussed laser beam was rather large in view of the size of the nanowire diameter, and that the use of high-order internal Mie resonances could help avoiding lateral scattering, so that it was thus natural to try to enhance it in a Fabry Perot cavity using a multi-pass interaction picture. Benjamin Besga who realized his PhD in Jakob Reichel group at Laboratoire Kastler Brossel was familiar with the fiber microcavities pioneered in their group, and we thus started a collaboration with Jakob, Romain Long and Jean Hare aiming at realizing a "nanowire in the middle" cavity optomechanical experiment. We designed a largely tunable experimental architecture where we could open widely the microcavity, insert the nanowire and progressively reduce its length down to around $10\,\mu$m, while keeping the possibility to adjust the fibers relative angles as well as the nanowire position within the optical mode. The extreme sensitivity of the experiment to external perturbations lead us to design a suspension of the vacuum chamber, to integrate an acoustic and thermal isolation enclosure and to implement a fully remote operation of the experiment in order to keep it locked over days in order to explore and map the peculiar optomechanical interaction. To readout the nanowire vibrations independently from the cavity mode, we decided to install a second probe beam (633 nm), channelled through the fibers, which could be exploited either in transmission, in reflection or from a lateral collection objective which was used to collect the IR and visible scattered photons. Altogether, this was certainly one of the most demanding experiment I worked on over the recent years.
Antoine Reigue joined the group as a postdoc and developed an involved modelisation of the experiment, which combined the peculiar light scattering properties of the nanowire in the non-paraxial regime and the intracavity field propagation [19, 20]. This allowed us to obtain a quasi-quantitative agreement with the experimental results obtained. By scanning the nanowire within the optical cavity mode, we could map the dispersive 2D optomechanical parametric interaction through the determination of the optomechanical coupling vector, $\mathbf{G} = \boldsymbol{\nabla}\omega_0(\mathbf{r})$ which naturally takes a vectorial character since the nanowire can equivalently vibrate along both transverse directions. By monitoring the nanowire-induced perturbations of the cavity finesse and of the transmitted, reflected and laterally scattered photon fluxes, we could explore the dissipative side of the optomechanical interaction. Those scanning probe measurements, realized with a sub-wavelength sized nanowire allowed to map the intracavity field structure and investigate one facet of the optomechanical interaction, namely how the nanowire perturbs the optical mode of interest. Exploring the reverse interaction requires measuring the optomechanical force exerted by the intracavity field on the nanowire. To do so we implemented pump probe measurements by modulating the intracavity optical power while demodulating the induced displacement with the red probe signal.
Beyond the dual mapping of the optomechanical coupling in the nanowire - cavity system, those measurement also allowed to realize the exceptional strength of the light-nanowire interaction, and could be realized at ultra-low optical powers, down to an intracavity mean photon population smaller than a single photon. Despite the finesse degradation caused by the scattering of the intracavity light field, it was possible to find locations in the intracavity mode where the optomechanical coupling was so strong to that the system could largely enter the single photon regime of the optomechanical interaction, when a single intracavity photon can displace the oscillator by more than its zero-point fluctuations. With Antoine Reigue we investigated different novel regimes arising with such large coupling strength. It also allowed to identify diameters for

which we could observe "anomalous" cavity shifts [21], for which one needs to increase the cavity length while inserting the nanowire inside the cavity mode, as if it had reduced the cavity optical path. We could experimentally observe and explore this peculiar situation at the occasion of the master internship of Lukas Schleicher.
The future cavity nano-optomechanics experiments will be conducted in the cryostat in order to lower the thermal noise of the nanowire so as to detect the single photon recoil, and to investigate the possibility to generate broadband optical squeezing, at ultra-low optical powers. The integration of the complete experiment in the cryostat is a true experimental challenge. An alternative approach, based on photonic crystals developed at C2N, in the group of Rémy Braive is currently under development. It should simplify the operation of the microcavities at dilution temperatures and will be the central topic of the PhD thesis of Chao Zhang, who started in October 2021.

All those experiments have allowed us to gain expertise in the detection of weak forces with the nanowires and can be viewed as parenthesis with respect to the long lasting goal of the hybrid spin qubit-nanomechanical experiment, aiming at detecting and exploiting the spin-dependent forces. In parallel, this research direction was also explored with a different hybrid system locally developed in the scientific presqu'île: photonic wires hosting a quantum dot at their basis. They are developed at CEA by Julien Claudon and Jean Michel Gerrard and were originally designed to efficiently optically address the quantum dot and collect its photo-luminescence [22]. This project started during joint discussions with Jean Philippe Poizat, Maxime Richard, Julien and Jean-Michel about the possibility to detect with the quantum dot the vibrations of the photonic wire through the dynamical strain it experiences. This parametric coupling is indeed of similar nature as the one involved in the spin-nanowire system, where the two-level system built out of the excited and fundamental states of the quantum dot sees its energy splitting being modified by the strain it experiences, which is dynamically modulated by the vibrations of the nanowire. Contrary to the spin qubit system which easily operates in the resolved sideband regime, the quantum dot lifetime is very small compared to the mechanical period, however the interaction strength was found to be extremely efficient, allowing to reach the so-called ultrastrong coupling regime, where the displacement caused by a quantum dot excitation generates a wire deformation larger than its zero-point quantum fluctuations. During the PhD of Inah Yeo, with the help of Pierre-Louis de Assis, we realized motionally averaged and time-resolved quantum dot spectroscopies, which permitted to quantify the parametric interaction strength [23] and also to localize the position of the quantum dot within the wire cross-section [24]. Then, Jan Kettler and Nitika Vaisch realized an amazing experiment, where they could investigate the hybrid interaction in the reverse direction, namely by detecting the mechanical deformation induced by a resonant optical excitation of the quantum dot: the resonant laser was time-modulated to create a temporal modulation of the quantum dot population, thus causing a mechanical actuation of the trumpet. This experiment was extremely tough in order to discriminate the mechanical action produced by the quantum dot from other "parasitic" effects at play, such as the direct photothermal actuation of the trumpet, which becomes extremely efficient at low temperatures. For what concerns the hybrid spin-qubit/nanowire experiments, Alex Fontana joined the group in September 2020, and we are currently building a new experiment aiming at observing and investigating the spin-dependent forces. The experiment will integrate the different actuation and force sensing techniques we recently developed, and the spin-dependent differential forces are expected at a level of a few attonewton, which is in principle largely within the force sensing capacities of the nanowire.

In parallel to those developments, we also investigated other nanomechanical structures, such as graphite or graphene membranes during the PhD thesis of Antoine Reserbat [25] and Cornelia Schwarz [26], from the hybrid group of the Institute in collaboration with L. Marty,

N Bendiab and V. Bouchiat. We investigated how the nanomechanical vibrations were affecting other internal degrees of freedom of those peculiar resonators, such as the Raman modes of a graphite membrane [27]. This analysis provided an interesting insight on the connection between high frequencies and low frequency vibrational modes, and opens perspective on their cross manipulations which presents direct analogies with the problematic arising in the hybrid experiments described above. With Cornelia, we explored the hybridization of the graphene vibrations with the modes of its supporting membrane, which lead to a deviation from the normal mode expansion when the two sub-systems generate different mechanical damping rates [28]. We also investigated the peculiar photothermal properties of the graphene membrane and how the pump-probe experiments we typically employed could be used to get information on the local structure of the material (multi- or mono-layers, presence of cracks or riddles, etc...) [26]. Similar photothermal analysis are currently employed in the exploration of the thermal properties of the nanowire at dilution temperatures.

We now turn to a more detailed description of the main research topics developed at Institut Néel since 2009.

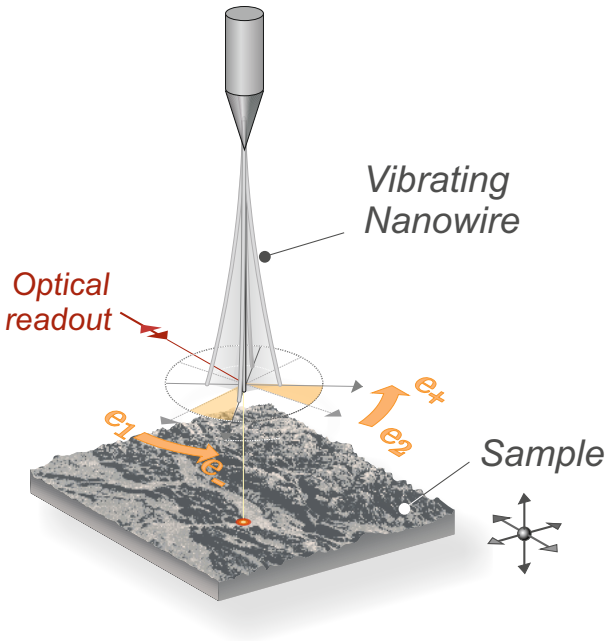

# Chapter 2

# Ultrasensitive force field sensing with suspended nanowires

In this chapter, we expose the different principles at play in the vectorial force sensing experiments realized with the suspended nanowires. We first present the mechanical and optical properties of the nanowires, as well as the 2D optical readout of the vibrations of their vibrating extremity. We then introduce the principles of force sensing, and the ones employed to image 2D force field gradients. While the original measurements were realized by analyzing the spectro-angular properties of the thermal motion of the nanowire, the measurement efficiency can be largely accelerated by exploiting coherently driven trajectories. We will finish this chapter by exposing some of the perspectives in the domain of force field sensing, such as the exploration of proximity forces, electrostatic and Casimir forces and their interest for surface analysis.

### Context

Force sensors are largely disseminated within fundamental and applied physics: from the early experiments by Cavendish or Coulomb on gravitational or electrostatic forces to the atomic force microscope [29] which allowed to observe spatially resolved atoms on a surface, they convert a force into a measurable displacement. The recent advances in micro- and nano-fabrication have allowed to significantly increase their force sensitivity, which can now approach a few attonewtons after 1 s of averaging in room temperature experiments, while operation with quasi molecular oscillators provides spectacular force sensitivities [30]. Our experimental configuration, made of an elongated mechanical oscillator vibrating above a sample under investigation has been employed in several domains, the most prominent one probably being the field of MRFM [31, 32, 33], which aimed at imaging single particles through the coherent manipulation of their internal spin degree of freedom and the magnetic force they apply on ultrasensitive force probes. In our case, the operation with a quasi-frequency degenerated nanowire, which oscillates similarly along both transverse directions in space is a configuration that was in general not widely spread, since it requires a careful analysis of their vibrations properties along both direction in space, as explained bellow. Then, the small nanowire diameter provided interesting perspectives in the light-nanowire interaction through the possibility to investigate forces at the sub-wavelength size. When compared to optically trapped particles approaches, the nanowires can be positioned at any position within the light field, which allows to realize vectorial force maps in non-trapping configurations and more generally brings a true scanning probe capacity for exploring confined optical fields.
In comparison to a degenerated force probe vibrating above a sample of interest, it can be rather difficult to operate with an ultra-soft and quasi-frequency-degenerated nanowire: its extreme sensitivity to lateral force field gradients generates large eigenmode rotations and instabilities can more easily develop when approaching too close to a non-homogeneous surface which provides a strongly structured force field. This appears typically below 30 nm above a sputtered

metallic layer, which approximately corresponds to the grain dimensions. This can be partly mitigated by developing different measurement techniques (such as multi-frequency excitations, see below) but, even with such a limitation, the nanowire provides a huge amount of information on the samples, such as residual electrostatic fields, surface contaminants, with a very limited alteration of the sample under test: the dielectric nanowires simply probe the local gradients of electrostatic fields, without strongly modifying their electrostatic environment (which is not the case when one approaches a metallized EFM voltage-bias tip). This weakly interacting character is certainly a strength for future force field imaging of surfaces.
Then, for what concerns the measurement of Casimir forces above nano-structures, the possibility to measure with the same nanomechanical probe the surface electrostatic imperfections (such as patches [34]) and the Casimir force is of a certain interest, since the local parasitic electric field could be compensated if they are properly measured. In comparison, in traditional Casimir configurations, the patches dimensions are on the contrary much smaller than the objects dimensions, so that their contributions are spatially averaged.

## 2.1 The nanowires

Most of the experiments realized in the group over the last decade were done with suspended silicon carbide nanowires. They come in the form of a powder, and we glue the selected nanowire on a sharply etched metallic tungsten tip, which then permits to handle them safely. The selection and the attachment are realized under an optical microscope equipped with a micromanipulator. The nanowire length $L$ is directly determined optically, while its diameter $d$ is deduced from its coloration observed under white light illumination. Due to its large refractive index, around 2.6 in the visible, the nanowire can host internal optical resonances, called Mie resonances, which structure the light-nanowire interaction. The colors observed in reflection depends on the nanowire diameter and on the light polarization employed, as shown in the color charts of Fig. 2.1c. The density of silicon carbide is around $\rho_{\mathrm{SiC}} = 3210\,\mathrm{kg/m^3}$, which is rather light compared to other materials and furthermore it presents a pretty large heat conduction coefficient of $\lambda_{\mathrm{SiC}} \simeq 400\,\mathrm{W/m/K}$ so that the heat deposited by the absorbed fraction of the readout power can be efficiently carried out of the nanowire. The nanowires can be found with a very large aspect ratio, often above 1000, with lengths up to 1.4 mm and diameters ranging from 100 to 500 nm.

The abacus given in Fig.2.1d illustrates how the mechanical properties and the force sensing capacities of the nanowires depend on their geometry (length and diameter). In the experiments it is rather important to adapt the nanowire dimensions to the experiment envisioned: choosing a low frequency nanowire will bring a higher mechanical susceptibility but also a larger sensitivity to external perturbations such as vibrations and to the force field gradients: they will cause more significant eigenmode rotations which can create difficulties in the eigenmode tracking protocol for example. On the contrary, a high frequency nanowire will in general present a lower force sensitivity, but will provide access to interesting dynamical regimes and more generally will permit to image faster a given force field landscape. Following the beam theory, the fundamental eigenmodes of the suspended nanowire oscillate at a frequency $\Omega_{\mathrm{m}}/2\pi = 1563\,\mathrm{Hz.m\,D/L^2}$, while higher order longitudinal eigenmodes can also be employed for sensing purpose, especially when the force field gradients are too intense. When using a readout probe measuring the local vibrations of the nanowire extremity, the effective mass amounts to one fourth of the nanowire physical mass, so that $M_{\mathrm{eff}} = 0.25\rho_{\mathrm{sic}}\pi(D/2)^2L$ which is generally found around 1 pg for our standard nanowires. The force sensitivity, when limited by the thermal vibrations is given by $\delta F_{\mathrm{min}} = \sqrt{2M_{\mathrm{eff}}\Gamma k_B T} \propto D^{3/2}L^{-1/2}$. The force iso-lines are depicted in blue in Fig. 2.1 at a temperature of 20 mK using a quality factor of $Q = 10^5$. From these estimations, the largest force sensitivities are achieved with long and thin nanowires, however there are many

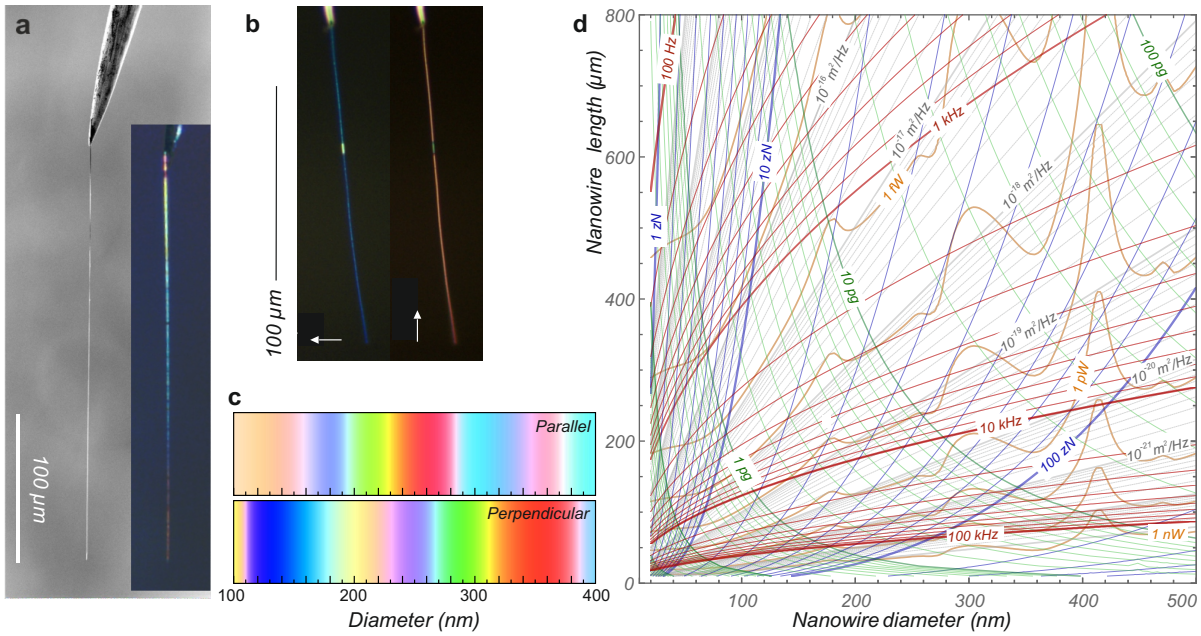


Figure 2.1: **Silicon carbide nanowires a**: Scanning electron microscope image of a suspended nanowire of conical shape, and its corresponding optical image obtained under white light illumination (conical from 240 nm (top) to 120 nm ). Optical images of a 140-nm-diameter nanowire obtained under polarized white light illumination. The color chart shown in panel **c** permit to determine its diameter. **d** Abacus of the mechanical and optical properties of the nanowire as a function of their length and diameter [18]. The effective mass is shown in green, the oscillation frequency of their fundamental eigenmode in red. The force sensitivity at 20 mK is shown in blue, assuming a quality factor of $10^5$, while the thermal noise peak level is shown in grey. The orange lines represent the optical power needed to obtain a unitary signal to background ratio on the thermal noise peak at 20 mK for a measurement wavelength of 633 nm, when accounting for the Mie resonance contributions to the light-nanowire interaction.

other parameters to consider: the readout efficiency, the mechanical linewidth (which should not be too small for fast sensing), the excess of low frequency environment noise, etc.. For what concerns the optical readout, it is important to also consider the signal to background ratio that can be obtained which can be properly compared using an interferometric readout such as the one implemented in the cryogenic experiment, where the measurement background is limited by the shot noise of the probe light. More details are given in [18].

The nanowire of interest is glued at the extremity of a sharp tungsten tip, and subsequently baked at 600 degrees in vacuum in order to harden the glue. The quality factors obtained are typically around 10 000 at room temperature, and improve to 100 000 at dilution temperatures, a limitation that is attributed to the dissipation in the amorphous oxyde crust surrounding the nanowire [18].

## 2.2 The optical 2D readout

The vibrations of the nanowires are readout by optical means. A probe laser is focused on their vibrating extremity by means of a high numerical aperture objective (100x/0.75), and the reflected light is sent on a vertically split photodetector that records the light reflected by the nanowire. A home-made low noise photo-amplifier, developed by Daniel Lepoittevin, provides the difference and sum of the photocurrents recorded on each quadrant ($0.2 - 20 \times$

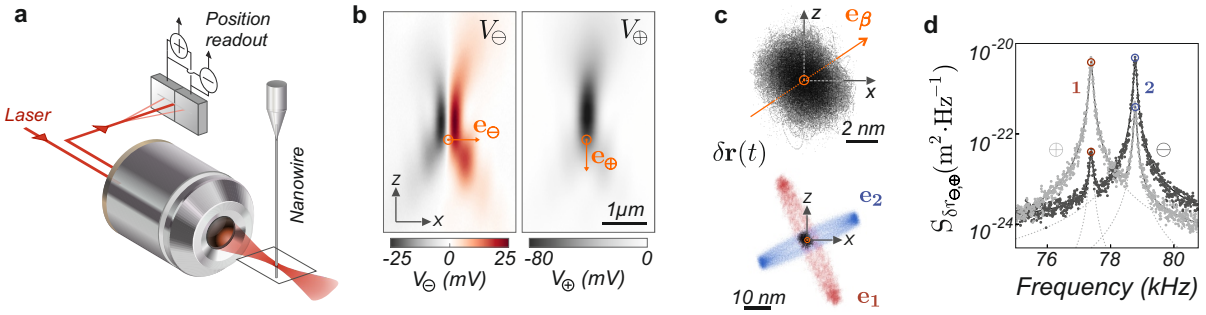


Figure 2.2: **Optical readout of nanowire transverse vibrations in 2D. a**: Principle of the optical readout: a laser is focused on the vibrating extremity of the nanowire and the reflected light is recorded on an amplified split photodiode providing the sum and difference of the photocurrents, whose DC components $V_{\ominus,\oplus}(\mathbf{r})$ serve to image the reflected light field, as shown in **b**, while the vibrations of the nanowire are encoded on their high frequency outputs. Positioning the laser at the position $\odot$, where the measurements vectors $\mathbf{e}_{\ominus,\oplus} \equiv \boldsymbol{\nabla} V_{\ominus,\oplus}/|\boldsymbol{\nabla} V_{\ominus,\oplus}|$ are quasi perpendicular, allows to readout the nanowire vibrations in 2D, such as their thermal noise or driven response as shown in **c**. A spectral analysis of the photocurrents permits to reveal the 2 non-degenerated transverse eigenmodes of the first longitudinal family appearing in the thermomechanical noise spectra shown in **d**. A quantitative analysis of those signals allows to determine the orientations of the 2 transverse eigenmodes, which can also be revealed under resonant excitation as shown in **c** bottom.

$10^6$ V/A conversion depending on the models). The low frequency outputs $V_{\ominus,\oplus}(\mathbf{r_0})$ allow to image the light spot in space by scanning the nanowire rest position $\mathbf{r_0}$. The vibrations of the nanowire extremity $\delta\mathbf{r}(t)$ are encoded as voltage fluctuations, visible in the high frequency output channels of the detector: $V_{\ominus,\oplus}(t) = V_{\ominus,\oplus}(\mathbf{r_0} + \delta\mathbf{r}(t)) \approx V_{\ominus,\oplus}(\mathbf{r_0}) + \delta\mathbf{r}(t) \cdot \boldsymbol{\nabla} V_{\ominus,\oplus}|_{\mathbf{r_0}}$. Each output channel thus provides, after calibration, a projective measurement $\delta r_\beta(t)$ of the nanowire motion, projected along a measurement direction $\mathbf{e}_\beta$:

$$\delta r_\beta(t) = \delta\mathbf{r}(t) \cdot \mathbf{e}_\beta \quad \text{where} \quad \mathbf{e}_\beta \equiv \left. \frac{\boldsymbol{\nabla} V_{\ominus,\oplus}}{|\boldsymbol{\nabla} V_{\ominus,\oplus}|} \right|_{\mathbf{r_0}} \tag{2.1}$$

are the measurements vectors at the position $\mathbf{r_0}$. They can be determined by calculating the local gradients of the reflection maps measured while scanning the nanowire position horizontally over a calibrated grid in the waist area. We chose an operating point where the 2 measurements vectors, $\mathbf{e}_\ominus, \mathbf{e}_\oplus$ are non-collinear and if possible perpendicular, and where the gradients are of maximum slope in order to efficiently convert position fluctuations into voltage fluctuations. There exists two sweet spots where those conditions are simultaneously met, on the optical axis and a bit before or after the waist position, indicated by a symbol $\odot$ in Fig.2.2.

We can then reconstruct the nanowire 2D trajectory $(\delta r_x, \delta r_z)$ in the Cartesian basis using the inversion matrix:

$$\begin{pmatrix} \delta r_x \\ \delta r_z \end{pmatrix} = \begin{pmatrix} \partial_x V_\ominus & \partial_z V_\ominus \\ \partial_x V_\oplus & \partial_z V_\oplus \end{pmatrix}^{-1} \cdot \begin{pmatrix} \delta r_\ominus \\ \delta r_\oplus \end{pmatrix}. \tag{2.2}$$

One can then compute the projected displacement $\delta r_\mu$ along any unitary measurement vector $\mathbf{e}_\mu$ forming an angle $\theta_\mu$ with the $\mathbf{e_x}$ axis: $\delta r_\mu(t) = \cos\theta_\mu\, \delta r_x(t) + \sin\theta_\mu\, \delta r_z(t)$. It is worth mentioning that the reflected optical power can also record non vibrational contributions such as the light shot noise fluctuations, or changes in the nanowire reflectivity which can have an experimental interest but are always found decades below than the motion-induced reflectivity fluctuations.

## 2.3 Nanowire dynamics, thermal noise and driven response

The volumic deformations of the nanowire are readout by the optical probe whose spatial extension (waist of approx. 500 nm) remains small compared to the length of the nanowire and to the typical size over which varies the shape of the eigenmodes of interest. We can thus assimilate the optical readout to a point-like measurement of the nanowire deformations. The vibrations of the nanowire extremity $\delta\mathbf{r}_\beta$ are dominated by the dynamics of the 2 fundamental longitudinal modes, which oscillate at frequencies $\Omega_{1,2}/2\pi$ along perpendicular orientations $\{\mathbf{e_1}, \mathbf{e_2}\}$ which are arranged by definition as a direct basis. The dynamics of the nanowire deflection can thus be described by the equation:

$$\ddot{\delta\mathbf{r}} = -\begin{pmatrix} \Omega_1^2 & 0 \\ 0 & \Omega_2^2 \end{pmatrix} \cdot \delta\mathbf{r} - \Gamma\dot{\delta\mathbf{r}} + \frac{\delta\mathbf{F}_{\rm th}}{M_{\rm eff}} + \frac{\mathbf{F}(\mathbf{r_0}+\delta\mathbf{r})}{M_{\rm eff}} \tag{2.3}$$

where the restoring force matrix is written in the $\mathbf{e_{1,2}}$ basis. $\Gamma$ is the mechanical damping rate of the nanowire, assumed isotropic here, associated to the Langevin force noise vector $\delta\mathbf{F}_{\rm th} = (\delta F^1_{\rm th}, \delta F^2_{\rm th})$ where each component is driving the nanowire randomly along each eigenmode orientation according to the normal mode expansion. The last term represents the contribution of the external forces exerted on the nanowire, which can vary in space or in time.
In absence of external force, the Fourier transform of the above equations [1] reads:

$$\delta\mathbf{r}[\Omega] = \boldsymbol{\chi}[\Omega]\cdot\delta\mathbf{F}_{\rm th}[\Omega] \quad \text{where} \quad \boldsymbol{\chi}^{-1} = M_{\rm eff}\begin{pmatrix} \Omega_1^2-\Omega^2-i\Omega\Gamma & 0 \\ 0 & \Omega_2^2-\Omega^2-i\Omega\Gamma \end{pmatrix} \tag{2.4}$$

is the inverse 2D mechanical susceptibility matrix of the unperturbed nanowire. This expression allows to calculate the fluctuations of the projected nanowire displacements $\delta r_\beta[\Omega] = \delta\mathbf{r}[\Omega]\cdot\mathbf{e}_\beta$ and their noise spectral density $S_{\delta r_\beta}[\Omega]$ defined by $\langle\delta r_\beta[\Omega]\delta r_\beta[\Omega']\rangle = 2\pi\delta(\Omega+\Omega')S_{\delta r_\beta}[\omega]$. In absence of external force, it can be expressed as:

$$S_{\delta r_\beta}[\Omega] = \sum_{\rm m=1,2} (\mathbf{e}_\beta\cdot\mathbf{e_m})^2 \frac{2\Gamma k_B T}{M_{\rm eff}\left((\Omega_{\rm m}^2-\Omega^2)^2+\Omega^2\Gamma^2\right)}, \tag{2.5}$$

where we have used the force spectral density of the individual Langevin force vectors, $S_F^{\rm th} = 2M_{\rm eff}\Gamma k_B T$ given by the fluctuation dissipation relation. The spectro-angular representation of the nanowire thermal noise is shown in Fig. 2.3. It allows to clearly identify the eigenmode orientations and eigenfrequencies. From the above expression one can directly formalize the ideas behind the projection measurement: the peak heights at the mechanical resonances in the spectra will be maximized when the measurement vector is aligned with the corresponding eigenvectors. These considerations will remain unchanged in presence of an external force field. Driving the nanowire at resonance, with a time-modulated reference force $\delta\mathbf{F}(t) = \delta F\cos\Omega t\,\mathbf{e_F}$ and recording the driven displacement in 2D also allows to determine the eigenmodes orientations. In absence of external force field gradients, the projected driven displacements $\delta r_\beta[\Omega]$ are given by:

$$\delta r_\beta[\Omega] = \sum_{\rm m=1,2} \frac{\delta F(\mathbf{e_F}\cdot\mathbf{e_m})(\mathbf{e}_\beta\cdot\mathbf{e_m})}{M_{\rm eff}\left(\Omega_{\rm m}^2-\Omega^2-i\Omega\Gamma\right)}. \tag{2.6}$$

As shown in Fig. 2.2c the coherently driven trajectories are superimposed on the 2D thermal noise of the nanowire. By recording the driven trajectories in 2D or by demodulating the projected driven amplitudes, $\delta r_{\ominus,\oplus}[\Omega_\pm]$, it is then possible to infer the direction and magnitude of the driving force, and its dephasing with respect to the excitation signal. This principle was originally employed to image the optical force exerted by the probe light on the nanowire by time-modulating the intensity of the incoming light field and reproducing this measurement in various locations in the waist area. As illustrated in Fig. 3.1c, the non-rotational character of the optomechanical force field could directly be visualized.

[1] The conventions employed are: $\delta r[\Omega] \equiv \int \delta r(t) e^{i\Omega t} dt$ and $\delta r(t) = \int \delta r[\Omega] e^{-i\Omega t} d\Omega/2\pi$

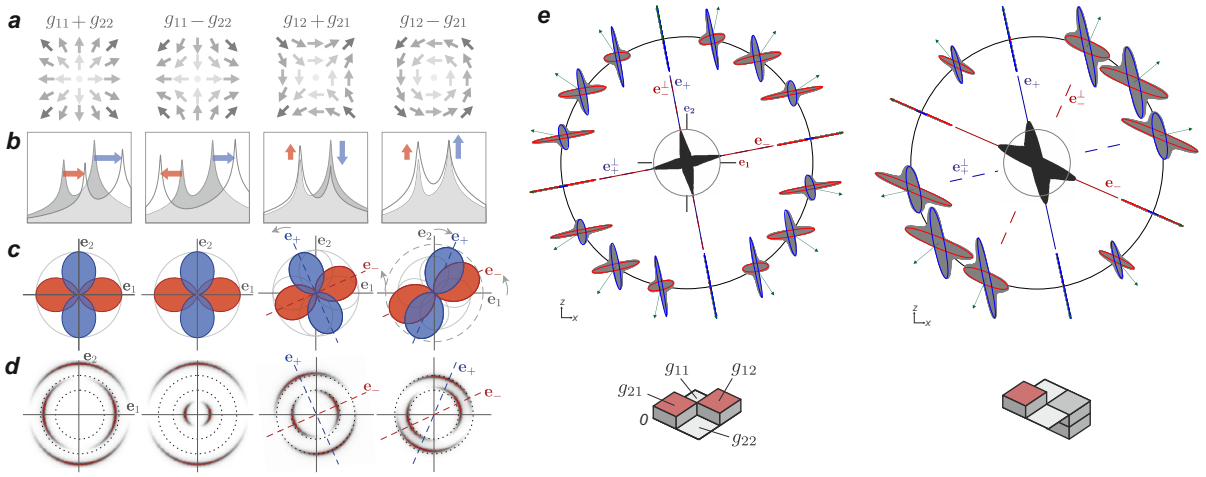


Figure 2.3: **Action of an external force field on the nanowire eigenmodes a**: sketches of the 4 component basis of the 2D force field gradients, displayed in the $\{\mathbf{e_1}, \mathbf{e_2}\}$ spatial basis and their action on the nanowire thermal noise spectra **b**. **c** The tomographic plots represents $S_{\delta r_\beta}[\Omega_\pm]$ as a polar function of the measurement angle $\mathbf{e}_\beta$. The complete spectro-angular signals $S_{\delta r_\beta}[\Omega]$ are shown as polar density plots in **d**, where the radial axis is now the measurement frequency. The unperturbed eigenfrequencies and eigenvectors are shown in gray. This representation allows to clear identify the dressed eigenmode orientations, as well as the frequency shifts, and the evolution of the noise spectral density under the action of an external force field. **e**: the stationary driven trajectories $\mathrm{Re}(\delta\mathbf{r}[\Omega]e^{-i\Omega t})$ shown in the transverse $\mathbf{e_x}, \mathbf{e_z}$ plane are plotted for different driving frequencies swept across the 2 fundamental mechanical resonances, while the resonant cases are highlighted in red and blue. The orientation of the driving force is rotated in the different subplots (with a constant magnitude). The left panel corresponds to a conservative force field, while the right panel corresponds to a non-conservative force field. The corresponding force field gradient matrix are shown in each case. While driving the dressed nanowire along its eigenvectors generates a uniaxial response of the system, a transverse actuation can lead to a larger displacement amplitude along the eigenvectors in the non-conservative case.

## 2.4 Principle of 2D force field sensing

We have thus illustrated how it is possible to determine a force vector when one can control its magnitude, by measuring the induced displacement in 2D. However this measurement is not suited for all forces, and in particular for proximity forces that cannot be simply time-modulated. In an atomic force microscope, the non-contact measurement technique which measures mechanical frequency shifts while oscillating above a surface under investigation allows to image the gradients of the force exerted by the sample on the vibrating cantilever tip, evaluated along the oscillation direction. We extrapolated this measurement principle to our 2D force field sensor, by investigating the perturbation of the nanowire mechanical eigenmodes induced by the transverse spatial gradients of the force field under investigation.
When the force experienced by the nanowire depends on its position in space, for example when it is scanned above a sample under investigation, and when the establishment time of the force is instantaneous on mechanical time-scales, we can formalize it as a position-dependent force field, $\mathbf{F}(\mathbf{r_0}+\delta\mathbf{r})$ in which the nanowire evolves. We note that this 2D vectorial force field is computed through the overlap of the volumic force density with the eigenmode deformation profile (a given eigenmode will not respond when the force is applied at a node of its deformation profile). One

can expand the force field at first order as:

$$\mathbf{F}(\mathbf{r_0}+\delta\mathbf{r})-\mathbf{F}(\mathbf{r_0})\approx\delta\mathbf{r}\cdot\boldsymbol{\nabla}\mathbf{F}|_{\mathbf{r_0}}=M_{\text{eff}}\begin{pmatrix}g_{11}&g_{21}\\g_{12}&g_{22}\end{pmatrix}\cdot\delta\mathbf{r}\quad\text{where}\quad g_{ij}\equiv\frac{1}{M_{\text{eff}}\partial_i F_j}\tag{2.7}$$

represents the 4 spatial gradients of the force field under investigation, calculated in the unperturbed eigenmode basis. The static force term is responsible for a redefinition of the system working point, $\mathbf{r_0}\rightarrow\mathbf{r_0}+\delta\mathbf{r_0}$, solution of

$$\mathbf{F}(\mathbf{r_0}+\delta\mathbf{r_0})=M_{\text{eff}}\boldsymbol{\Omega}_{\mathbf{m}}^{\mathbf{2}}\cdot\delta\mathbf{r_0},\tag{2.8}$$

which can potentially lead to exotic vectorial multistability regimes in non-linear force fields if the external force gradients are comparable to the nanowire stiffness. In our experiments, the static displacements are generally negligible (nanometers) when exploring weak force fields (forces smaller than fN). The linearized force field can be introduced in the dynamical equation, which can be expressed as:

$$\delta\mathbf{r}=\boldsymbol{\chi}_{\mathbf{eff}}\cdot\delta\mathbf{F}\quad\text{where}\quad{\boldsymbol{\chi}_{\mathbf{eff}}}^{-1}=M_{\text{eff}}\begin{pmatrix}\Omega_1^2-\Omega^2-i\Omega\Gamma-g_{11}&-g_{21}\\-g_{12}&\Omega_2^2-\Omega^2-i\Omega\Gamma-g_{22}\end{pmatrix},\tag{2.9}$$

is termed the inverse dressed mechanical susceptibility since the force field gradients generate a cross coupling of the 2 original eigenmodes of the nanowire. This can be viewed as an extension of the traditional cross-coupling of a dual system, when the coupling mechanism takes a complete vectorial form. The external force field will thus change the mechanical properties of the nanowire, by modifying its eigenfrequencies:

$$\Omega_{\pm}^2\equiv\frac{\Omega_1^2+\Omega_2^2-g_{11}-g_{22}}{2}\pm\frac{1}{2}\sqrt{(\Omega_2^2-\Omega_1^2-g_{22}+g_{11})^2+4g_{12}g_{21}},\tag{2.10}$$

and its eigenvectors:

$$\mathbf{e}_-=\frac{1}{\sqrt{g_{12}^2+(\Omega_{2\|}^2-\Omega_-^2)^2}}\begin{pmatrix}\Omega_{2\|}^2-\Omega_-^2\\g_{12}\end{pmatrix}\quad\text{and}\quad\mathbf{e}_+\equiv\frac{1}{\sqrt{g_{21}^2+(\Omega_+^2-\Omega_{1\|}^2)^2}}\begin{pmatrix}-g_{21}\\\Omega_+^2-\Omega_{1\|}^2\end{pmatrix}\tag{2.11}$$

where we have introduced $\Omega_{i\|}^2\equiv\Omega_i^2-g_{ii}$.
The above equations can be mathematically inverted [11] so that one can determine the 4 components of the local force field gradients, the $g_{ij}$ terms, by measuring the perturbation caused on the eigenmodes of the nanowire. This is the core principle behind the sensing of 2D force fields: one simply needs to track the eigenmode orientations and the eigenfrequencies, which can be done using the principles of the spectro-angular analysis of the nanowire thermal noise, or via a resonant excitation of the eigenmodes.

To clarify the phenomenology, one can consider the different basis elements of the 2D force field gradients, whose corresponding vector flows are illustrated in Fig. 2.3a. The divergence of the force field, $\text{div}\mathbf{F}\propto g_{11}+g_{22}$, does not depend on the basis orientation and is responsible for a common frequency shift. If the force field presents a trapping character, it will adds up to the restoring force field and generates a stiffening of the nanowire leading to an increase of its mechanical frequencies. Since the determination of the eigenfrequencies almost does not require any calibration, the force field divergence is in general the simplest component to acquire. Similarly, if the force field presents an opposite trapping/antitrapping structure aligned with the eigenmodes orientations, it will cause an asymmetric frequency shift (second column). The same force field but rotated by 45 degrees (third column) will have a very different impact on the nanowire: a displacement along one direction will make the nanowire experience a force along

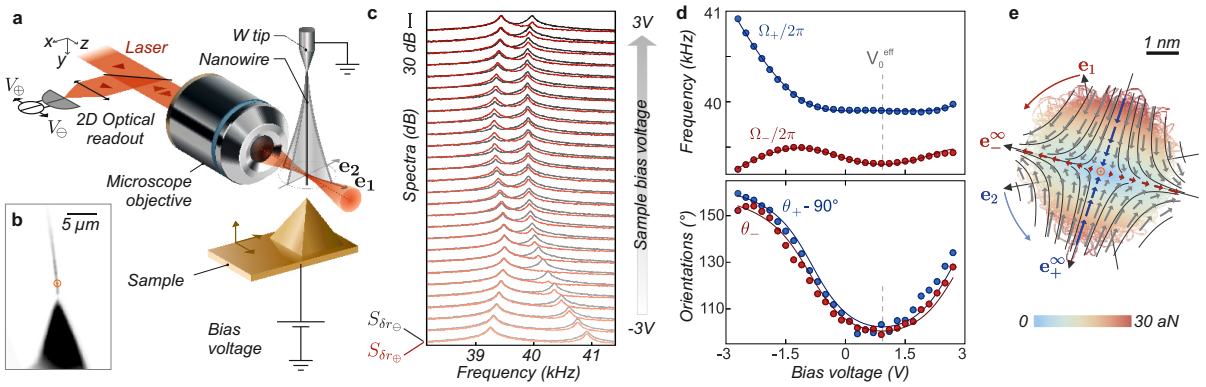


Figure 2.4: **Principle of electrostatic force field sensing a**: Sketch of the experiment [11]: a voltage-biased sample - a metallic tip here - can be piezo scanned below the nanowire vibrating extremity. **b**: Evolution of the thermal noise spectra measured on both measurement channels, for varying voltage bias, at a given position 100 nm above and on the side of the tip. Their analysis allows to determine the eigenmode orientations and the eigenfrequencies, which are reported in **d** as a function of the bias voltage. A pronounced rotation of the eigenvectors is induced by the force field gradients, as well as peculiar frequency shifts, which are connected to the rotation of the eigenmode basis, which preserves here its perpendicularity. The full lines are fits with a quadratic dependence of the electrostatic force gradients. **e**: Local map of the force field around the chosen measurement point, deduced from the previous measurements for a bias voltage 1 V away from the extremum value. When increasing the bias voltage, the eigenvectors tend to get aligned with the eigendirections of the force field. The vector flow is plotted over the spatial extent of the nanowire thermal noise, whose spectro-angular analysis was used to determine the force field structure.

the transverse direction, thus cross-coupling the 2 eigenmodes. This hybridization will cause a modification of the eigenmode basis, a rotation of the basis in that case, with a magnitude that depends on the initial frequency splitting of the nanowire. Our quasi-frequency degenerated nanowires are then very sensitive to such shear components of the force field. The last component, the rotational one, does not depend neither on the eigenmode orientation. It also couples both directions in space, and thus rotates the eigenvectors but leads to a breaking of their orthogonality. This force field has a very peculiar status, since it does not derive from a potential energy, it can be produced by exploiting the radiation pressure force in a focused light beam and will be further discussed in section 3.1.

## 2.5 Illustration on the case of an electrostatic force field

We will now illustrate the principle of 2D force field sensing on the specific case of an electrostatic force [11] generated by a sharp metallic tip approached in the vicinity of the nanowire vibrating extremity, and voltage biased with a tunable voltage to clearly separate the electrostatic contribution from the force environment (which will be discussed later). The sketch of the experiment is given in Fig. 2.4a.

The nanowire thermal noise was first recorded for varying bias voltages $V$, on the 2 measurement channels, at a given position above the electrostatic tip, located at a typical distance of 200 nm on one side of the tip. By fitting the thermal noise spectra, it was possible to reconstruct the eigenfrequencies and the eigenmode orientations, and to map their dependence on the bias voltage, see Fig. 2.4d. At a given position, the electrostatic force presents a quadratic

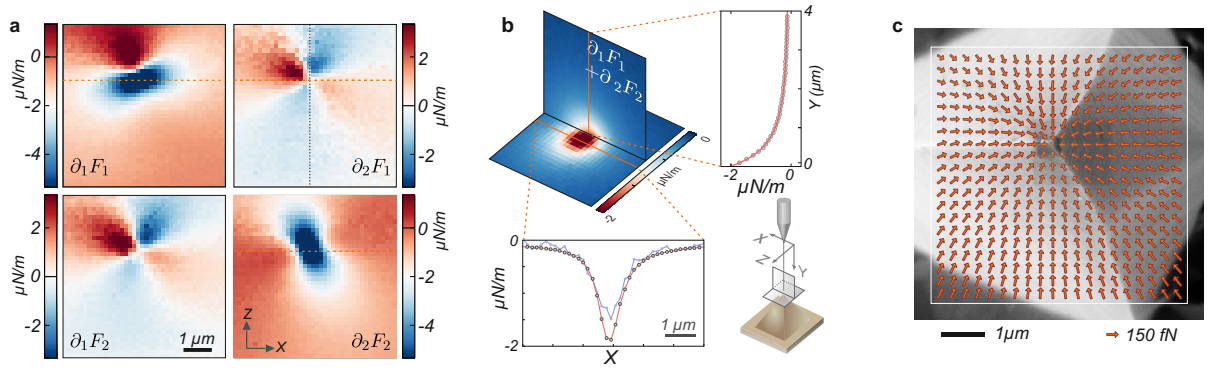


Figure 2.5: **Mapping of the electrostatic force field a**: Map of the electrostatic force field gradients $\partial_i F_j$, obtained by reproducing the previous local measurements at different positions above the sharp electrostatic tip. The eigenmode orientations can be identified as the white lines, where no shear force is measured ($g_{12} = g_{21} = 0$), as expected for a quasi-central force field. **b**: The measurement can be realized at different positions above the tip, the divergence of the force field which only depends on the eigenfrequency shifts represents an interesting resource for rapid imaging. The surfaces can be detected at distances of a few $\mu$m. **c**: After integration of the force field gradients, one can reconstruct the electrostatic force field experienced by the nanowire above the metallic EFM tip shown in the background. The integration constant is chosen so that the force vector above the tip is zero.

dependence on the bias voltage: $\mathbf{F}_{\text{el}} = \mathbf{f}_{\text{el}}(V - V_0)^2$, and so do the force field gradients. Due to the non-trivial evolution of the eigenfrequencies and eigenvectors with the external force field gradients, their parabolic behavior is not directly observed in the mechanical parameter changes. The electrostatic force field responsible for such a modification of the mechanical properties is shown in Fig. 2.4e. One can notice that the eigenvectors turn and their rotation stops once they get aligned with the eigen-directions of the force field gradients while the eigenfrequencies never stop evolving at large positive or negative bias. We note that such a measurement is conducted in a regime where the electrostatic force field gradients dominate the mechanical properties of the nanowire, which behaves as a "compass" pointing towards the force field eigenvectors.
Such a measurement was reproduced at varying positions around the electrostatic tip, which allows to map the force fields gradients as shown in Fig. 2.5. One can notice that the 2 transverse components are measured as being almost identical, as expected for a conservative force field.
Then, a last integration step can be done to reconstruct the force field from the force field gradient maps:

$$F_i(\mathbf{r}) = F_i(\mathbf{r}_\infty) + \int_{\mathbf{r}_\infty \to \mathbf{r}} \mathbf{dr} \cdot \boldsymbol{\nabla} F_i$$

where $i = x, z$ and where the integration path $\mathbf{r}_\infty \to \mathbf{r}$ can be arbitrary, which provides multiple evaluation possibilities. A computation procedure, which was elaborated with the help of Benjamin Canals, is then implemented to reconstruct the force field profile, using an integration constant chosen so that the force above the tip has a zero horizontal projection. The resulting integrated force field is shown in Fig.2.5c.

We have thus illustrated the procedure to measure force field gradients, in the case of a conservative force field. The case of a non-conservative force field will be discussed in the next chapter.

## 2.6 Advanced protocols

The above described universal force field sensing protocol was realized by extracting and tracking the eigenmodes properties out of thermal noise measurements. However this was an extremely lengthy measurement since recording a proper thermal noise spectrum requires a few seconds of averaging, and a significant subsequent data analysis in order to determine the eigenmode orientations and frequencies following the spectro-angular analysis exposed above. To accelerate the measurement, Philip Heringlake developed several key elements. First the projective measurement vectors are now probed in quasi real-time: the experiment is coherently shaken with respect to the probe laser along both transverse directions, at 2 different frequencies around 80-100 Hz along each axis using the piezo stage that supports the core experiment (nanowire and sample). This calibrated displacement is demodulated on each measurement channel, which permits to record in real-time the measurement slopes ($\boldsymbol{\nabla} V_{\ominus,\oplus}$). This function is realized with a FPGA card, that has been completely reprogrammed by Philip with the help of J. Minet from the electronic department.
Then, to track the eigenmode orientations, we now make use of coherently driven trajectories instead of using the random thermal motion of the nanowire. To do so a second green laser beam is co-injected with the probe laser, and is intensity modulated at the 2 mechanical resonances in order to simultaneously drive both mechanical modes. This generates coherent trajectories, which are then analyzed on each measurement channel in order to determine the eigenmodes orientations. Two feedback loops are activated to maintain the excitation frequencies at resonance, which is necessary when approaching a sample which can generate significant frequency shifts (for strong electrostatic force field it is common to observe a relative frequency shift of a few percent). After a few calibration steps, it is possible to reconstruct the eigenvectors and eigenfrequencies directly out of the signals demodulated by the PLL and the associated lock-in, and thus to obtain the complete structure of the local force field gradients experienced by the nanowire. To reach its steady state, the nanowires needs a $1/\Gamma$ duration, which sets a minimum measurement time in each position. In practice we operate with a measurement time of typically 100 ms, which is 100 times faster than before. This acceleration of the measurement rate, allowed us to approach the nanowire closer from surfaces without being afraid of "touching", and scanning measurement parameters on a broader range, by suffering less from experimental drifts.
One difficulty associated with this dual PLL scheme is the fact that when the force gradients are too strong - or the nanowire too sensitive -, the eigenmodes can rotate and change their orientations with respect to the measurement vector $\mathbf{e}_\beta$ or to the drive vector $\mathbf{e}_\mathbf{F}$, thus causing an impossibility to lock the PLL since it changes the resonant phase by 180 degrees. Philip developed a FPGA module- termed the "radar" module- which allows to rotate the measurement angle, which partly solves the problem, but we should still rotate the driving force vector, which requires a dual excitation to be fully capable of getting rid of those eigenmode rotations. Philip developed an alternative approach consisting in implementing an artificial force field, which could compensate the force field under test, using a real-time 2D feedback. With the FPGA modules he developed, he could synthesize the 2D displacement projected along an arbitrary orientation $\mathbf{e}_\mu$ and apply a force in a direction $\mathbf{e}_\mathbf{F}$ proportional to $\delta r_\mu$, so that the nanowire is subjected to a new force $\delta\mathbf{F} = g\,\mathbf{e}_\mu \cdot \delta\mathbf{r}\mathbf{e}_\mathbf{F}$, which presents the same characteristics as a force field gradient. Depending on the relative orientation of the measurement and feedback vectors, it was possible to emulate axial or transverse synthetic force fields [13].
Then, another method employed was based on multi-frequency excitation tones, which did not require locking the PLLs: instead of using 2 resonant tones, we exploit the large linearity of the nanowire by driving each mode with a comb of frequencies, so that we can reconstruct the frequency, damping rates and eigenvectors directions of each mode. This method was for example used in the cavity nano-optomechanical experiment, where we imaged the optomechanical force

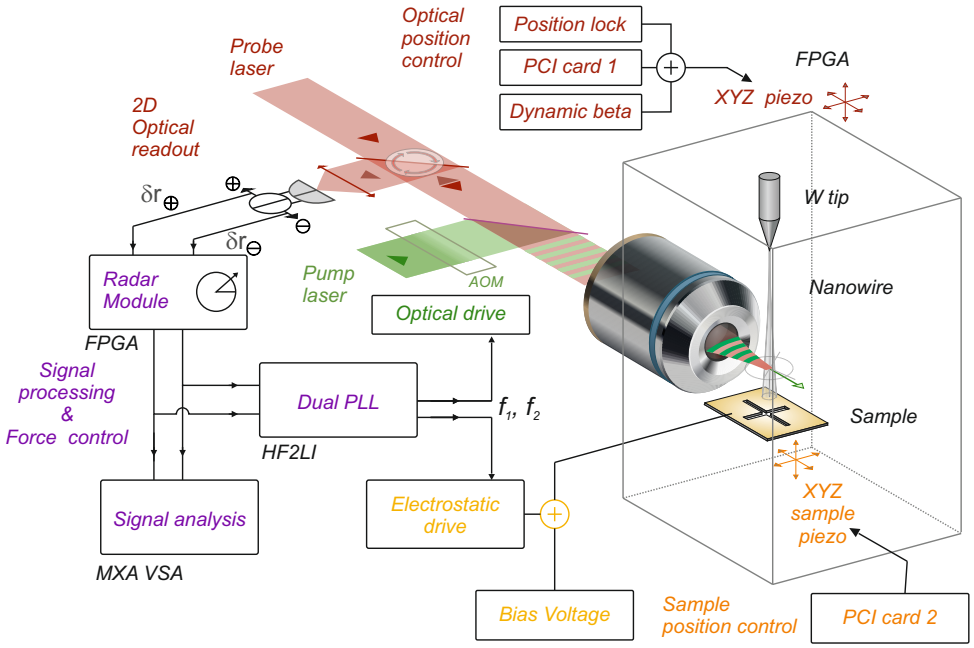


Figure 2.6: **Measurement architecture implemented in advanced protocols**

exerted by the intracavity light field on the nanowire [19], which is discussed in section 3.2.

## 2.7 Perspectives in 2D force field sensing

The typical experimental architecture we now employ is depicted in Fig. 2.6. In addition to the readout and force sensing modules discussed above, we can approach the sample by controlling the force field experienced by the nanowire in real time. We then scan the sample in the vicinity of the nanowire vibrating extremity to establish force maps, and we have to manage the bias voltages to activate and control the electrostatic forces at play at the surface. The latter are often the dominant forces at the nanoscale, and we exploit them to get quantitative or qualitative information on the sample under test.

### 2.7.1 Exploration of surfacic electric fields

As discussed above, as a dielectric the nanowire is attracted towards regions of large electric field. When the electric field is rapidly vanishing with the altitude, the force experienced by the nanowire fundamental eigenmode can be assimilated to the total electrostatic force, which is calculated from the integration of the Maxwell stress tensor $\mathcal{T}$ on the periphery $S$ of the nanowire:

$$\mathbf{F} = -\int_S \mathcal{T}\mathbf{d^2S}, \tag{2.12}$$

where the tensor components are quadratic in the electric field: $\mathcal{T}_{ij} = \epsilon_0 E_i E_j - \epsilon_0 E^2 \delta_{ij}$. For a perfect voltage-biased metallic structure it is the geometry of the surface that governs the field distribution above it. The quadratic contribution of the force in the bias voltage then serves to get topographic information on the nano-structure. Several samples were produced and investigated: sharp and round (250 nm radius of curvature) tips, micro-disks, holes and trenches, with the help of Jean François Motte, Gwénaëlle Julie and Bruno Fernandez from Nanofab, and Simon Le Denmat. A pot-pourri of the different force field divergence maps measured above them is shown in Fig. 2.7. One can observe that the nanowire gets attracted towards the tips and

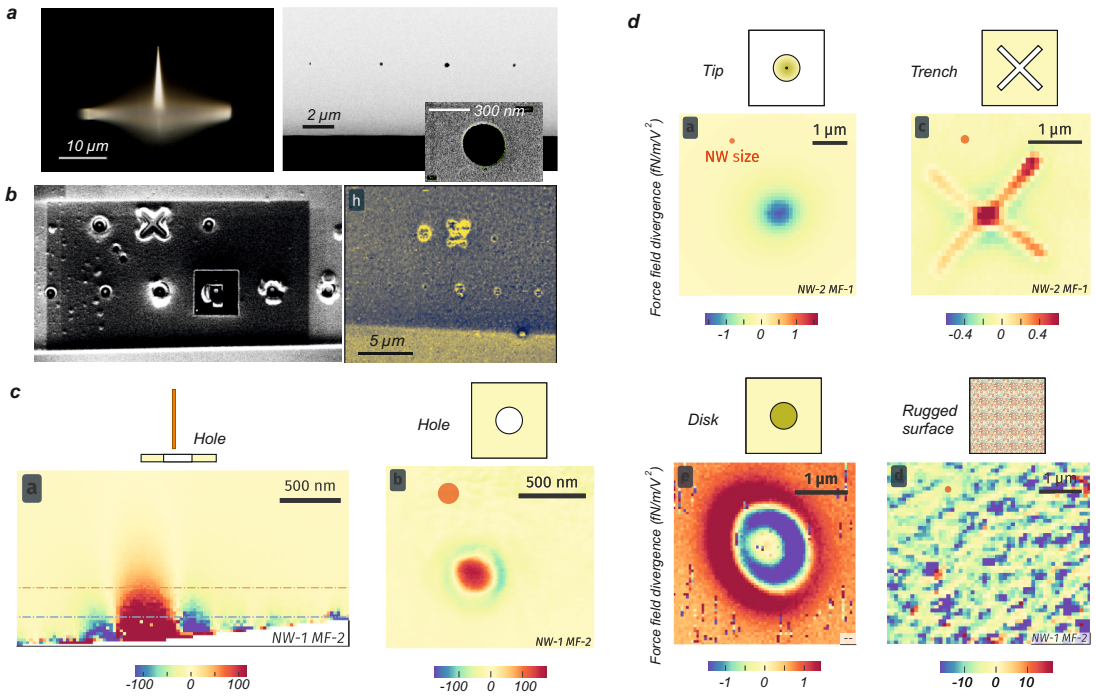


Figure 2.7: **Electrostatic forces above nanostructured samples a** Images of the sampled employed: a sharp tip and FIB etched cantilevers providing cylindrical holes and trenches of 100-1000 nm typical lateral extensions (viewed here from the bottom to avoid contamination of the front surface). The force divergence measured above the sample allows to identify the nanostructures' topography. **c** Quadratic contribution of the force field divergence in the sample bias voltage, $V$: $\partial^2 \mathrm{div}\mathbf{F}/\partial V^2$ measured above a hole (horizontal and vertical scan planes). **d** Images of the quadratic components in the bias voltage of force field obtained above a sharp conductive tip, a cross trench drilled in a metal plane, a metallic disk, and a silicon plane covered with a metal layer, where the grain structure becomes apparent. The nanowire diameters are indicated as orange disks.

to the sharp edges in general, so that the force divergence is measured as being of anti-trapping character above the hole (or above the trench) because it is isotropically attracted towards the edges of the nano-structure. Vertically, we can detect the electrostatic force produced by a quasi-flat surface at a micron distance (due to the residual tlts), which allows to safely approach the sample without being afraid of crashing the nanowire.

Biasing the sample thus allows to clearly identify the electrostatic force produced by the bias dependent electric field ($E_V \propto V$) - leading to a quadratic dependence of the force in $V$ - and thus to potentially minimize it by choosing the appropriate bias voltage. In general the minimum of the electrostatic force parabolas is not found a zero bias voltage, because there always exists some residual electric field that do not depend on the bias voltage: this is for example the case if the nanowire support and the sample materials present a different work function, if there exists trapped charges in the system or when the metallic surface presents some electrostatic patches (regions of different work functions). For example sputtered metallic layers are generally made of grains presenting varying work functions so there always remain residual fields at their surface even in absence of bias voltage. In the case of gold, the work extraction value can vary up to 80 mV between the different crystal orientations, whose dimensions are of a few tens of nanometers, thus generating huge residual electric fields (100 kV/m) at the sample surface, which can be partly screened by surface contamination. In the calculations of the electrostatic

force (eq. 2.12), those residual fields $E_{\mathrm{res}}$ get combined with the bias depended electric field $E_V$, generating an additional linear contribution of the force in the bias voltage ($\propto E_{\mathrm{res}}E_V \propto V$) - which displaces and change the parabola extrema - and to a supplementary offset contribution $\propto E_{\mathrm{res}}^2$. The nanowire thus allows to image not only the sample structure via the quadratic contribution in the bias voltage, but can also be used to investigate the residual electrostatic fields, generated by the grainy structure of the metal as well as by other sources of contaminations (such as carbonated residues consecutive to SEM imaging, which are clearly observable in the force measurement map). This grainy structure was in parallel characterized with AFM/ KPFM measurements (realized with the help of Simon Le Denmat), allowing a direct comparison to the nanowire-based measurements. While the former, realized at a closer distance (approx 5-10 nm) presented a sharper lateral resolution in the topographic measurements, the nanowire-based measurements provided a significantly larger amount of information on the electrostatic landscape above the sample, which could not be visualized otherwise. As such, the nanowire could serve as an efficient characterization tool of the electrostatic properties of samples employed in nano-science, allowing a rapid and sensitive diagnostic of the different growth and deposition methods used in sample preparations.

### 2.7.2 Casimir force field imaging

When the electrostatic fields are properly canceled, the nanowire is in principle only submitted to the Casimir forces, arising from the quantum fluctuations of the electromagnetic field in the surrounding vacuum. A theoretical paper by Johnson and colleagues in 2010 [16] predicted the possibility to observe a repulsive Casimir force in a needle-hole geometry in vacuum and we are currently exploring the possibility to detect them with our nanowires. The paper also suggested that the needle would experience a laterally instable force, meaning a laterally anti-trapping force field for the nanowire, with magnitudes hardly measurable in existing experiments. Numerical simulations of our system realized by Philip on Scuff-EM, a FDTD program and interactions with Romain Guśout and Serge Reynaud from LKB, have convinced us that they should be well within reach with the detection capacity of the nanowires, since we estimated Casimir force gradients of a few 10 aN/nm in our geometries. This magnitude is however far smaller compared to the strength of the electrostatic and optical force fields experienced by the nanowire so that measuring them properly is a current experimental challenge. The most delicate point is to correctly assess the force contribution of the residual electrostatic fields: from the above discussion, they do not only displace the parabolas through the linear contribution ($\propto E_V E_{\mathrm{res}}$) but also contribute to a force background ($\propto E_{\mathrm{res}}^2$), which may hide the Casimir contribution ($\propto \delta E_{\mathrm{vac}}^2$). The measurement of the parabola shifts with respect to a mean canceling voltage value allows to compensate for the linear contribution of the residual electric fields, but not for their quadratic contribution. After compensating the linear contributions of the electrostatic surface field, we obtained a residual force field presenting a spatial profile and a magnitude in qualitative agreement with our numerical simulations [13], see Fig. 2.8. The surface patch contributions were clearly visible at short distances above the sample, while the weakly vanishing contribution observed at larger altitudes can in principle be explained by a tilt of the nanowire with respect to the sample surface: the attractive vertical forces are around 10 times larger than the horizontal contributions, and are responsible for an apparently anti-trapping contribution to the force gradient experienced by the nanowire along its tilted oscillation plane on each side of the hole structure. However such a procedure is not expected to provide a completely quantitative result since the quadratic contributions arising from the surface field cannot be fully eliminated. Improvements in the sample fabrication techniques could help reducing their impact: for example, one could think of producing samples out of a mono-crystalline layer or, alternatively, working with metallic patches presenting a smaller size distribution whose stray field will more rapidly vanish with the altitude above the sample.

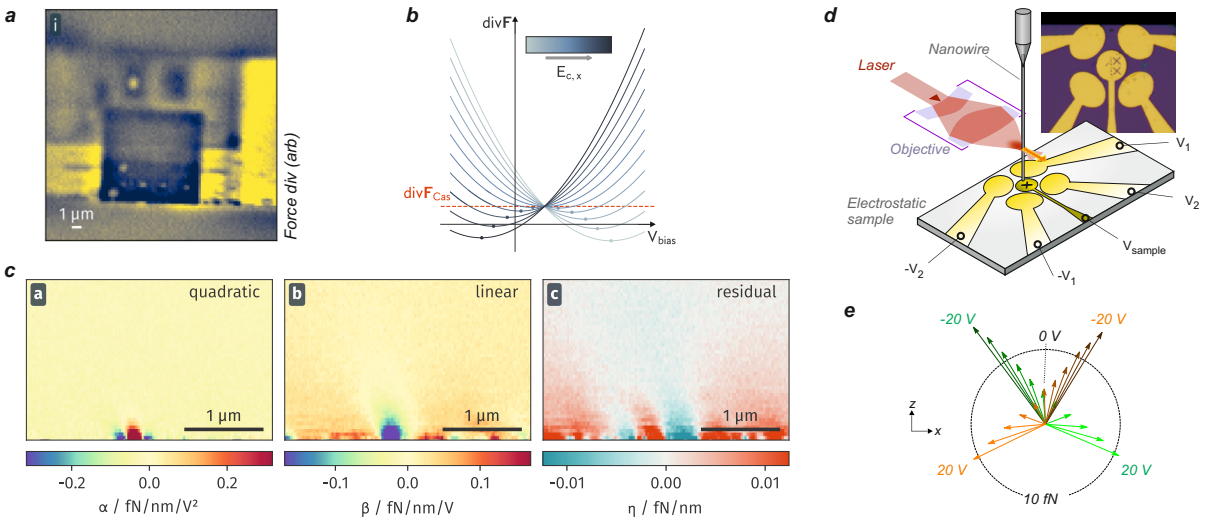


Figure 2.8: **Proximity forces a** Force divergence scanning image (at a given bias voltage) of the top face of a first generation FIB-milled cantilever observed after SEM imaging: in addition to the force field emerging from the nano-structures, the SEM scanning frames are clearly visible, indicating a surface contamination (probably carbon deposition). **b** Force parabola expected in presence of a parasitic surface field (which do not depend on the bias voltage) of varying magnitude, which accordingly displaces and vertically shifts the parabolas. **c** Quadratic, linear and residual force divergence maps obtained above a 500 nm hole, defined from $\mathrm{div}\mathbf{F} = \alpha(V - V_0)^2 + \beta(V - V_0) + \gamma$ with $V_0 = -0.39\,V$. The residual contribution is in agreement in magnitude (tens of attonewton) and in spatial profile (anti-trapping character above the hole) with numerical simulations of the Casimir force field, but is not yet quantitative due to the contribution of residual electrostatic fields. **d** Principle of lateral compensation electrodes, that will help compensating the surface electrostatic fields. **e** Variability of the optically driven force vector observed in presence of a transverse electric field: in addition to the radiation pressure force observed at zero lateral bias voltage, one can observe the apparition of an intense transverse force, aligned with the compensation electrostatic field.

For all those suggestions, a direct nanowire-based imaging of electrostatic residual fields will significantly help the optimization of the Casimir compatible samples.
To obtain a more quantitative assessment of the Casimir force fields, one could aim at locally compensating the residual electric fields seen by the nanowire: since they can rapidly vary above the nano-structure, it is necessary to realize this compensation at each position above the sample. To do so we have developed new samples where we added 4 control electrodes on each side of the sample under test, see Fig. 2.8d. They are employed to create a quasi-homogeneous electric field around the nanowire (so that alone, they do not induce additional forces) which serves to compensate for the local residual electric fields in the measured electrostatic force. This homogeneous field will not have the same spatial shape as the residual electric fields, which are in principle confined on the sample surface, so the compensation will not be complete, but since the electrostatic volume forces are essentially localized at the nanowire extremity, we believe this could be a good strategy to obtain a better quantitative agreement. Furthermore, those control fields will also help investigating in greater details the residual electric fields above a surface, which should have some direct applications in surface imaging and characterization at the nanoscale.

Other perspectives in the thematic of force field imaging will require a specific functionaliza-

tion of the nanowire, for example with micro/nanomagnets to obtain a magnetic force sensing capacity. Jean-Fran cois Motte succeeded in attaching micro-beads of a approx 300 nm diameter at the extremity of nanowires, using micro-manipulators and Platinum "soldering" in a SEM, they will be studied in the PhD thesis of Hugo Weltz. The vectorial and ultrasensitive force sensing properties of the nanowire, will in principle allow to explore weak magnetic structures, which could be destroyed by the stray field of a more macroscopic traditional MFM probe, or give new insights on the stray field emitted by peculiar magnetic structures such as vortices or skyrmions.

Furthermore, we recently observed a novel actuating force when combining optical and electrostatic fields on the nanowire, see Fig.2.8e. We believe they originate from the action of electrostatic fields on the laser-induced electron-hole pairs created when operating with a wavelength close to the silicon carbide bandgap (515 nm for the 3C phase): the pair is first spatially separated by longitudinal fields, which prevents from a direct recombination and creates a net charge distribution along the nanowire which is in turn sensitive to the inhomogeneous transverse fields via the action of a direct Coulomb force. The total electro-optic transverse force is aligned with the transverse electric field and presents a linear dependence with its magnitude. An electric field of $1\,\mathrm{V}/\mu\mathrm{m}$ combined with an optical power of $10\,\mu\mathrm{W}$ generates forces in the 10 fN range. It represents a interesting avenue for directly imaging the vectorial structure of electrostatic fields (and not the gradients of a quadratic electrostatic term).

# Chapter 3

# Nano-optomechanics with sub-wavelength-sized nanowires

This chapter is dedicated to the optomechanical interaction between the nanowire and light fields, we present the different studies realized over the past years and describe the future perspectives of the work.
The force exerted by a focused laser beam produces a rotational force field in the waist area, as expected from the converging-diverging structure of the Poynting vector, which was mapped with sub-wavelength sized nanowires during the PhD thesis of Arnaud Gloppe [8]. This rotational structure has a very peculiar impact on the nanowire dynamics. At large powers it can generate a new kind of dynamical instability, while at lower powers, prior to the onset of the instability, it is responsible for a breaking of the eigenmode orthogonality and for a violation of the fluctuation-dissipation relation, by bringing the nanowire in a out of equilibrium state. Those different aspects, which were investigated during the PhD thesis of Laure Mercier de Lépinay [10] and pursued with Philip Heringlake' synthetic force fields [13] are summarized in the first section.
In the last section we describe the cavity nano-optomechanical project realized in collaboration with the group of J. Reichel at the Laboratoire Kastler Brossel, which was investigated during Francesco Fogliano's PhD thesis [17]. By inserting the nanowire in the mode volume of a tiny fiber micro-cavity, we could generate an intense optomechanical interaction which we have mapped using the force sensing protocols exposed above. The coupling strength is indeed so large that we could measure and map the optical force exerted by a very weak intracavity field corresponding to less than a single photon in the optical mode.
We will present the project and its perspectives towards the exploration of the field of cavity nano-optomechanics in the single photon regime.

### Context and positioning of our approach

Optomechanics explores the interaction between a probe light field and a deformable object, a mechanical oscillator, possibly enhanced by a high finesse cavity which was early recognized as an ideal platform to explore the quantum limits of ultrasensitive measurements, ultimately limited by the quantum fluctuations of the light field and the oscillator position [35, 36, 37, 38] and their crossed interactions provided by dynamical backaction for example. The optomechanical interaction carries an intrinsic Kerr-like non-linearity [39] efficient down to the single photon regime, which has for the moment remained far from experimental reach since most of the impressive results achieved, such as ground state cooling, mechanical detection of radiation pressure quantum noise, advanced correlation between light and mechanical states or optomechanical squeezing [40, 41, 42, 43, 44, 45, 46, 47, 48, 49, 50, 51, 52, 53, 54] were obtained by making use of large photon numbers to compensate for the weak single photon interaction strength obtained with macroscopic oscillators. The single photon regime is achieved when a single photon in the cavity pushes the static rest position of the mechanical resonator ($\delta x^{(1)}$) by more than the spreading

of its zero point fluctuations $\delta x_{\mathrm{zpf}}$. A very strong optomechanical interaction is indeed needed, requiring $g_0 > \Omega_{\mathrm{m}}$ where $g_0$ is the single photon optomechanical coupling and $\Omega_{\mathrm{m}}$ the resonant angular frequency of the mechanical oscillator. Depending on the relative values of the cavity linewidth, oscillator frequency and single photon coupling strength $(\kappa, \Omega_{\mathrm{m}}, g_0)$, different novel dynamical phenomena were theoretically anticipated [55, 56, 57, 58, 59, 60, 61, 62, 63, 64, 65, 66]. For the moment only atom-based optomechanical experiments [67, 68] could approach such a regime, while recent developments with highly deformable photonic crystals [69, 70] or trampoline [71] resonators represent interesting platforms in that perspective.
Our sub-wavelength-sized nanowires produce significant photon scattering out of the cavity mode so that we largely operate in the *single photon adiabatic regime* ($\Omega_{\mathrm{m}} \ll g_0 \ll \kappa$), where the cavity field instantaneously follows mechanically induced perturbations. A precise positioning of the nanowire within the intracavity stationary wave will be required and thus calls for a mapping and understanding of the optomechanical interaction in this peculiar configuration. We have shown that already at room temperature, the nanowire can detect variations of the mean intracavity photon number smaller than unit and that its mechanical properties are governed by the intracavity field. Operating at cryogenic temperature should allow to enter a regime where the position fluctuations of the nanowire are completely dominated by the intracavity field quantum fluctuations, down to the single photon level. This represents an interesting resource for quantum optics since the optomechanical interaction to the oscillator is sufficient to generate non-classical states of light down to very small mean photon numbers and on a broad frequency range, not restricted to the vicinity of the mechanical resonance [39, 38]. Furthermore significant deviations from the commonly employed semi-classical description can be expected since the optical field fluctuations can have an optomechanical impact comparable to the mean field at low photon number, which should also opens the road towards the investigation of vacuum Casimir forces in confined optical resonators.
Finally, the fact that the nanowire equally vibrates along both transverse direction provides two degrees of freedom for building up the optomechanical interaction. The different observations we made in the cavity free case, where the rotational structure of the optical/optomechanical force field played a critical role should be transposable to the cavity case. Our theoretical investigations [20] have shown that the optomechanical force field will remain non-reciprocal, so that one can anticipate a rich optomechanical phenomenology.

## 3.1 Non-conservative optomechanical force fields

Very rapidly after having inserted the nanowire in the optical waist of a high numerical aperture objective in a vacuum chamber, we observed a peculiar modification of the nanowire dynamics, which became instable only on one side of the optical axis: there the nanowire was oscillating with a very large amplitude, hundreds of nanometers, sufficient to blur the optical DC maps, while its eigenfrequencies were merging prior to the onset of instability. This evolution towards the instability was very peculiar, very different from the optomechanical or photothermal ones observed in 1D optomechanical systems (cavity with a movable mirror or equivalent), and its precise location in space, lead us thinking that it should be connected to the spatial topology of the force field. This led us analyzing the impact of a 2D force field varying in space on our 2D oscillator. We theoretically identified the specific role of the rotational structure of the force field, which was subsequently measured experimentally [9] using pump-probe techniques, as shown in Fig.3.1c.

Following those experimental observations, we further explored theoretically the light-nanowire interaction, and in particular the contribution of the Mie internal optical resonances. Guillaume Bachelier developed numerical simulations under Comsol and Matlab, where he modeled the non-paraxial structure of the incoming light field, and computed both the scattering profiles

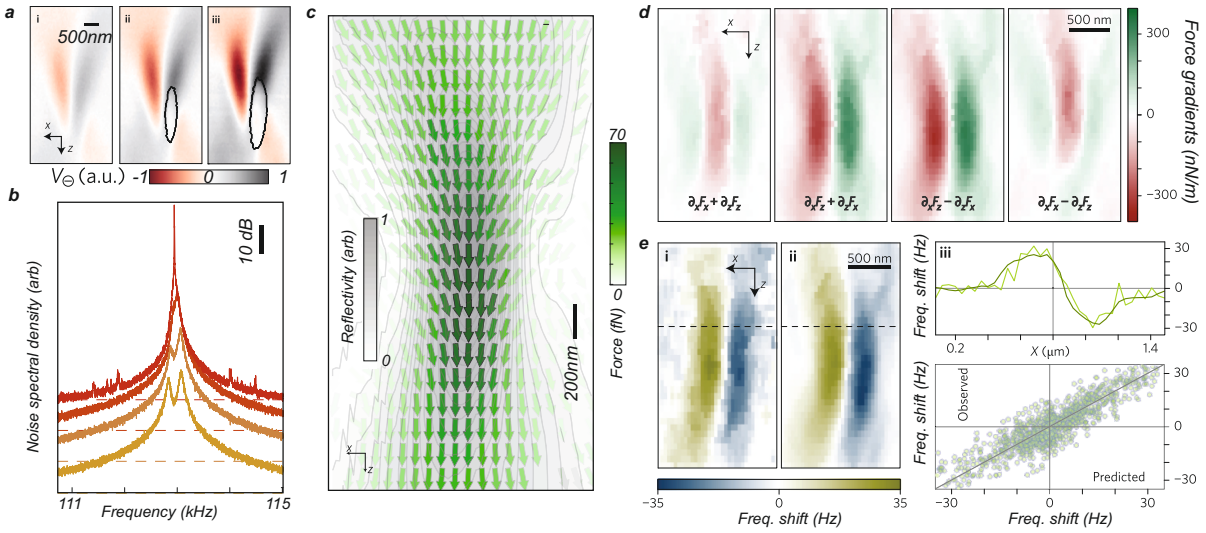


Figure 3.1: **Rotational instability and optomechanical force field experienced in a focused laser waist. a** Reflection images ($V_\ominus$ channel) measured for increasing optical powers (140, 260 and 380 $\mu$W). The area over which the rotational instability appears is contoured in black. **b** Noise spectra measured for increasing optical powers (including a vertical offset for visibility) showing the initial frequency merging followed by a transition towards the rotational instability, where the nanowire eigenmodes acquire an additional damping/antidamping component arising from the non-conservative structure of the optomechanical force field. **c** Optomechanical force field map obtained by realizing response measurements at multiple positions within the optical waist [9]. The force field presents a rotational character on each side of the waist. **d** Different components of the force field gradients derived from the force map, and in particular the rotational of the force field $\partial_x F_z - \partial_z F_x$ (third plot). **e** Comparison of the measured relative frequency splitting $(\Omega_+ - \Omega_-)/2\pi - (\Omega_2 - \Omega_1)/2\pi$ (*ii*) to the value predicted from the measured force field gradients (*i*) using expression 2.10: full maps, line cuts and full map comparisons. The mechanical properties of the nanowire are thus governed by the spatial structure of the optomechanical force field. This comparison also validates the complete force measurement protocol.

and the optical force maps within the waist area for different colors and nanowire diameters. Antoine Reigue pursued this investigation, by exploiting the seminal book of Bohren [72] to obtain analytical expressions of the optomechanical force field [20]. For a dipolar object, a small nanowire in our case, the light forces can be separated between the dipolar gradient forces and the radiation pressure forces. The latter generate a rotational structure, which can be understood from the converging/diverging structure of the Poynting vector in the waist area.
In this section, we will explore the impact of the rotational force field, on the nanowire dynamics, by presenting its effect on the eigenmode structure, on the thermal noise dynamics and its relation to the fluctuation dissipation relation, on the nanowire optically dressed mechanical susceptibility and on the trajectories followed by the nanowire extremity.

### 3.1.1 Dressing the nanowire with a rotational optical force field

The optical force experienced by the nanowire has been shown to respond instantaneously, on mechanical time scales, to an intensity modulation (photothermal effects present a frequency cut-off in general 100x slower than the mechanical period). As such, when the nanowire evolves in the light beam, the force experienced by the nanowire instantaneously change with its position changes. Furthermore, it presents a rotational structure, so that it can be written and locally

expanded as:

$$\mathbf{F}(\mathbf{r_0}+\delta\mathbf{r}) = \mathbf{F}(\mathbf{r_0}) + \delta\mathbf{r}\cdot\boldsymbol{\nabla}\mathbf{F} \quad \text{with} \quad \mathrm{rot}_{2\mathrm{D}}\mathbf{F} = M_{\mathrm{eff}}(g_{21}-g_{12}) \neq 0.$$

In the case of a pure rotational force field, verifying $g_{12} = -g_{21} \equiv g_{\circlearrowleft}$ the eigenfrequencies become:

$$\Omega_{\pm}^2 = \frac{\Omega_1^2+\Omega_2^2}{2} \pm \frac{1}{2}\sqrt{(\Omega_2^2-\Omega_1^2)^2 - 4g_{\circlearrowleft}^2}. \tag{3.1}$$

The force field gradients $g_{\circlearrowleft}$ linearly increase with the optical power, so that at a certain point the argument of the square root can become negative, which arises more easily with quasi frequency-degenerated nanowires. In such a situation, the nanowire eigenfrequencies merge towards each other, the eigenmodes then also acquire an imaginary part, meaning that they are not linear anymore but become partly elliptic. The later means that depending in which direction they rotate, the geometrical damping they acquire will add up or get subtracted from their intrinsic damping rate, and at a certain point, the damping of the anti-damped eigenmode will become negative, meaning that the system becomes dynamically unstable. This peculiar instability then only arises from the rotational topology of the optical force field, and is precisely responsible of our preliminary observations. In the following we will restrict our analysis to the stable situation, at low optical powers, prior to the bifurcation.

### 3.1.2 Eigenmode orthogonality breaking

If we now inspect the expression of the eigenvectors, we can observe that their cross product verifies:

$$\mathbf{e_y}\cdot(\mathbf{e}_-\wedge\mathbf{e}_+) \propto g_{12}-g_{21} \propto \mathrm{rot}_{2\mathrm{D}}\mathbf{F} \tag{3.2}$$

meaning that their orthogonality is broken in presence of a rotational force field. We verified this puzzling observation by measuring the eigenmode orientations as a function of the optical power [12], by realizing spectro-angular analysis of the nanowire thermal noise, and by measuring driven trajectories in 2D to identify the eigenmode orientations. Those observations are summarized in Fig. 3.2. This specificity arises from the cross-coupling of 2 eigenmodes, with a non-reciprocal coupling term. This situation does not exist in conservative systems, where the coupling force field derives from a potential energy for which $\mathbf{F} = -\boldsymbol{\nabla}U$ so that $\partial_1 F_2 = \partial_{12}^2 U = \partial_{21}^2 U = \partial_2 F_1$.

### 3.1.3 Perturbed mechanical response

From the above 2D analysis of the response measurements (Fig. 3.2a), one can also observe a peculiar phenomenon: while all the responses were taken with the same amplitude of the modulated driving force, the amplitude of the driven displacements largely increases at large mean optical power, even when the drive vector is not aligned with the eigenmodes. This perturbation of the mechanical response is also visible on the thermal noise spectra: the noise power measured at resonance, $S_{\delta r_{\ominus,\oplus}}[\Omega_{\pm}]$ significantly increases, by a factor of 30 when approaching the bifurcation. Furthermore, the thermal noise resonant peaks, get deformed and become asymmetric, as if the two modes were driven by a common force noise which can generate cancelations between the individual response of each mode. Both observations are rather counter-intuitive: the mechanical damping rates are not modified below the bifurcation, so that one does not expect a significant increase of the resonant mechanical response. A more complete picture of the response patterns is shown in Fig. 2.3e, where the response were simulated for different orientations of the optical force drive, in 2 situations: in absence or in presence of a non-conservative force field. Having observed that the rotational optical force field is responsible for a modification of the mechanical response of the nanowire as well as an excess of noise, it was important to

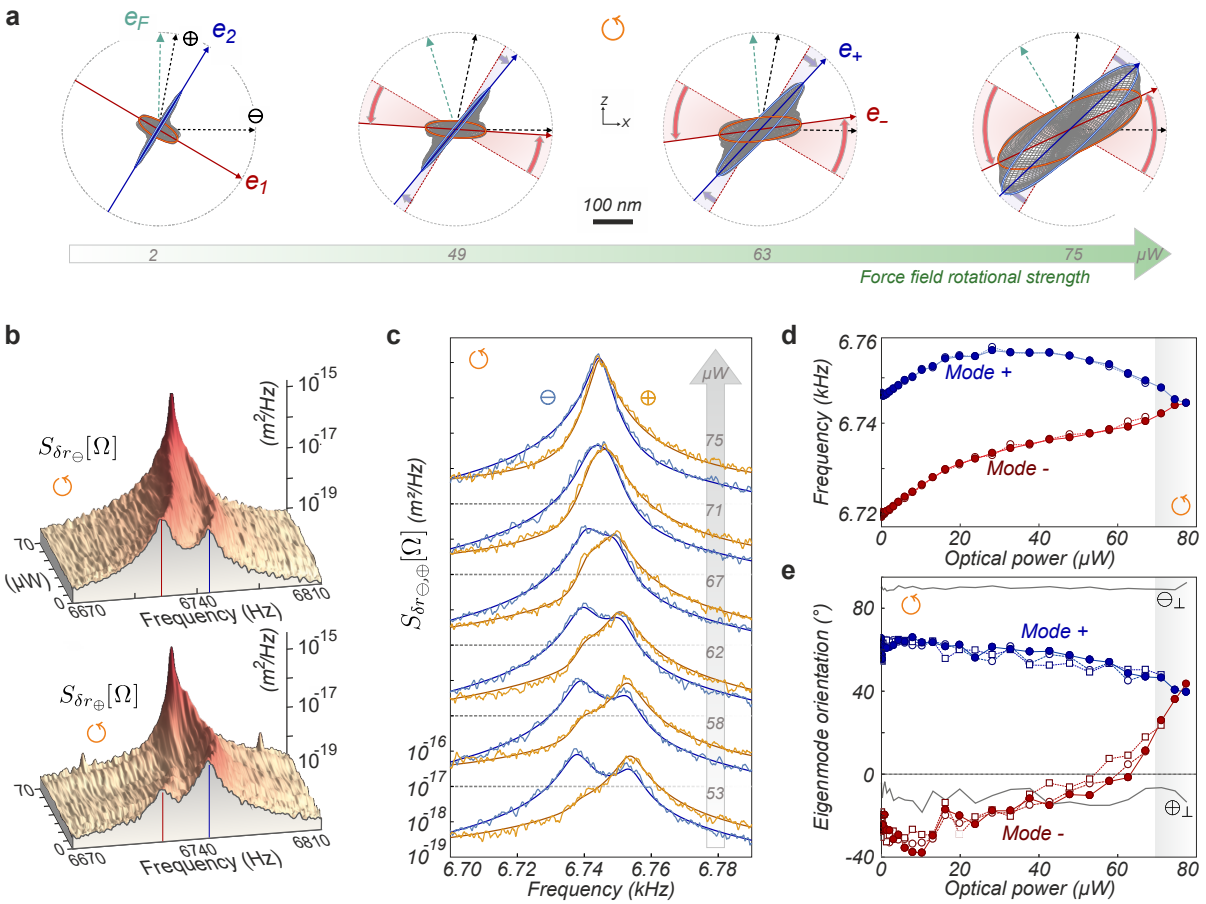


Figure 3.2: **Eigenmode orthogonality breaking.** **a** 2D representations of the elliptical driven trajectories measured while sweeping the drive frequency across both eigenfrequencies, for increasing optical powers generating an increasing force field rotational. Each grey ellipse corresponds to a different driving frequency, while the resonantly driven cases are highlighted in red/blue. The measurement vectors are shown as black dashed lines, as well as the undressed and dressed eigenvectors and the drive orientation. **b** Set of thermal noise spectra $S_{\delta r_{\ominus,\oplus}}[\Omega]$ measured on both measurement channels for increasing optical powers, also shown in **c**. The full lines are fits to the model, which allow to determine the evolution of the optical force field gradients $g_{ij}$ with the optical power. Under the action of the rotational force field, the eigenvectors converge towards each other, while the frequencies merge. At larger optical powers, the system enters into the rotational instability.

investigate if the fluctuation-dissipation relation remains valid in presence of a non-conservative force field.

### 3.1.4 Violation of the fluctuation dissipation relation

The projected thermal noise fluctuations of the nanowire are given by the expression:

$$\delta r_\beta[\Omega] = \mathbf{e}_\beta \cdot \boldsymbol{\chi}[\Omega] \cdot \delta \mathbf{F}_{\mathrm{th}}. \tag{3.3}$$

When the nanowire presents an isotropic damping rate, the Langevin force noise is made of a set of 2 independent perpendicular random force vectors whose orientation can be chosen in any perpendicular basis of the (xz) space, such as the basis attached to the measurement orientation

$\mathbf{e}_\beta$ and the perpendicular orientation $\mathbf{e}_\beta^\perp$. If one introduces the 2D susceptibility tensor:

$$\chi_{\mu\nu} \equiv \mathbf{e}_\mu \cdot \boldsymbol{\chi} \cdot \mathbf{e}_\nu \tag{3.4}$$

which can be measured by driving the nanowire along the direction $\mathbf{e}_\nu$ while measuring the projected displacement along a direction $\mathbf{e}_\mu$. We can recast the projected thermal noise fluctuations as:

$$\delta r_\beta[\Omega] = \chi_{\beta\beta}\delta F_\beta + \chi_{\beta\beta^\perp}\delta F_\beta^\perp \tag{3.5}$$

where we have introduced the axial ($\chi_{\beta\beta}$) and transverse ($\chi_{\beta\beta^\perp}$) mechanical susceptibilities. The fluctuation dissipation relation would tell us that the thermal noise measured along a given orientation is connected to the axial susceptibility according to:

$$S_{\delta r_\beta}^{\mathrm{FDR}}[\Omega] = \frac{2k_BT}{\Omega}\mathrm{Im}\chi_{\beta\beta}. \tag{3.6}$$

On the contrary, our formalism based on the 2D dressing of the nanowire by the force field gradients proposes the following expression for the thermal noise:

$$S_{\delta r_\beta}[\Omega] = \left(|\chi_{\beta\beta}|^2 + \left|\chi_{\beta\beta^\perp}\right|^2\right) S_F^{\mathrm{th}}. \tag{3.7}$$

To verify if the FDR expression was valid, we realized pump-probe measurements to measure the mechanical response of the nanowire in 2D, and measured the thermal noise of the nanowire at different locations and powers within the waist area. The response measurements allow to reconstruct the coefficients of the 2D mechanical response, which can be subsequently employed in expressions 3.6 and 3.7 and compared to the spectra measured experimentally, along both measurement channels.
A first measurement sequence was realized on the optical axis, where the force field rotational is zero. There we found a quasi-perfect agreement of the measured thermal noise spectra with

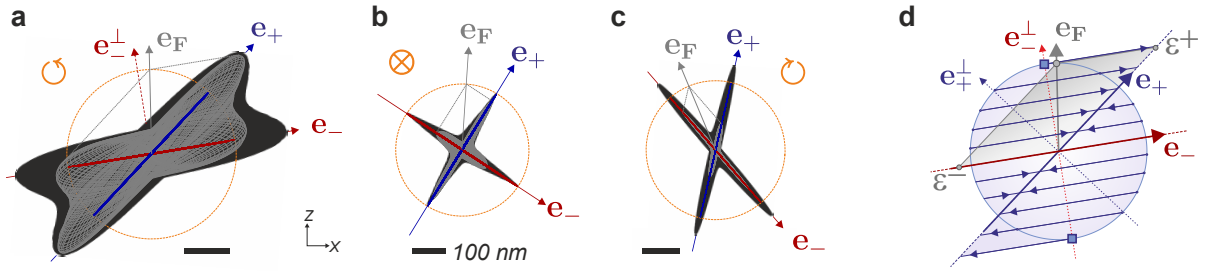


Figure 3.3: **Warped mechanical susceptibility.** Stationary trajectories (gray) shown in the horizontal xz plane followed by the nanowire under monochromatic excitation along the direction $\mathbf{e_F}$, for different driving frequencies, swept across both fundamental resonances when inserted in a force field of positive (**a**), null (**b**) and negative (**c**) rotational. The resonantly driven trajectories are highlighted in red / blue. The black area represents all the different trajectories that can be generated while rotating the drive orientation ($\mathbf{e_F}$). All responses are taken with the same drive amplitude. The resonantly driven amplitude can be schematically obtained by projecting the drive vector in the warped eigenmode basis (**d**). As expected, the resonant mechanical susceptibility remains uniaxial when the drive vector is aligned with the eigenmode. However in presence of a rotational force field, it is possible to generate a resonant oscillation amplitude in the direction of one mode larger than in the non-rotational case, when the drive vector becomes perpendicular to the other eigenmode. This statement is also valid in the non-rotational case.

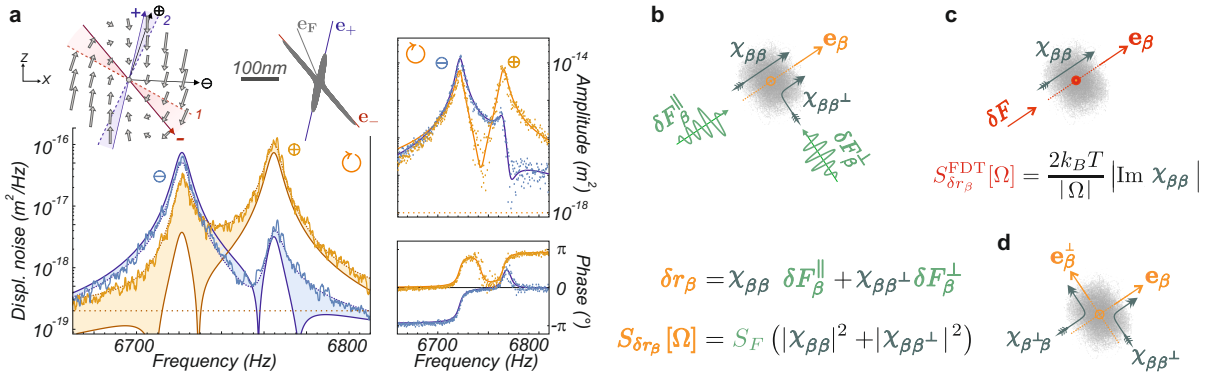


Figure 3.4: **Violation of the fluctuation dissipation relation.** Thermal noise spectra $S_{\delta r_{\ominus,\oplus}}[\Omega]$, resonantly driven trajectories (amplitude and phase) measured on the side of the optical waist, in a region of negative rotational, as indicated in the sketched measured force field landscape. In the noise plot, the dotted lines are fits using the model, which present a quasi perfect agreement with the data, while the full lines are the thermal noise spectra expected from the fluctuation dissipation relation $S^{\mathrm{FDR}}_{\delta r_{\ominus,\oplus}}$ and the deviation is colorized. b,c Scheme of the uniaxial and transverse mechanical susceptibilities involved in the model and in the FDR relation. **d** Scheme of two reciprocal mechanical susceptibilities involved in expression 3.8.

both expressions, meaning that the FDR relation was verified by our system, and furthermore that the 2D dressing model was in agreement with the measurements and the FDR.
However measurements realized on each side of the optical axis, in areas of positive or negative rotational strength of the optical force field, for different optical powers, showed that the FDR expression was largely invalidated, presenting deviations larger than 10dB, while the 2D dressing model remained pertinent to describe the thermal noise of the nanowire in a regime where the eigenmodes were largely warped by the rotational force field.

By composing a bit more with the theoretical description given above, we found a patch to the fluctuation dissipation relation in the following 2D form:

$$\sum_{\mu=\beta,\beta^\perp}\left(S_{\delta r_\mu}[\Omega]-\frac{2k_BT}{\Omega}\mathrm{Im}\chi_{\mu\mu}\right)=\left(\chi_{\beta\beta^\perp}-\chi_{\beta^\perp\beta}\right)^2 S_F. \tag{3.8}$$

This expression simply states that the sum of the deviations from the FDR measured along 2 transverse orientations, is simply given by the difference of the 2 transverse susceptibilities constructed along those perpendicular orientations. The last term is simply proportional to $(\mathrm{rot}\mathbf{F})^2$, which is positive for any frequency.

The nanowire dynamics can then strongly deviate from the fluctuation dissipation relation when dressed by a non-conservative force field, meaning that one of the founding hypothesis is violated. This is not the system linearity criteria, since we have already mentioned that the nanowire responses remain linear up to very large oscillation amplitudes (hundreds of nanometers), but instead the equilibrium criteria. The nanowire extremity undergoes a randomly driven trajectory in a rotational force field, where the work accumulated during a trajectory connecting one point to itself, is non-zero anymore, depends on the loop trajectory and changes sign for example between clockwise or counter-clockwise trajectories. However, when averaged over many random trajectories, this would not bring a mean additional work if the trajectories themselves were not modified. Indeed the rotational force field favors random trajectories turning in the direction of its curl, which creates a non-zero average work, bringing the nanowire out of equilibrium. We will come back on this aspect in the next section where we will record and

analyze the nanowire trajectories. This discussion also leads to the fact that it is not possible to define a proper noise temperature for the nanowire in presence of a non-conservative force field.

In practice, it is often difficult to verify or assess if a system is at the thermal equilibrium condition, especially when the SNR is small which occurs for example at low temperatures. However the expression 3.8 suggests a very simple and practical experimental implementation: it is sufficient to measure if there exists a difference between a set of 2 mirrored transverse mechanical susceptibilities, a response measurement that can still be realized for small SNR since the response measurements can be repeated and averaged for a long duration.

### 3.1.5 Thermal noise squeezing and apparition of a circulation in the nanowire trajectories

The above analyses were realized on noise spectral densities and driven responses of the nanowire, but it is also interesting to investigate the real-time trajectories $\delta\mathbf{r}(t)$ followed by the nanowire extremity in presence of a rotational force field. To do so, we recorded the projected trajectories $\delta r_{\ominus,\oplus}(t)$ measured along the measurement vectors $\mathbf{e}_{\ominus,\oplus}$ forming an angle $\beta_{\ominus,\oplus}$ with $\mathbf{e_x}$, out of which we can reconstruct the trajectories in the (xz) plane using:

$$\begin{pmatrix} \delta r_x(t) \\ \delta r_z(t) \end{pmatrix} = \begin{pmatrix} \cos\beta_\ominus & \sin\beta_\ominus \\ \cos\beta_\oplus & \sin\beta_\oplus \end{pmatrix}^{-1} \cdot \begin{pmatrix} \delta r_\ominus(t) \\ \delta r_\oplus(t) \end{pmatrix}, \tag{3.9}$$

and compute any projected trajectory along an orientation $e_\mu$:

$$\delta r_\mu \equiv \cos\theta_\mu \delta r_x + \sin\theta_\mu \delta r_z. \tag{3.10}$$

In particular one can measure the variances of the projected displacements:

$$\Delta r_\mu^2 \equiv \int dt\, \delta r_\mu^2 = \int d\Omega\, S_{\delta r_\mu}[\Omega] \tag{3.11}$$

or the variances of the projected speed components $\delta v_\mu = \delta\dot{r}_\mu$:

$$\Delta v_\mu^2 \equiv \int dt\, \delta v_\mu^2 = \int d\Omega\, \Omega^2 S_{\delta r_\mu}[\Omega]. \tag{3.12}$$

The spatial distribution of the position of the nanowire extremity is shown in Fig. 3.5 in absence (middle) and in presence (left/right: positive/negative circulation) of a rotational force field (here a pure shear force field produced with the synthetic 2D feedback). One can observe a large noise enhancement in the direction towards which converge the dressed eigenvectors at large rotational, and a noise reduction in the orthogonal orientation. The reduction can amount to -3 dB with respect to the initial variance. This noise reduction, which is commonly observed in quantum optics using non-linear resources ($\chi^2, \chi^3$ optical non-linearities employed in optical squeezers), arises here in a linear but 2D system featuring a non-reciprocal interaction between its internal degrees of freedom.

Equivalently puzzling is the fact that the same noise compression is observed in the speed space $(v_x, v_z)$. So that in the direction of noise compression, perpendicular to the dashed lines in Fig. 3.5, one can reduce simultaneously the noise variances in the position and speed spaces. One can wonder whether such noise reduction could also be observed if the nanowire was found in the quantum ground state of its 2 transverse eigenmodes. Since the only ingredient is a noiseless non-reciprocal interaction, the response is in principle positive, meaning that one could in principle reduce the variance product below the initial Heisenberg limited value. Those important

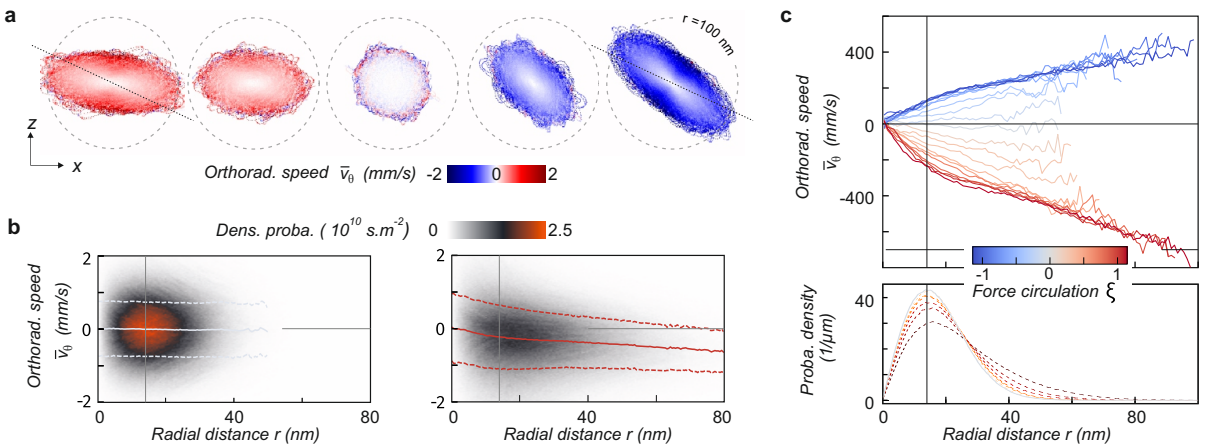


Figure 3.5: **Thermal noise compression and apparition of an orthoradial circulation in a rotational force field. a** Thermal noise trajectories recorded in the xz plane in absence (center) and in presence of a shear force field ($g_{21} \neq 0$) with increasing positive (left) or negative (right) circulation. The color scale gives the spatial distribution of the mean local orthoradial speed, averaged over the sampled dataset. **b** Computed densities of probability in the $(r, v_\theta)$ space, in absence (left) and in presence (right) of the shear force field. A bias appears in the distribution, and the mean orthoradial speed measured at a given distance from the center is indicated as a full line, while the width of the distribution is indicated by dashed lines. **c** Evolution of the mean orthoradial speed (above) and density of probability (bottom) with the distance to the rest position, for varying force field circulations. The grey lines indicate the position and speed variances ($\Delta r_{\text{th}}$, $\Delta v_{\text{th}}$) measured in absence of external force field. From [13, 73]

.

questions lead us investigate what are the conjugate variables of the position in presence of a rotational force field. Since it does not derive from a potential energy, the question was delicate to answer. However we found a seminal work by M.Berry and Sukhla [14], where they precisely investigated particle trajectories in what they called circulating force fields, and propose an effective Hamiltonian which could describe the nanowire dynamics: it requires a non-isotropic kinetic mass Hamiltonian, of the form $H = \frac{p_x^2}{2M_x} + \frac{p_z^2}{2M_z} + \frac{1}{2}k_x x^2 + \frac{1}{2}k_z z^2$. By carefully tuning the parameters of a similar quadratic form, we could describe the nanowire dynamics at first order, and verify that the conjugate variable to the position in the squeezed direction was a linear combination of the speed components in the squeezed and in the anti-squeezed directions. Since the anti-squeezing amplitude is significantly larger than the squeezing amplitude, the variance product never gets reduced below their initial value.

Last, we investigated the speed distribution in the thermal noise cloud: our interpretation of the out-of equilibrium state suggested that the nanowire trajectories get biased, and start to turn in the direction of the rotational. We could verify this by plotting a map of the mean ortho-radial speed, locally averaged over many trajectories, see Fig.3.5. One could see that in absence of rotational, the mean ortho-radial speed is almost zero in each point of the distribution, so that there are as many trajectories turning clockwise and anticlockwise. The situation is different when the rotational force field is activated: one can notice a bias in the mean ortho-radial speed, which becomes larger and larger as the nanowire gets away from its rest position. The evolution of the mean ortho-radial speed as a function of the distance to the nanowire "galactic" center is shown in Fig. 3.5c. This is not a surprise that one measures a non-zero mean ortho-radial speed, since the nanowire is subjected to an ortho-radial acceleration, but the analogy to the missing mass curves found on the ortho-radial speed of stars within galaxies will certainly deserve further

investigations.

## 3.2 Cavity nano-optomechanics, towards the single photon regime

The above-described experiments gave us an introduction to the rich optomechanical interest of the nanowires when coupled to a freely propagating light field. The light-nanowire interaction was early found to be rather strong: a 150-nm-diameter nanowire is capable of almost entirely suppressing the transmission of a 500 nm focussed red laser beam, despite its sub-wavelength sized dimensions. Furthermore, the optical force was measured at the few fN/$\mu$W level, which was very close to the $2P/c$ force exerted by a fully reflected light beam of power $P$ on an infinite mirror (6 fN/$\mu$W). Also, the mapping of the optical force experienced by the nanowire allows to investigate confined optical field with a measurement tool complementary to more traditional scanning probe measurements based on the measurement of optical signals. We were also interested in investigating the non-conservative character of the light-nanowire interaction when implemented in a cavity nano-optomechanical experiment built around our nanowires. To do so we engaged a collaboration with the group of J. Reichel, the PhD group of B. Besga, which helped a lot in establishing the collaboration. This was (one of) the central topic of the PhD thesis of Francesco Fogliano and we made use of the high finesse fiber micro-cavities, developed for atomic QED experiments, in order to enhance the light-nanowire interaction by simply inserting the nanowire in the middle of the cavity mode.

In the following we will rapidly introduce the experiment, the steps realized so as to map the strength of the 2D optomechanical coupling vector and the optomechanical force exerted by the intracavity field on the nanowire. The extreme interaction strength obtained allowed us to measure optical forces down to the single intracavity photon level, and we verified that the optomechanical force field was the dominant external force field exerted on the nanowire, even at sub-unity mean intracavity photon number. We will also introduce the theoretical model developed by Antoine Reigue to correctly account for the nanowire interaction to the different cavity modes

### 3.2.1 The experiment

The experiment is sketched in Fig. 3.6. A long aspect ratio nanowire is inserted between 2 optical fibers whose center have been laser-etched to form a concave depression where is subsequently deposited a highly reflecting optical coating featuring a maximum reflection at 820 nm where the micro-cavity finesse reaches approx. 50 000. The finesse can be adjusted by pumping the cavity at shorter wavelengthes, and most of the following measurements were realized around 780 nm where it approaches 1000. To align the cavity, one of the fiber is mounted on a gimbal mount, which allows to adjust their respective angle, while the other is mounted on a motorized XYZ stage, which allows to finely tune their lateral position. The cavity length can be adjusted with two annular piezo elements supporting each fiber: a thick one serves to tune it over approx. 1.5 $\mu$m while it can be dithered by a faster piezo for active locking purpose. The nanowire is first rotated along its axis to bring it in the plane perpendicular to the optical axis, so that it can be safely inserted in the volume between the fibers, even for small cavity lengths ($\leq 10\,\mu$m). It is mounted on a XYZ piezo stage used for fine positioning supported by a motorized XYZ stage used for the coarse pre-positioning.
The cavity is first pre-aligned at room pressure in particular to optimize the fiber angles, while the final alignments are realized at low pressure. The cavity length is reduced down to a small separation with the nanowire already positioned between the fibers, on the side of the optical axis. The cavity geometry is then finely adjusted to the desired configuration, using the trans-

mission and reflected signals to maximize the injection into the mode(s) of interest, in general a $\mathrm{TEM}_{00}$ mode, whose spatial profile can be tested by scanning the nanowire extremity in the cavity mode volume.
The experiment is extremely sensitive to environmental noises and drifts. A 1° C temperature change typically leads to a relative displacement in the nanowire-fibers apparatus of a micrometer. We installed a suspension apparatus around the vacuum chamber, surrounded by an acoustic and thermal shield made of different wood and foam layers, to reduce the long term temperature drifts. The long lasting measurements were automatized and remotely operated, to minimize the acoustic noise in the room.
We used tunable pump lasers, either a Ti:sapphire laser or a diode laser, but the parametric shifts of the cavity resonance were so large (hundreds of GHz) so that we chose instead to lock the cavity length on the laser wavelength, using the fast and slow piezo elements supporting the fibers. The cavity length was also dithered at 400 kHz to produce the error signal for the cavity lock. The locking was ensured by the Pyrpl module [74], running on a Red Pitaya FPGA card, which allowed to maintain the cavity at resonance for hours and even days, even while scanning the nanowire position within the cavity mode.
A red laser was used to probe the mechanical vibrations of the nanowire independently from the cavity pump lasers. It was co-injected in the cavity fibers, using a wavelength divider module, and since the coatings of the cavity mirrors are inefficient at 633 nm, we could build an interferometric readout of the nanowire motion by monitoring the red reflection on a separate detector. Two side-objectives were installed, one to monitor the relative positions of the nanowire and fibers, and a second to collect the light scattered out of the cavity mode by the nanowire. This gave us a way to monitor the position dependent losses induced by the nanowire, and a convenient lateral readout channel of the nanowire vibrations. Its very low background and the sharp slopes observed lead to large signal to background ratios in the measurements.

### 3.2.2 Mapping the optomechanical coupling strength

The parametric optomechanical coupling strength was determined by measuring the dependence of the cavity resonance frequency $\omega_0(\mathbf{r})/2\pi$ on the nanowire position $\mathbf{r}$ within the optical mode volume. Such measurements are shown in Fig. 3.6def, where the cavity transmission is measured as a function of the cavity length, for different positions of the nanowire. When scanning the nanowire transversally, the cavity resonant shift reproduces the lateral Gaussian profile of the cavity mode with a waist of $1.8\,\mu$m, causing a maximum cavity resonant length shift of $\Delta L = -12\,$nm, which corresponds to an equivalent frequency shift of $\Delta\omega_0 = -\omega_0\,\Delta L/L = 2\pi \times 400\,$GHz. When scanning the nanowire along the cavity axis, the nanowire allows to reveal the standing wave structure of the cavity field, and its $\lambda/2$ periodicity. These measurements allow us to spatially map the vectorial parametric coupling strength $\mathbf{G} \equiv \boldsymbol{\nabla}\omega_0|_{\mathbf{r_0}}$, which has to be evaluated at the nanowire rest position $\mathbf{r_0}$. The maximum slopes observed are $G_x/2\pi \approx 0.3\,$GHz/nm and $G_z/2\pi \approx 3\,$GHz/nm, which translates into single photon vectorial coupling strength of $g_0^z/2\pi = 1.2\,$MHz when considering the isotropic zero point fluctuations of the nanowire of $\delta r_{\mathrm{zpf}} = \sqrt{\hbar/2M_{\mathrm{eff}}\Omega_{\mathrm{m}}} \approx 0.4\,$pm. Those measurements also allow to estimate the additional cavity losses induced by the nanowire when inserted in the cavity mode, and investigate their spatial dependence, at the origin of a dissipative coupling mechanisms.
One can also analyze the optomechanical system by locking the cavity at resonance while scanning the nanowire in the cavity mode and monitoring the different optical signals, such as the cavity transmission and reflection or the correction of the cavity lock (out of which we measure the parametric cavity shifts) but also the side-scattered light flux which is collected through the lateral microscope objective. The different scanning probe images obtained are shown in Fig. 3.6g where one can clearly identify the standing wave structure of the intracavity mode in the transmission map. The scatter channel presents a peculiar pattern, with a ring structure

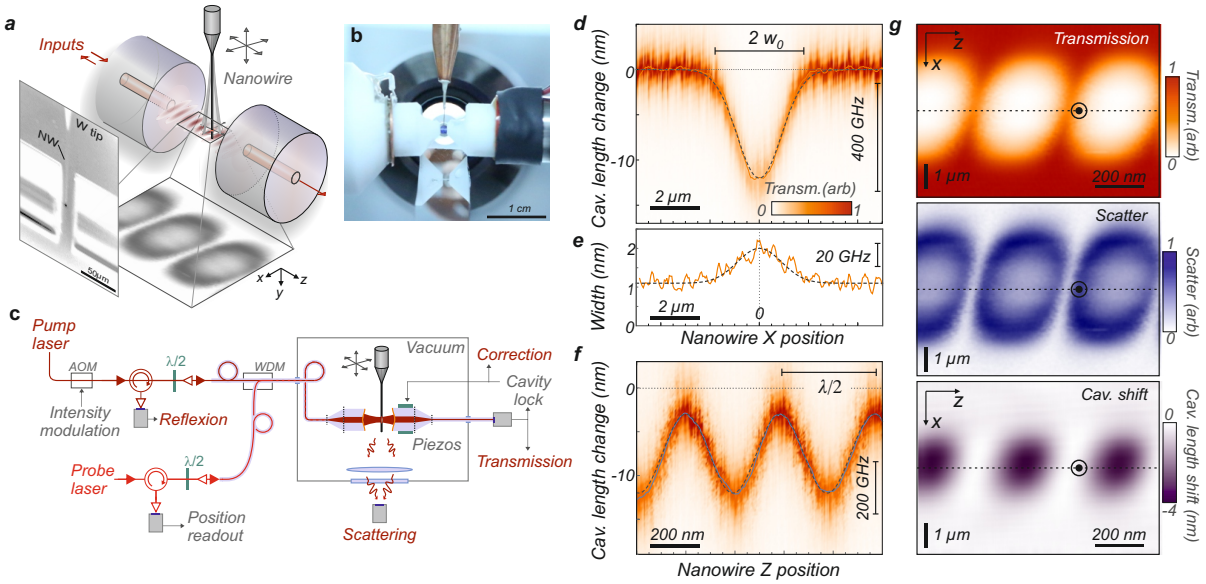


Figure 3.6: **Nanowire in the middle cavity nano-optomechanics.** **a** Sketch of the experiment (inset: CCD image taken from the side objective showing the cavity light scattered by the nanowire). **b** Optical image of the core part of the experiment, the fibers and nanowire support are visible, as well as the lateral collection objective. **c** Sketch of the experiment: an IR pump laser is used to pump the cavity mode, while a red laser serves to independently probe the nanowire vibrations. **d** Transmission signals recorded while scanning the cavity length around a $TEM_{00}$ mode resonance, while scanning the nanowire across the optical mode, which generates a large parametric shift. **e** Evolution of the optical mode linewidth as a function of the nanowire position. **f** Similar measurements obtained while scanning the nanowire along the optical axis, revealing the periodic structure of the cavity mode (nodes and antinodes). **g** Dependence of the cavity transmission, of the side-scattered light flux and of the lock correction measured when locking the cavity length at resonance using the piezo elements supporting the fiber supports, while scanning the nanowire extremity across the cavity mode, in the horizontal xz plane.

surrounding the anti-nodes of the intracavity field. When progressively entering the intracavity mode, the nanowire is first responsible of an increased scattering, but at some point the nanowire becomes responsible for a finesse degradation which reduces the intracavity flux and thus the side-scattered intensity. Outside of the rings the initial cavity finesse has been degraded by less than a factor of 2, so that the cavity properties are somehow preserved.

### 3.2.3 Mapping the optomechanical force within the cavity mode

The above measurements allowed to quantify the optomechanical coupling in one direction: how the nanowire position affects the cavity field. However this study could not be complete without investigating the reverse mechanism which consists in measuring the optomechanical force exerted by the intracavity field on the nanowire. To do so, we realized response measurements to measure the optomechanical force exerted by the intracavity field on the nanowire. The cavity length was locked on resonance, and the injected intensity was modulated with an acousto-optic modulator to dynamically change the intracavity photon number, and thus the optomechanical force experienced by the nanowire. Sweeping the modulation frequency across both fundamental mechanical modes allowed to determine the complex force vector. Those measurements were realized with a largely frequency split nanowire (50-60 kHz), so that its eigenmodes are protected

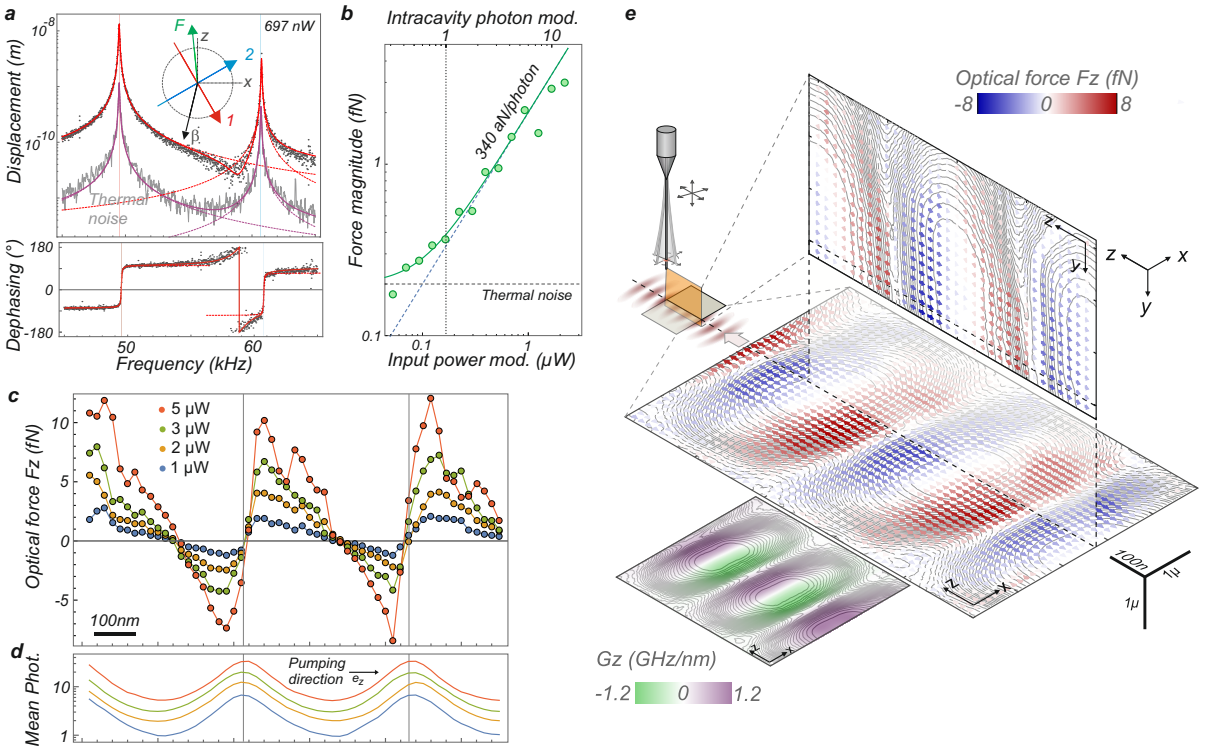


Figure 3.7: **Optomechanical force field sensing within the cavity mode. a** Thermal noise and mechanical response obtained at resonance while modulating the intracavity power, which allows to determine the orientation and magnitude of the optomechanical force experienced by the nanowire. **b** Dependence of the force amplitude for increasing modulation depth, down to a modulation of the intracavity photon number smaller than unity. Evolution of the force magnitude (**c**) and of the cavity transmission (**d**) as a function of the nanowire position along the optical axis, for increasing injected powers. **e** Map the the z-component of the optomechanical force in the horizontal and vertical planes. The lower left inset represents the parametric coupling strength derived from the spatial variations of the correction signal of the cavity lock.

against the action of shear components of the force field, and one can safely assume that they preserve their orthogonality and their orientations at any position within the cavity field.
The optomechanical response was first characterized by positioning the nanowire on the optical axis, on the side of a node of the intracavity field, for an increasing modulation strengths, as shown in Fig. 3.7a. The instantaneous optical force behaves linearly, with a sensitivity of approx. 340 aN per intracavity photon number, over a dynamically modulated photon number change spanning from 10 down to 0.3, while the nanowire thermal noise provides a limiting sensitivity of 0.07 photon/$\mathrm{Hz}^{1/2}$, so that the nanowire is capable of detecting changes in the intracavity photon mean occupation significantly smaller than unity.
Similar measurements were realized at different positions along the optical axis, see Fig. 3.7c, for different mean injected powers. The $\lambda/2$ periodicity is clearly visible, and the optomechanical force is found to repel the nanowire from the nodes of the electromagnetic field, which can be localized as regions of large cavity transmission. The advanced force sensing protocols were then employed to realized wider maps, such as the one shown in Fig.3.7e. The orders of magnitude obtained were in good agreement with the numerical simulations realized by A. Reigue[20], which combined the Mie scattering regime to a input-output matrix formalism to describe in optomechanical interaction between the confined light field and an infinite cylinder.

### 3.2.4 A giant coupling interaction strength - perspectives

These dual measurements allowed us to characterize the optomechanical interaction in the "nanowire in the middle" experiment. Combining an ultrasensitive force sensor with a small mode volume microcavity, and operating at positions of maximum interaction strength allowed to reach the regime where a single photon stored in the cavity mode is capable of displacing the nanowire by more than its zero-point quantum fluctuations ($\delta x^{\rm zpf} \equiv \sqrt{\hbar/2M_{\rm eff}\Omega_{\rm m}}$). Using the canonical parametric interaction Hamiltonian $\hat{H} = -\hbar g_0 \hat{a}^\dagger \hat{a}(\hat{b} + \hat{b}^\dagger)$, which couples the light and mechanical degrees of freedom (associated to the operators $\hat{a}$, $\hat{b}$ respectively) with a single photon coupling strength $g_0$, the static force exerted by a single photon can be written as $F^{(1)} = -\nabla H = \hbar g_0/\delta x^{\rm zpf}$. This force generates a static deflection of the nanowire of $\delta x^{(1)} = \chi[0]F^{(1)} = F^{(1)}/M_{\rm eff}\Omega_{\rm m}^2$, which can also be expressed as :

$$\delta x^{(1)}/\delta x^{\rm zpf} = 2g_0/\Omega_{\rm m}$$

The above ratio largely exceeds unity in the experiment (up to 100), meaning that this configuration gives access to exceptional coupling strength, sufficient to enter the single photon regime of cavity optomechanics. As a confirmation, in our room temperature experiment, we could measure mechanically variations of the intracavity mean photon number smaller than unity, using pump-probe techniques. Future developments in the single photon regime will require reducing the thermal noise of the nanowire so that the spreading of the nanowire thermal noise $\delta x^{\rm th} \equiv \sqrt{k_B T/M_{\rm eff}\Omega_{\rm m}^2}$ becomes smaller than the static single photon recoil $\delta x^{(1)}$. In that regime, the nanowire dynamics (both the static and resonant response) becomes completely bound to the optical field dynamics, down to the single photon level, but this requires operating at cryogenic temperatures.
Moreover, these novel optomechanical regime will allow to investigate second order optomechanical effects, such as reaching the regime of single photon static bistability: the above described single photon recoil, $\delta x^{(1)}$, is in turn responsible for a parametric shift of the cavity resonance given by $\delta\omega_0^{(1)} = -g_0\,\delta x^{(1)}/\delta x^{\rm zpf} = -2g_0^2/\Omega_{\rm m}$. It will lead to a static bistability of the cavity, at the single intracavity photon level if it exceeds the cavity linewidth, $\kappa$, requiring that the so-called *static single photon parametric cooperativity* exceeds unity:

$$C^{(1)} \equiv \frac{2g_0^2}{\Omega_{\rm m}\kappa} > 1$$

As exposed in [20], the nanowire in the middle configuration is capable of approaching such a large interaction strength. Finally, the quantum fluctuations of the radiation pressure force noise in the single photon regime can become observable if they exceed the Langevin force fluctuations. The ratio of their respective force noise spectral densities can be expressed as $2C^{(1)}Q/n_{\rm th}$, which could approach $\approx 30$ at dilution temperatures. Up to now, the optomechanical squeezing has for the moment only been observed in the resolved sideband regime, at large photon numbers and was restricted to a frequency band in the vicinity of the mechanical resonances to benefit from their large mechanical susceptibility. The encouraging numbers given above suggest that it could be possible to generate some broadband squeezing in our optomechanical system (spanning from DC to $\Omega_{\rm m}$) at the condition to operate at sub-1 K temperatures, which is in principle well within reach, see below. Also, being able to produce some squeezing with such a low photon number would also allow to generate and investigate non-Gaussian states, as envisioned in [39].

Also, the theoretical simulations have also shown that it should be possible to observe "anomalous" positive cavity shifts in the system - when the cavity length must be increased to keep it at resonance while laterally inserting the nanowire in the cavity mode volume, and was subsequently observed experimentally [21] see Fig. 3.9c. This is a consequence of the Mie resonances contributions to the light scattering properties of the nanowire. This observation

means that the lateral parametric shift $\partial_x\omega_0$ can change of sign from one mode to another, meaning that the corresponding optomechanical force will also change its orientation and its magnitude. Since the nanowire has the sensitivity to detect only very few photons in the cavity mode, it can in principle be used to explore the Casimir force in such a confined geometry. The modelisation and the measurement of contributions of the different optical resonances to the total optical force in such a non-trivial geometry should be of particular interest to understand the Casimir force landscape.

### 3.2.5 Nano-optomechanics at dilution temperatures, measurements in the photon counting regime

As mentioned above, operating the nanowires at low temperatures allows increasing their force sensitivity, due to the concomitant reduction of their noise temperature and improvement of their mechanical coherence. This however requires preserving the capacity to readout their thermal vibrations without perturbing their quiet state. This last point becomes extremely difficult at low temperatures since the heat conductivity of the nanowire vanishes, so that a very small fraction of absorbed light can produce important temperature gradients within the nanowire. We thus developed a first experiment to verify if it was possible to operate the nanowires at dilution temperatures.
With the assistance of E. Eyraud and W. Wernsdorfer, we developed a home-made dilution fridge, of the sionludi type, where the coolest area is located on top of the cryostat, a configuration that is well suited for optomechanical experiments. The cryostat is described in greater details in [18, 17]. We developed cryogenic compatible interferometric fiber objectives to probe the nanowire vibrations down to dilution temperatures, see Fig.3.8. The incoming light is fiber-guided into the cryostat and focused on the nanowire vibrating extremity through 2 aspheric lenses which are also used to collect the back-scattered light. The latter interfere with the fraction of the incoming light which is reflected on the fiber output interface, leading to a very contrasted (close to 100 %) image in reflection. The interferometer presents an exceptional fringe stability (drifts around a nm per day) and the nanowire deformations are converted into reflected signal fluctuations. To minimize the optical heating, we had to lower the injected light below the picowatt level, which required operating with photon counters instead of standard continuous detectors. This measurement strategy requires a different calibration procedure: position fluctuations are not converted into continuous voltage fluctuations as in standard continuous measurement, but into a flux modulation, where the pulse density becomes time-modulated. This technique allowed to probe thermal noise spectra, but also response measurements down to extremely small optical fluxes, significantly smaller than the mechanical period, without suffering from the elevated dark noise of standard detectors. Typical calibrated noise spectra are shown in Fig. 3.8e, out of which one can determine the mechanical properties of the nanowire, and in particular its noise temperature. Reproducing those measurements while varying the optical power allows to evaluate the influence of optical absorption on the nanowire noise temperature, while changing the cryostat temperature allows to verify its proper thermalization. After having spent a lot of time trying to minimize the parasitic noise sources of mechanical and electrostatic origin - which required in particular developing a cold suspension apparatus to mitigate the parasitic vibration noise - we could observe a nanowire presenting a noise temperature around 32 mK when using 100 fW of optical probe light. This ultra-low optical probe power was necessary to reach sub-100 mK noise temperatures, which are reached for only a pW of probe light, see the heating curves of Fig. 3.8h. This traduces the extremely faint heat conductance of the nanowire at those dilution temperatures. Such optical heating curves allow to investigate the dependence of the nanowire heat conductance with temperature, a subject of interest in itself since the conductance is supposed to be rapidly dominated by ballistic conduction mechanisms, at temperatures lower than 1 K. The sub-linear dependence of the heating curves in the opti-

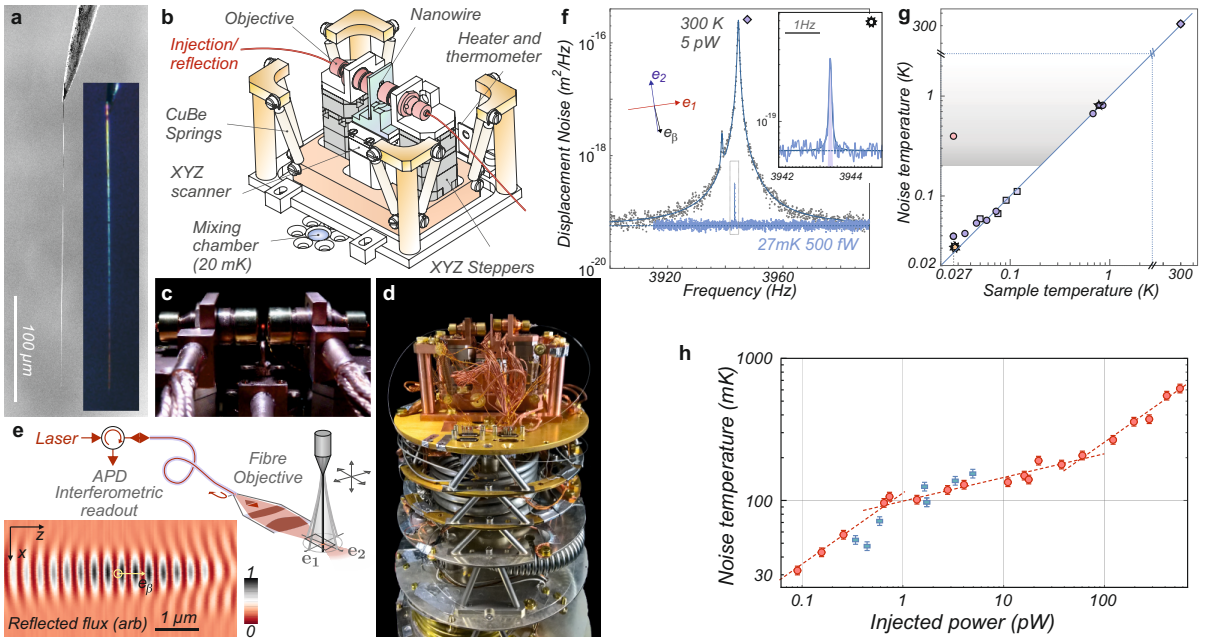


Figure 3.8: **Operating the nanowires in a dilution temperature environment. a** SEM and optical images of an ultrasensitive nanowire employed in the cryostat. **b** Sketch of the optical head. **c, d** Images of the cryostat and a close-up of the optical head, where the light scattered by the nanowire is visible. **e** Sketch of the interferometric fiber objectives and of the optical readout in reflection. The inset is a map of the reflected photon flux, obtained while scanning the nanowire in the waist area. The interference signal permits to image the wavefronts of the focus laser beam. **f** Thermal noise spectra obtained while positioning the nanowire on the side of the interference fringe, on the optical axis, at room and dilution temperatures out of which one can determine the noise temperature of the nanowire (300 K and 32 mK respectively), and investigate its dependence on the injected optical probe power (**h**) or on the cryostat temperature (**g**), where the greyed area represents the minimal noise temperatures obtained in absence of suspension.

cal probe power is a signature that the nanowire conductance increases with the temperature. Furthermore it presents different characteristic regimes, which will be a subject of further explorations in collaboration with the local experts of heat transport at the nanoscale (O. Bourgeois, E. Collin in particular).

After having verified the proper thermalization of the nanowire, we investigated its force sensing properties. The force sensitivity improved to approx. $40\,\mathrm{zN/Hz^{0.5}}$, a record value for scanning probes, for a rather modest quality factor, around $Q = 100\,000$, corresponding to a mechanical linewidth of tens of mHz for our kHz nanowires. We also investigated the frequency stability of the nanowires, especially under "large" excitation amplitudes (around 1 nm for a 1 aN amplitude force drive), and measured relative frequency r.m.s. deviations around $4 \times 10^{-8}$ over hours. The relative Allan variance deviation was measured at the level of $5 \times 10^{-11}$ for a gate time of $\tau = 2\pi/\Gamma_\mathrm{m} = 40\,\mathrm{s}$, which conveys an exceptional sensitivity to external force field gradients, at the level of 1 fN/m. Those rather astonishingly low values are comparable to the spatial gradients associated to the radiation pressure force of a 100 fW focused optical probe beam (0.6 zN varying over 300 nm laterally), and traduces the interest of the nanowire force probe for optomechanical purposes, at ultra-low photon fluxes.

Those measurements at dilution temperatures also lead us to investigate the temperature dependence of the nanowire mechanical properties. We could observe the characteristic signatures of amorphous defects both in the frequency and mechanical damping rates dependence, such as a logarithmic increase of the relative frequency shifts: $\Delta\Omega_{\rm m}/\Omega_{\rm m} = C\,\ln(T/100\,{\rm mK})$ with a constant $C = 1\times10^{-6}$ which is only 1% of the universal value obtained for amorphous oscillators [1]. This can be understood as a consequence of the presence of an amorphous crust covering the crystalline core of the nanowire, as can be viewed in TEM images. Removing the nanowire amorphous layer should thus lead to an improvement of their mechanical quality factors, but this happens to be a challenging task since it requires hydrogen etching at very high temperatures. The nanowire surface rugosity plays a significant role in the transition from the diffusive to the specular phonon reflection regimes, which could thus influence the overall nanowire heat conduction properties, and thus the measured optical heating curves.
Further measurements, realized during the PhD of Clément Gouriou, also lead us observe that the heating efficiency can be doubled when positioning the laser at less than 2 $\mu$m from its extremity, which hints towards an optical wave guiding mechanism. Also, response measurements conducted using a pump-probe scheme allowed to investigate the dynamical evolution of the heat waves within the nanowires at various temperatures ranging from 300 K down to 1 K. Pursuing those measurements at dilution temperatures should provide additional complementary tools to investigate the dynamical heat conduction properties of the nanowire in the ballistic regime.

### 3.2.6 Perspectives

The perspective of developing cavity nano-optomechanical experiments at dilution temperature is thus a central objective and holds the promise to operate deeply in the single photon regime of cavity optomechanics. We already introduced the static criteria ($\delta x^{(1)} \gg \delta x^{\rm th} \gg \delta x^{\rm zpf}$). Reaching those exotic regimes of cavity optomechanics remains a very challenging experiment however, but will be the central objective of the coming years. Since the operation of fiber microcavities at dilution temperature with a nanowire in the middle is risky, an alternative consists in exploiting photonic crystal microcavities, developed in the group of R. Braive at C2N, see Fig. 3.9d. Their proper thermalization will be facilitated, as well as their combined integration with a nanowire, which will be scanned above the photonic crystal cavity, thus limiting the risk of contact with the crystal. The smaller mode volume and the evanescent character of the cavity mode should in principle increase even more the parametric coupling strength while partly reducing the nanowire-induced light scattering.
Some of the perspectives of those experiments follow. The rotational character of the optomechanical force field expected from the numerical simulations opens interesting questions on the extrapolation of the observations done in the case of the focused laser beam to the cavity force field. In particular, it would be interesting to investigate the contributions from the quantum fluctuations of the radiation pressure force in such a non-conservative force field, and study the type of correlations it generates on the oscillator position fluctuations and on the outgoing light fields. Will the thermal noise squeezing observed in free space would be preserved and which kind of light fluctuations will emerge from the cavity: will the "traditional" optomechanical squeezing observed will be preserved and which type of correlations could be found between the different light fields emerging from the cavity. To respond to those questions, it is necessary to correctly account for the light scattering induced by the nanowire between different modes of the microcavity, which will involve the multimode quantum optics toolbox. This intrinsically multimode character of the system - the nanowire is free to move along 2 transverse directions and the nanowire couples the different modes of the cavity - makes a great difference with the canonical 1D optomechanical system of a cavity with a movable mirror. It has already been formalized in [20] but we first focused ourselves on the description of the mean fields so as to

evaluate the vectorial parametric coupling strength and the optomechanical force fields. This study already underlined some peculiar effects. It confirmed the rotational character of the intracavity optomechanical force field (even if the standing wave alone is a sum of two counter-propagating waves, so that one could think that it would annihilate the rotational components of the optical force), or the possibility to observe anomalous positive cavity shifts, see Fig. 3.9c. The objective will now reside in correctly describing the quantum fluctuations of the fields in this multimode system.

Another important perspective concerns the investigation of the spatial structure of the vacuum Casimir forces in such a geometry. We introduced the interest of using the nanowires as scanning probes of electromagnetic field vacuum fluctuations in confined geometries, will a peculiar structure arise in this configuration ? We already mentioned that the existence of positive cavity shifts makes that the mean field lateral (x) optical force changes its orientation and magnitude depending on the optical modes involved. This question also allows to connect the traditional optomechanical approach, when only one optical mode (or a few) is involved and optically pumped, to the Casimir description where the quantum fluctuations of all optical modes have to be taken into account. Traditionally these two domains are largely separated since one needs to inject a lot of light in the systems to generate a measurable optomechanical force. In our case, we have shown a sub-single photon force sensitivity, so that we could in principle investigate the transition from the single photon optomechanical regime to the Casimir regime. An interesting experimental indicator would be the comparison between the gradients of the optomechanical force field measured using pump-probe techniques, as explained above, and the spatial dependence of the nanowire frequency shifts (a measure of the total force gradients) within the cavity mode. One can expect that at large photon numbers, both measurements agree, but they should differ for smaller photon number, since the nanowire is sensitive to all force gradients, including the Casimir force field gradients.

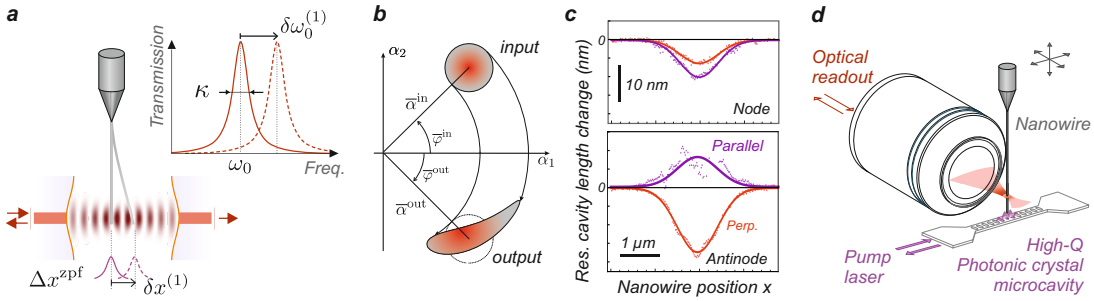


Figure 3.9: **Perspectives in cavity nano-optomechanics. a** Single photon static bistability: a single photon displaces the oscillator by a quantity $\delta x^{(1)}$, which in turn parametrically shifts the cavity resonance by $\delta\omega_0^{(1)}$. The cavity can become statically bistable (or multi-stable) if it exceeds the cavity linewidth. **b** Under such large interaction strengths, the optical noise exiting the cavity can be parametrically squeezed, over a large bandwidth, and can furthermore generate non-Guaussian states of light. **c** For larger nanowire diameters (160 nm here), whose optical response is governed by higher order internal Mie resonances, a positive cavity shift can be observed, here for the parallel polarization, when inserting the nanowire transversally through an antinode of the cavity field. **d** The alternative approach developed in collaboration with the group of R. Braive at C2N consists in inserting the nanowire in the evanescent tail of a photonic crystal cavity mode. We expect to reach even larger optomechanical interaction strengths, while facilitating the operation at cryogenic temperatures.

Another direction of future investigations concerns the possible interest in quantum optics of this optomechanical system featuring such a large parametric coupling strength, which is formally equivalent to a Kerr media inserted in an optical cavity. Since we largely operate in the adiabatic regime ($\Omega_{\mathrm{m}} \ll \kappa$), one could in principle use this resource to generate a broadband squeezed state, see [38], which would go beyond the optomechanical squeezing experiments which demonstrated squeezing performance in the resolved sideband regime, in a narrow frequency window around the mechanical resonance. Some estimations conducted with A. Reigue have shown that it could be possible to measure appreciable squeezing for intracavity photon numbers close to unity at the condition to operate at dilution temperatures. Further investigations would also be to investigate the possibility to generate non-Gaussian squeezed states [39]. One could also think of exploiting the large single photon parametric interaction to realize Quantum Non-Demolishing measurement of light intensities at ultra-low photon fluxes. More generally, the nanowire in the middle configuration should be viewed as an interesting resource for quantum optics, operating at low optical powers.

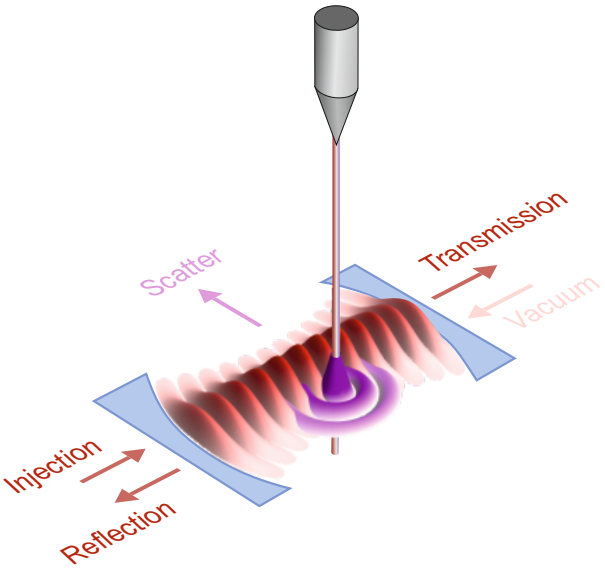
Scatter
Transmission
Vacuum
Injection
Reflection

# Chapter 4

# Hybrid qubit - nanomechanical systems

This chapter is dedicated to the description of the research activities conducted on the exploration of the interaction between a nanomechanical oscillator and a single-two-level system (TLS), thus defining an hybrid qubit-mechanical system [75, 76]. The long term motivations of the present activities are to investigate the possibility to generate of non-classical states of motion by exploiting spin-dependent forces, as originally employed in trapped ion physics [77, 78] through the quantum manipulation of their internal optical and mechanical states.
We have investigated two systems. First the single spin qubit of a Nitrogen-Vacancy (NV) color center hosted in a diamond nano-crystal, attached to the vibrating extremity of a nanowire and inserted in a strong magnetic field gradient to couple the spin state to the nanowire position fluctuations via the Zeeman effect. Second, a quantum dot located in a micro-mechanical photonic wire parametrically coupled to its deformations via internal strain modulation. In both cases, the interaction between the mechanical oscillator and the qubit state can be formalized by the Hamiltonian:

$$\hat{H} = \hbar\Omega_{\mathrm{m}}\hat{b}^{\dagger}\hat{b} + \hbar\omega_0\hat{\sigma}_z + \hbar g_0(\hat{b} + \hat{b}^{\dagger})\sigma_z, \tag{4.1}$$

where $\hat{\boldsymbol{\sigma}}$ is the Pauli operator of the qubit, $\omega_0/2\pi$ its frequency splitting and $\Omega_{\mathrm{m}}/2\pi$ the oscillator resonant frequency. This parametric interaction presents a certain analogy with the optomechanical Hamiltonian, the cavity mode being replaced by the qubit, whose dynamics is now bounded on the Bloch sphere, so that it presents a natural non-linearity under external excitation. Both TLS present some important differences: the NV spin qubit has a resonance frequency in the GHz domain and can be prepared and manipulated using well established protocols, and also presents a very long coherence time that can overpass the mechanical period, so that it will allow to enter interesting dynamical regimes in the resolved sideband regime ($\kappa < \Omega_{\mathrm{m}}$). The quantum dot presents a frequency splitting in the optical domain instead, so that it is naturally polarized at room temperature, and a modest temporal coherence (ns) which brings the system in the adiabatic regime. However the interaction strength was found to be extremely large, allowing to reach the ultrastrong adiabatic coupling regime of the parametric interaction ($g_0 \gg \Omega_{\mathrm{m}}$).

### Context and positioning

A hybrid system composed of a mechanical oscillator coupled to a two level system aims at reproducing with a macroscopic oscillator the seminal operations at play in ion trapped experiments to entangle the ion position to its internal degrees of freedom. Following the ground state cooling in optomechanics, this unconventional combination [79, 75] was seen as a promising route towards the generation of non-classical states of motion of macroscopic objects. Hybrid systems made of a mechanical oscillator interfaced to Bose Einstein Condensates

or atomic clouds [80, 81, 82, 83], superconducting qubits [84, 85, 86], solid state single spins [31, 87, 4, 88, 89, 90, 91, 6, 92, 93, 7], molecules [94] or quantum dots [95, 96, 97, 98, 23, 99] have already been explored. Few groups have engaged experiments based on NV spin qubits, using either magnetic [88] or strain coupling [92, 93] to mechanical deformations. The strength of strain mediated interaction between the fundamental ground states of the NV defect is of similar magnitude as what can be achieved with magnetic coupling. However it can be significantly larger if exploited within the excited states of the defect, but this requires a resonant laser excitation and operating at low temperatures. There the photo-physics of the NV defect is much more delicate to handle than at room temperature and can be less convenient to operate than other hybrid platforms based on quantum dots for example. Also, the great tunability of the magnetic interaction and the control one can gain on the spatial structure of the interaction was seen as a important asset for our experiments.
The hybrid interaction, coupling phonons and qubits presents large similarities with quantum electrodynamics (QED) systems where hallmark experiments revealing the interplay between atomic and photonic excitations have permitted exploring the foundations of quantum mechanics. The observation of a Mollow triplet in atomic fluorescence spectra [100] is one of the characteristic signatures of the strongly driven Jaynes-Cumming interaction, characterized by the apparition of sidebands on each side of the pump frequency featuring a splitting proportional to the laser field amplitude. Along with the Autler-Townes doublet [101] or vacuum Rabi oscillations, it expresses the dressing of the atom with the optical photon field [102]. Since then, Mollow triplets were reported in atomic vapors [103, 104], single molecules [105, 106], single quantum dots [107, 108] or superconducting qubits [109] coupled to photon fields in the optical or microwave (MW) domains. This motivated us to investigate this peculiar dynamics in our hybrid spin-nanowire experiment.

## 4.1 Nitrogen-vacancy spin qubit

The NV defect in diamond is now a largely spread resource for quantum information and magnetic field imaging, it represents both a robust single photon source and a long lived spin qubit. The capability to isolate single NV defects made it an early recognized bright single photon source presenting an extreme optical stability [110] and operable in biological or extreme physical environments, such as low temperature [111] or high pressure [112].
The NV defect (NV-) is a color center hosted in the diamond matrix constituted of a Nitrogen atom replacing a Carbon atom associated to a vacancy, supplemented by an additional electron. The defect can be optically pumped, its excited states being associated to a zero phonon line around 637 nm with two transition dipole perpendicular to the NV axis. Its fundamental state is a spin triplet, degenerated by the spin-spin interaction of the 2 electrons which are populating its higher occupied orbital. The ground state presents a frequency splitting around 2.87 GHz between the $m_S = 0$ and $m_S = \pm 1$ states with a gyromagnetic ratio of $g \approx 2$. The simplified energetic diagram of the defect is shown in Fig. 4.1f.
The great interest of the spin qubit arises from the demonstrated possibility to spin polarize, to optically readout their spin state and to manipulate them with a combination of optical and microwave pulses, already at room temperature, associated to an extremely long lifetime with $T_1$ duration approaching the ms level in ultra pure samples. The optically excited states of the defect also possesses a spin 1 triplet structure, duplicated over two orbital choices. Under optical excitation, the system can emit red photons through an alternation of absorption/emission cycles at a maximum rate of 40 MHz, when limited by the $\approx 12.5$ ns finite lifetime of the excited state. Such optical cycles do preserve the NV spin state. However the excited NV can also decay to a meta-stable set of spin 0 states, and more efficiently from the $m_S = \pm 1$ states. There, the system will more likely decay into the $m_S = 0$ ground state, so that those peculiar selection

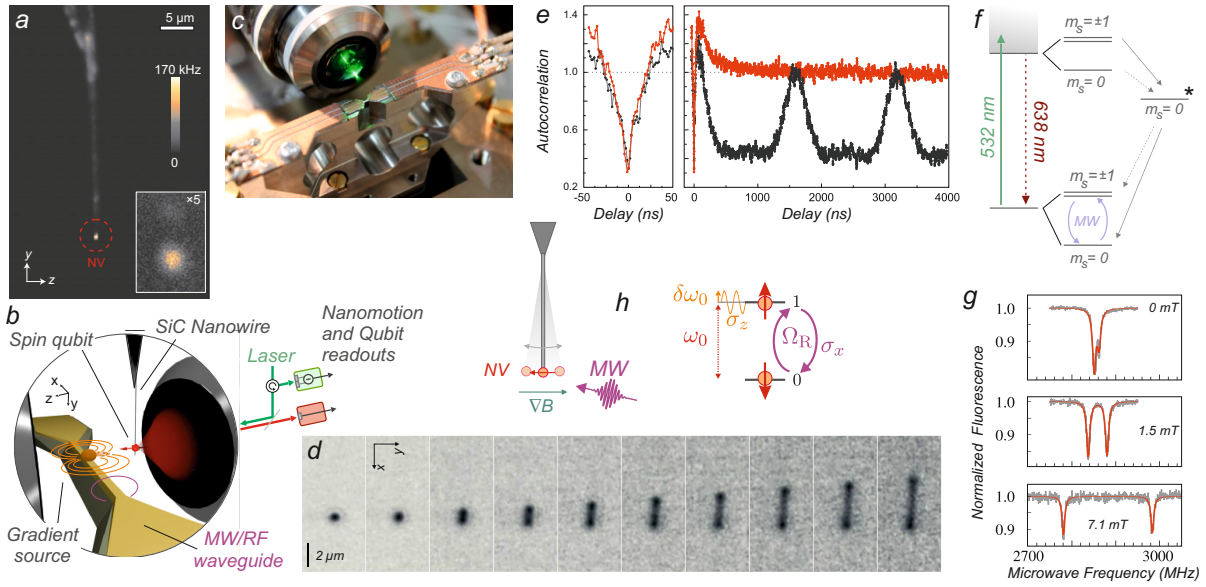


Figure 4.1: **The hybrid spin qubit -mechanical experiment.** **a** Fluorescence scanning image of a nanowire functionalized with a NV defect. **b** The system is inserted in a strong magnetic field gradient to couple the nanowire position to the spin state, via a position dependent Zeeman effect. **c** Photograph of the microwave waveguide supporting the magnetic bead and the objective used for NV readout and spin polarization. **d** CCD images of the time averaged NV fluorescence under increasing mechanical excitation: the movable single photon source acquires a spatial degree of freedom, which can be investigated through cross-correlation [118] or autocorrelation [4] measurements as shown in panel **e** black: oscillating, red: at rest. **f** Simplified scheme of the energy diagram of the NV defect. **g** Optically detected magnetic resonance (ODMR) measurements under varying magnetic field strength, illustrating that a strong magnetic field gradient will allow to render the spin-qubit resonant frequency dependent on the oscillator position, thus generating a parametric coupling scheme as illustrated in panel **h**.

rules enable an optical pumping of the NV state: under optical illumination, the NV defect will be spin polarized in its fundamental ground state. The NV spin state can subsequently be manipulated by quasi-resonant transverse microwave fields, in the GHz range, and its spin population can be determined by measuring the amount of light it emits after an optical excitation: after averaging over several iterations, the system will emit up to approx. 30 percent more light in its excited states than in its ground state due to the possibility to transit towards the metastable dark state. This capacity to detect optically the NV spin population and manipulate it with microwave fields was early used to measure Rabi oscillations of the spin qubit [113], and implement other dynamical protocols at the single spin level. It is now a powerful resource for magnetic field imaging at the nanoscale [114, 115] but also for NMR-like experiments exploring the surrounding magnetic field landscape [116, 117].

The nanowires were functionalized with single NV defects by iteratively dipping their vibrating extremity into a liquid drop containing diamond nanocrystals hosting either zero or one NV defect and stopping the process as soon as one NV was identified by fluorescence analysis. Its unicity could be verified with autocorrelation measurements, see Fig.4.1e. The NV orientation was subsequently determined using the Zeeman effect produced by the calibrated magnetic field of magnets approached from different orientations in space. If the mechanical properties of the nanowire can be efficiently determined with the optical readout techniques described above, this novel mechanical degrees of freedom acquired by the suspended vibrating NV defect gave us the

occasion to investigate a bit further the principles of nano-optomechanical readout in the photon counting regime. In particular, we explored how the temporal and spatio-temporal correlation measurements were altered with such a movable single photon source [4, 118] that can emit photons from different positions in space, that can be optically resolved for sufficiently large oscillation amplitudes, in a configuration that reminds the original Hanbury Brown and Twiss experiment. Those second order correlation measurements, represent indeed an interesting avenue for position sensing at ultralow optical fluxes [118], still operating when the photon flux becomes smaller than the mechanical damping rate.

The coupling between the NV spin and the nanowire vibrations proceeds through a position-dependent Zeeman effect, realized by inserting the NV-functionalized nanowire extremity in a strong magnetic field gradient. The NV spin is sensitive to the external magnetic field $\mathbf{B}$ through the Zeeman effect, which is formalized through the Hamiltonian:

$$\hat{H}_{\mathrm{NV}} = \hbar\omega_0\hat{\sigma}_z^2 + g\mu_B\ \hat{\boldsymbol{\sigma}}\cdot\mathbf{B}, \tag{4.2}$$

$\mu_B$ being the Bohr Magneton ($9.27\times10^{-24}$ J/T). A magnetic field parallel to the NV-axis (z axis) will induce frequency shifts of the qubit resonance with a sensitivity of $g\mu_B/h \approx 28\,\mathrm{MHz/mT}$, while an hybridization of its eigenstates will be caused by a transverse static B-field. Since this perturbation equally affects the excited states, it will cause a reduction of the mean fluorescence and of the spin-dependent fluorescence contrast due to the intermixing of excited spin states which modifies the selection rules for the transition towards the metastable state. As such the orientation of the local magnetic field with respect to the NV axis will be extremely important in our experiments.

When a NV defect is attached at the vibrating extremity of the nanowire and inserted in a magnetic field $\mathbf{B}(\mathbf{r})$ presenting large spatial gradients, it becomes coupled to the nanowire vibrations $\delta\mathbf{r}$ around its rest position $\mathbf{r_0}$ according to the linearized Hamiltonian:

$$g\mu_B\ \hat{\boldsymbol{\sigma}}\cdot\mathbf{B}(\mathbf{r_0}) + g\mu_B\hat{\boldsymbol{\sigma}}\cdot((\delta\mathbf{r}\cdot\boldsymbol{\nabla})\mathbf{B}|_{\mathbf{r_0}}), \tag{4.3}$$

and the interaction term can also be expressed as:

$$g\mu_B\hat{\sigma}_i\,\partial_j B_i\,\hat{\delta}r_j. \tag{4.4}$$

Depending on the structure of the magnetic field gradients and on the orientation of the nanowire motion, one can generate a parametric ($\propto\hat{\sigma}_z$) or transverse interaction ($\propto\hat{\sigma}_{x,y}$) to the spin. The phonon fields associated to the vibrational modes of the nanowire thus play an equivalent role as time-modulated magnetic fields, acting on the spin state from different directions on the Bloch sphere, depending on the Pauli operator involved. In view of the large frequency separation between the mechanical and spin qubit resonances, we have first focussed on the parametric interaction regime, where the spin energy becomes position dependent, so that it gets modulated by the deformations of the nanowire. In that case, the parametric coupling strength can amount to $g\mu_B\partial_z B_z/h = 2.8\times10^{16}\,\mathrm{Hz/m}$ (or 28 MHz/nm) for a gradient of $\partial_z B_z = 10^6\,\mathrm{T/m}$. The single phonon or single spin excitation parametric coupling strength is then given by

$$g_0 = \frac{g\mu_B\partial_z B_z}{\hbar}\,\delta x^{\mathrm{zpf}} \tag{4.5}$$

and can reach $g_0/2\pi = 17\,\mathrm{kHz}$ for the nanowire we routinely employ (150 $\mu$m, 100 nm, 4 kHz, 5 pg) in force sensing experiments featuring $\delta x^{\mathrm{zpf}} = 0.6\,\mathrm{pm}$. In analogy with the previous chapter, this suggests that the spin-dependent force should be capable of statically displacing the nanowire by more than its zero-point-fluctuations.

In practice, as mentioned above the magnetic field at the rest position $\mathbf{B}(\mathbf{r_0})$ should also remain aligned with the NV axis to preserve its ability to be optically readout and spin polarized.

Then, one needs to generate a strong magnetic field gradient where the spin energy $\hbar\omega_0(\mathbf{r})$ varies in the direction of motion. As a micromagnet we used a NdFeB micrometric structures (beads) deposited on a microwave waveguide, whose magnetic orientation was adjusted by inserting the sample in a large external magnetic magnetic field (see Fig 4.2). It was important to mechanically bind the magnet and the microwave waveguide to avoid spatial drifts between the DC and MW magnetic fields landscapes.
We mapped the spatial dependence of the spin qubit energy $\hbar\omega_0(\mathbf{r})$ by scanning the micro-bead position and measuring the NV fluorescence for different microwave tones (see Fig 4.2b). When the magnetic field of the bead is not aligned with the NV axis, we observe a reduction of its fluorescence due to the intermixing of the NV excited states. This effect is pretty convenient to identify the sweet spots in space where the magnetic field remains aligned with the NV axis and where strong magnetic field gradients are expected. Also, at positions where the spin resonance hits the microwave tone ($\omega_0(\mathbf{r}) = \omega_{\rm mw}$), we observe the typical ODMR dip in the fluorescence, out of which one can extract the spatial map of the spin resonance, $\omega_0(\mathbf{r})$, and thus compute the vectorial parametric coupling strength $\boldsymbol{\nabla}\omega_0$ as shown in Fig. 4.2cd.
In a first experiment [4], we positioned the NV-functionalized nanowire in a region of large magnetic field gradient and investigated how the ESR resonance was broadened by the coherent oscillations of the nanowire, see Fig. 4.3 left. This allowed a first investigation of the parametric coupling strength, which reached $1.3 \times 10^{15}$ Hz/m (1.3 MHz/nm) in a magnetic field gradient of 45 000 T/m in an adiabatic regime, where the spin resonance was intentionally microwave-broadened to accelerate the measurement sequence.
In a second experiment [7], see Fig. 4.3 right, we investigated the coherent dynamics of the spin under mechanical and microwave excitations, in the resolved sideband regime, when the spin coherence time overpasses the mechanical period $\Gamma_{\rm spin} < \Omega_{\rm m}$ (in view of the different coherence times associated with the spin evolutions under different excitation protocols ($T_1$, $T_2$, $T_2^\star$), the resolved sideband criteria should be examined in each situation). Since the nanowire can move identically along both transverse directions, it was necessary to integrate a complete 2D description of the hybrid system, and investigate how the movement of the nanowire in the 2D space was affecting the spin properties.

In presence of a large parametric coupling strength, the spin state energy becomes position dependent $\hbar\omega_0(\delta\mathbf{r})\,\hat{\sigma}_z$ , meaning that in turn the oscillator experiences a spin dependent force given by

$$F = -\hbar\boldsymbol{\nabla}\omega_0\ \hat{\sigma}_z = g\mu_B\,\nabla B\,\hat{\sigma}_z. \tag{4.6}$$

The differential force, between the spin up and spin down cases amounts to 18 aN in a magnetic field gradient of $10^6$ T/m. This magnitude is in principle well within the force detection capacity of the nanowires, and should be within experimental reach. This spin dependent force is indeed the key ingredient to transfer the spin excitation to the mechanical oscillator, and represents a direct analogy to the Stern and Gerlach experiment (1921), where a strong magnetic gradient was used to spatially separate a flux of silver atoms depending on their spin orientation. These spin dependent forces are also at the base of quantum information processing with trapped ions [77].
The hybrid force is thus proportional to the spin population $\sigma_z$. In order to enhance the hybrid interaction and develop experimental schemes capable of detecting it in the surrounding force environment experienced by the nanowire, it is interesting to modulate the spin population at the mechanical resonance frequency in order to benefit from the enhanced mechanical response of the nanowire. To do so we realize a set of experiments aiming at driving the spin qubit with a resonant microwave tone adjusted so as to produce a Rabi precession of the spin approaching the mechanical resonance. We realized an initial study during the PhD thesis of Sven Rohr, where we observed that the spin precession could be locked on an external time-varying magnetic field responsible for a parametric modulation of the spin energy [6] at a frequency close to the one

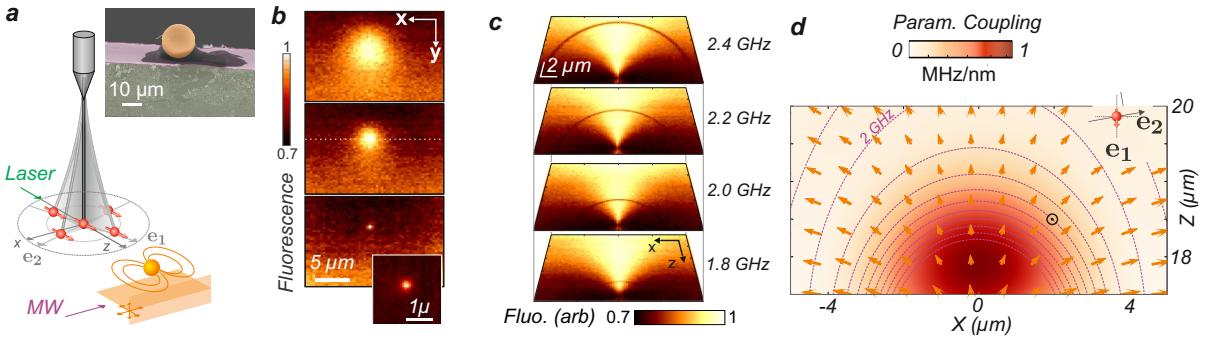


Figure 4.2: **Magnetic field alignment and vectorial parametric coupling strength a** A 20 $\mu$m NdFeB bead is glued on a microwave guide, and its magnetisation is oriented along the NV axis. The sample can be displaced by a piezo stage in front of the NV, to reach the suitable interaction strength. **b** The NV fluorescence drops when the external field is not aligned with its axis, so that the coarse approach can be realized by progressively shrinking the bright area in the vertical plane. **c** Fluorescence images obtained by scanning the magnet in the horizontal plane, while injecting a constant microwave tone of progressively decreasing frequency. The areas where the NV energy splitting is resonant with the microwave tone appears as a thin line in the horizontal xz space. **d** This method allows to measure the spatial dependence of the spin energy $\hbar\omega_0(\mathbf{r})$ in the 2D oscillating plane, as shown with iso-energy lines. The vectorial parametric coupling strength is proportional to the gradient $\boldsymbol{\nabla}\omega_0$, shown as a flow of arrows.

of the driven Rabi precession. In NMR experiments this phenomenon is called "spin locking" (in a continuous version here). In our experiments, it can be difficult to properly adjust the spin precession due to long measurement times, and drifts in the microwave powers and in position. The spin locking mechanism helps making the spin precess precisely at the resonantly driven oscillation frequency, where the associated spin dependent force generates the largest displacements and presents a direct interest for mechanical readout of the spin dynamics.
When one realizes a Fourier transform of the Rabi precession measured in presence of the quasi resonant mechanical driving tone, see Fig. 4.4ef), one observes that in addition to the central frequency, which corresponds to the mechanical vibration, it is possible to observe two lateral tones, of smaller amplitudes, whose frequency splitting linearly increases with the driving strength (see Fig. 4.4g). This peculiar non-linear observation is a direct consequence of the bound character of the spin dynamics on the Bloch sphere.

The spin locking mechanism can be seen as a double dressing of the spin qubit with both the microwave and phonon fields and leads to an analogy to the Mollow triplet in quantum electrodynamics: when one measures the fluorescence spectrum of an atomic cloud illuminated by a resonant laser field, it is possible to detect not only the laser frequency, but also 2 sidebands whose frequency splitting linearly increases with the laser electromagnetic field strength.
Here follows a brief explanation of this analogy. First, the {spin qubit - microwave photon} subsystem whose uncoupled eigenstates are $|m_s, N\rangle$ ($m_s = 0, 1$ is the qubit state restricted to one transition and $N$ the microwave photon number) is subject to the resonant transverse interaction $\hbar g\hat{\sigma}_x(\hat{a} + \hat{\dagger}a)$, see Fig. 4.4a. For a quasi-resonant driving condition ($\omega \approx \omega_0$), in the rotating wave approximation, the coupled eigenstates $|\pm_N\rangle$ are built among the dressed multiplicities $\{|0, N\rangle, |1, N-1\rangle\}$ which share a similar number of spin or photonic excitations, and the energy splitting between the dressed states scales as $\hbar g\sqrt{N}$. For a coherent microwave driving tone with a large mean photon number $\bar{N}$, the photon number distribution is peaked around $\bar{N}$, and the global system dynamics can be approximated to the one reduced to the main multiplicity ($\bar{N}$), which is the one of a pseudo spin, with eigenstates $|\pm_{\bar{N}}\rangle$ presenting an energy splitting of

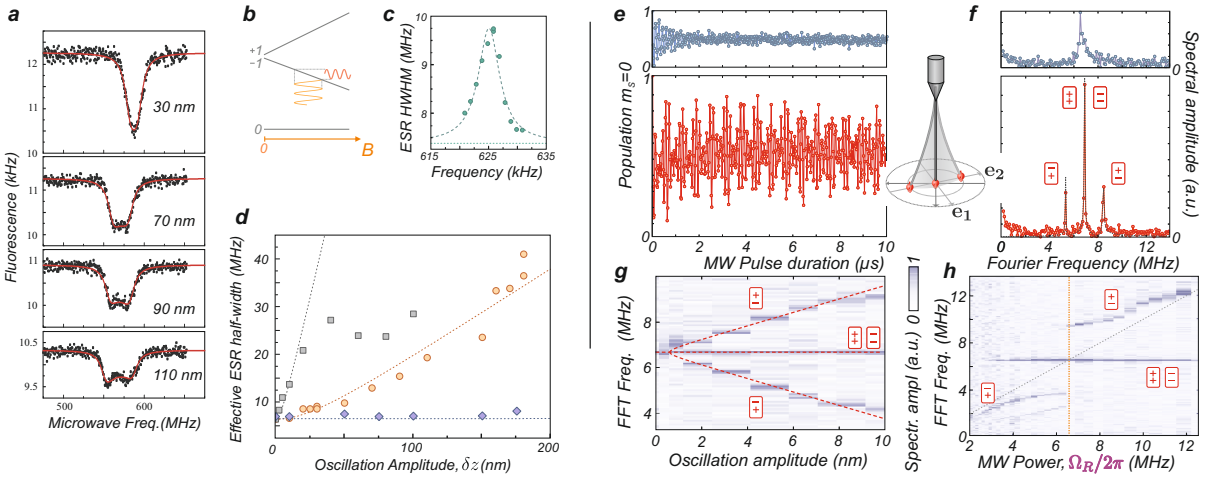


Figure 4.3: **Parametric modulation of the vibrating NV spin** in the adiabatic (left [4]) and resolved sideband (right [7]) regimes. **a** Evolution of the ODMR response of the spin qubit measured for increasing resonantly driven oscillation amplitudes. In the adiabatic regime, the motion-averaged ESR resonance gets broadened and then transforms into an inverted camel-back shape, the oscillator spending more time in its oscillatory trajectory at the extrema positions (**b**). The broadened ESR linewidth is reported in **d**. **c** Similar measurements reproduced at a constant drive amplitude while scanning the drive frequency. The experiment being conducted in air, the nanowire presents a reduced quality factor. **d** Evolution of the ESR linewidth with the oscillation amplitude at different positions in space, presenting a 0, 6700 and 45000 T/m magnetic field gradient. At large coupling strengths, one observes a deviation from the linear coupling regime at large oscillation amplitudes, since the magnetic field gradient is no more homogeneous over the oscillation amplitude. **e** Rabi precession measurements realized with a microwave power generating $\Omega_R/2\pi \approx 6.3\,\mathrm{MHz}$ in absence (above, blue) and presence of a resonant mechanical drive at a similar frequency. One observes a longer lived precession, characterized by the apparition of sidebands in the amplitude of the Fourier Transform (**f**) as well as a spectacular narrowing of the central peak. **g** Evolution of the spin population spectra for increasing driving amplitude, showing the progressive splitting of the triplet, linear in the oscillation amplitude. **h** Spin precession spectra observed for increasing microwave powers, generating an increasing Rabi frequency, which crosses the mechanical oscillation tone (6.3 MHz). One observes a characteristic synchronization of the spin precession on the parametric modulation tone, called "spin locking" in NMR protocols.

$\Omega_R = g\sqrt{\bar{N}}$, quantified along the $x$ axis on the Bloch sphere, as sketched in Fig. 4.4b.
For this pseudo spin, the parametric phononic modulation - involving $\sigma_z$ - acts as a transverse driving field (along the vertical axis of the Bloch sphere). Furthermore, when one measures the time evolution of the NV spin population (projection along the vertical axis of the Bloch sphere), it also corresponds to a measurement of the dipole evolution of the pseudo spin (in its equatorial plane). We are thus is a situation similar to the Mollow triplet configuration, where the light field is replaced by phonons, and the atom by the pseudo spin. The resonant pumping condition requires $\Omega_\mathrm{m} \approx \Omega_R$, which is precisely the spin locking condition, and one can then expect to detect the mechanical driving frequency and the sidebands in the time evolution of the pseudo-spin, i.e. in the Rabi precession of the spin qubit. The origin of the Mollow triplet signature can also be explained by a second dressing of the pseudo spin by the phonon field. The undressed eigenstates are now $|\pm_{\bar{N}}, M\rangle$, where $M$ is the phonon number, which can be sorted in multiplicities $\{|-_{\bar{N}}, M\rangle, |+_{\bar{N}}, M-1\rangle\}$ within which acts the "transverse" interaction term: $\hbar g_0(\hat{a}+\hat{a}^\dagger)\sigma_z$, knowing that the spin population operator $\sigma_z$ partly acts as a creation/annihilation operator for

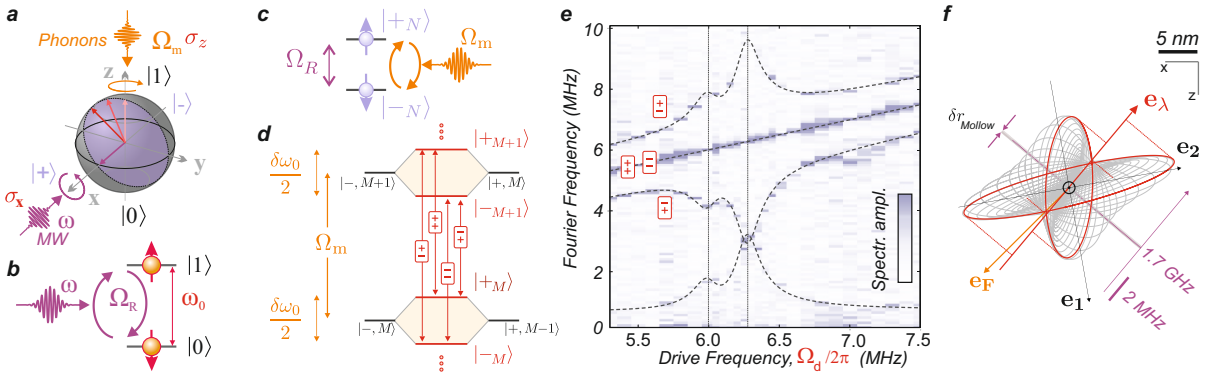


Figure 4.4: **A phononic Mollow triplet. a** Sketch of the Bloch sphere and of the microwave and mechanical driving tones at play: a transverse MW field drives Rabi oscillation of the spin qubit while subjected to a parametric mechanical modulation acting along the vertical axis of the sphere. **b** The MW field is resonant with the spin transition and generates a Rabi precession at a rate $\Omega_R$. For large photon numbers, the dynamics of the qubit can be assimilated to the one of a pseudo-qubit, of energy splitting $\Omega_R$, quantized in the horizontal plane of the Bloch sphere, a direction along which the mechanical drive appears as a transverse drive as sketch in panel **c**. The interaction efficiency is maximized when the mechanical drive is resonant with the pseudo-qubit energy splitting, i.e. $\Omega_m \tilde{\Omega}_R$, and leads to a second dressing ladder as sketch in panel **d** between the phonon and pseudo qubits states. The different transitions observed in the Mollow triplet structure are indicated as red labels. **e** Mollow triplet spectra observed while sweeping the mechanical driving frequency $\Omega_d/2\pi$ across both fundamental mechanical eigenfrequencies while simultaneously adjusting the microwave power to preserve the condition $\Omega_R \tilde{\Omega}_d$. The Mollow triplet structure reflects the doubly resonant mechanical response with a frequency splitting reflecting the parametric modulation strength generated for the different driven trajectories undergone by the nanowire $\delta\omega_0[\Omega_d] = \boldsymbol{\nabla}\omega_0 \cdot \delta\mathbf{r}[\Omega_d]$, which are analyzed in 2D in panel **f**. the gradient of the spin qubit energy is indicated, as well as $\delta r_{\text{Mollow}}$, the minimum distance along the energy gradient over which it is necessary to oscillate to produce a resolvable Mollow triplet ($\delta\omega_0 > \Gamma_{\text{spin}}$).

the pseudo spin (we note that the rotating wave approximation is not completely valid since the parametric coupling strength can approach the mechanical frequency, but most of the observed phenomenology can be explained by the dressing process. The parametric modulation thus acts as a second dressing, where the energy splitting in the multiplicities now becomes $\hbar g_0 \sqrt{M}$ or $\hbar\delta\omega_0/2$ which corresponds to half the amplitude of the parametric modulation caused by the resonant motion. Since the Rabi measurement represents a measurement of the time evolution of the pseudo-spin dipole, the frequencies observed in the Rabi spectrum are thus the ones connecting the different dressed states, between the different multiplicities: $\Omega_m$ and $\Omega_m \pm \delta\omega_0/2$, as well as the intra-multiplicity one, at $\delta\omega_0/2$. They are indicated in the different plots of Fig. 4.3 and 4.4.
When varying the microwave power across the spin-locking condition, see Fig. 4.3h, one can see that the Rabi frequency, which normally scales with the microwave field strength, gets locked on the parametric mechanical modulation tone, meaning that the spin precession gets synchronized on the oscillation period. The locking capture bandwidth, or more precisely the frequency mismatch over which the spin dynamics is dominated by the parametric modulation tone is of the order of $\delta\omega_0$.

To further explore the spatial structure of the parametric interaction in the Mollow triplet

regime, we performed a set of measurements, where the nanowire was driven with an electrostatic force generated by a RF tone co-propagating in the MW waveguide. It was injected by a first bias-T , while the waveguide was terminated by a second one to ensure an open circuit to generate a voltage modulation at the magnetic bead level. By sweeping the driving frequency $\Omega_\mathrm{d}/2\pi$ across both mechanical resonances, we generated driven trajectories of varying orientations, amplitudes and ellipticities in the magnetic field gradient landscape. For each driving frequency, we adjusted the microwave power to ensure the Mollow triplet configuration ($\Omega_R \approx \Omega_\mathrm{d}$) and recorded Rabi precessions of the driven spin qubit, whose Fourier transforms are shown in 4.4e. One can recognize the doubly resonant response of the nanowire which produces a large parametric modulation associated to a larger splitting of the triplet, while the central tone which is associated to the driving tone $\Omega_\mathrm{d}$ linearly evolves across the map. The dashed lines are fits to the different Mollow triplet lines, $\Omega_\mathrm{d}$, $\Omega_\mathrm{d} \pm \delta\omega_0[\Omega_\mathrm{d}]/2$ and $\delta\omega_0[\Omega_\mathrm{d}]/2$ using

$$\delta\omega_0[\Omega] \equiv \left| \boldsymbol{\nabla}\omega_0 \cdot \sum_{m=1,2} \frac{\delta F(\mathbf{e_F}\cdot\mathbf{e_m})\mathbf{e_m}}{M_\mathrm{eff}\,(\Omega_\mathrm{m}^2 - \Omega^2 - i\Omega\Gamma_\mathrm{m})} \right| \tag{4.7}$$

with the fitting parameters indicated in 4.4f. The parametric coupling strength obtained amounts to $|\boldsymbol{\nabla}\omega_0| = 0.5\,\mathrm{MHz/nm}$ (corresponding to around 20 000 T/m) oriented along the unitary vector $\mathbf{e}_\lambda = \boldsymbol{\nabla}\omega_0/|\boldsymbol{\nabla}\omega_0|$ which are both in good agreement with the static coupling strength expected at position $\odot$ shown in Fig. 4.2e both in orientation and magnitude. The mechanical properties of the nanowire eigenmodes were independently determined by thermal noise analysis, while the force magnitude and its orientation can also be independently determined using driven trajectories analysis. In particular the force is pointing towards the magnetic bead center, which was electrically connected to the waveguide, and is thus imposing its orientation to the electrostatic actuation force at the measurement position. We also note that it was necessary to include a parasitic RF modulation tone to fully explain the non-vanishing value of the triplet splitting out of the mechanical resonance, which was directly parametrically modulating the spin qubit energy. This artefact could be later mitigated by using a different mechanical driving force such as a piezo (or optical) actuation, or by exploiting the quadratic dependency of the force on the bias voltage, which could be used to drive the nanowire at half its resonance frequency.

All these experimental observations on the Mollow triplet can also be quantitatively described by solving the Bloch equations of the spin precession under photonic and phononic drives, but the Mollow triplet analogy helps understanding the physics behind the spin locking mechanism. An interesting difference is that one can readout the time evolution of the dipole of the pseudo spin, while in the original experiment, it is only within the optical signals that it could be detected, with quadratic detectors, not capable of recording the temporal dynamics of the dipole. If one pursues the Mollow triplet analogy, it would be desirable to detect the presence of the Mollow triplet directly on the mechanical (photonic) side: the temporal evolution of the spin $\sigma_z(t)$ operator directly acts as a force drive on the nanowire and one should in principle be capable of detecting the Mollow sidebands in the position spectrum of the nanowire under continuous optical and microwave illuminations of the spin qubit.

A natural question that also arises in those investigations is how the random position fluctuations of the nanowire can affect the spin coherence: randomly modulating the energy of a qubit is a source of large decoherence for quantum superpositions in general. The nanowire thermal noise, which spreads over a few nanometers at room temperature, is also spectrally colored and can generate a significant loss of coherence when the spin is made to precess at a Rabi frequency close to the mechanical resonance. We have started investigating those questions [5, 10], both theoretically and experimentally in a simulated experiment (similar to [6] but using a noisy colored drive), and investigated how the spin was sensitive to the simulated position fluctuations,

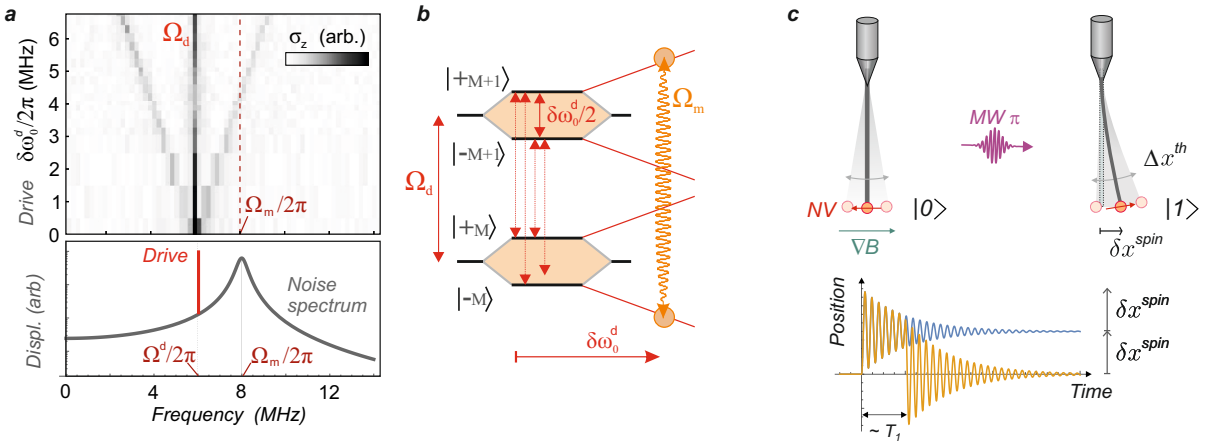


Figure 4.5: **Future developments. a** FFT analysis of the NV spin precession measured when subjected to a time-varying magnetic field which simulates the parametric modulation caused by a spectrally colored random motion combined to a coherently driven trajectory of increasing amplitude as shown in the bottom spectral plot. The mechanical resonance is at 8 MHz, while the detuned driving tone is at 6 MHz. When the upper Mollow sideband crosses the spectral window where the thermal noise is maximal, one observes a reduction of the spin-locking efficiency (reduced magnitude of the central peak). This can be understood by the presence of random magnetic fields which can induce transitions between the dressed multiplicities (see panel **b**). **c** Mechanical detection of the spin-dependent force: a microwave $\pi$- pulse excites the spin state, thus applying a static force on the nanowire during a duration lasting in average over $T_1$. The nanowire trajectory following the spin flip is shown in the lower panel (blue). The orange curve is the one obtained in presence of a subsequent spin relaxation. The maximum displacement obtained during the first oscillation period is $2\delta x_{\mathrm{spin}}$, and does not depend on the nanowire quality factor. The spin-flip-driven trajectory is however hidden in the nanowire thermal noise, but the latter can be averaged over several iterations of the protocol, especially when combined with active cooling techniques (see text).

see Fig. refFig-Hybrid-NV-perspectivesab. In the Mollow triplet regime, the spin is no longer sensitive to the noise present at the Rabi precession frequency, but to the noise present at the Mollow sidebands frequencies ($\Omega_{\mathrm{m}} \pm \delta\omega_0/2$), which can be understood from the fact that such a noise term can generate transitions between the dressed states and interrupts the equivalent "fluorescence cascade". As such, in presence of a modest resonant mechanical oscillation, for which $\delta\omega_0 > \Gamma_{\mathrm{m}}$, the Mollow triplet sidebands are brought beyond the noise bandwidth of the nanowire mechanical thermal noise. With the parametric coupling strength employed, of a few MHz/nm, this only requires a few pm of oscillation amplitude.

### Perspectives for the hybrid spin qubit experiment

The future perspectives of the work will thus aim at observing and investigating the action of the NV spin on the mechanical oscillator, using a coupling scheme similar to the Stern and Gerlach experiment. The orders of magnitude are promising, and the spin dependent forces are in principle well within the detection capability of the nanowires. It will however require to control all the other forces acting on the nanowire, of optical, microwave or electrostatic origin, but since one has the potential to independently readout and control the spin state using the standard toolbox of NV physics, this provides an avenue for efficiently suppressing forces not related to the spin evolution.

Let us inspect the feasibility of a direct detection of the trajectory followed by the nanowire consecutive to a spin flip triggered by a microwave $\pi-$ pulse, as sketched in Fig. 4.5c. In the rather modest magnetic field gradients employed here (20 000 T/m), we operated with parametric coupling strength around 1 MHz/nm, which corresponds to a spin-dependent differential force of $\hbar\nabla\omega_0 \approx 0.7$ aN. The latter could reach 20 aN in a stronger but realistic field gradient of $10^6$ T/m, which would in turn maximally displace a typical 5 kHz, 1 pg nanowire by $2\delta x^{\rm spin} \approx 40$ pm, where:

$$\delta x^{\rm spin} \equiv \frac{1}{M_{\rm eff}\Omega_{\rm m}^2} g\mu_B \nabla B \tag{4.8}$$

is the spin-driven recoil. This magnitude has to be compared to the $\Delta x^{\rm th} \approx 90$ nm rms spreading of the nanowire thermal noise at room temperature (2400 times larger). It would thus require a too long averaging sequence to detect the spin-driven recoil. However, using an active cooling technique, such as cold damping [13], one can concomitantly reduce the nanowire thermal noise and its mechanical quality factor by 3 orders of magnitude. This requires an initial SNR of 60 dB for a $Q = 10\,000$, which is realistic, while the 2D active feedback protocols based on electrostatic forces, deployed during the PhD thesis of Philip Heringlake [13] have already demonstrated their efficiency. The spin-driven recoil $2\delta x^{\rm spin}$ being unchanged in presence of cold damping, it would thus become of the same magnitude as the spreading of the cold-damped nanowire thermal noise, so that it would only require a few averaging cycles to be revealed. In that situation the cold-damped mechanical linewidth would be around 500 Hz, so that the spin recoil could be detected within a few seconds of averaging.
This duration remains however far too long to reach a regime of *single shot mechanical readout of the spin state*, for which the measurement time should be faster than the spin decay time, $T_1$ (ms at best at room temperature). However, operating the hybrid system at low temperatures will help to significantly increase the spin coherence and reduce the thermal noise of the nanowire force probes, so that the single shot readout regime should become accessible. However, operating at such low temperatures puts serious constrains on the experiments, and in particular significantly limits the optical powers that can be sent on the nanowire and thus on the NV. It will probably require to invert the experimental configuration by functionalizing the nanowire with a nano-/ micro-magnet while approaching a NV defect hosted in a diamond microstructure, more efficiently thermalized to the cold finger of the cryostat. In that view, the perspective of realizing magnetic force field imaging with a magnetically functionalized nanowire will allow to test this configuration.

In addition to the above-described perspective - which only makes use of the static mechanical response of the nanowire- many other dynamical protocols could be investigated with the magnetically coupled NV-nanowire hybrid system. In particular, the spin-locking mechanism allows the spin to precess exactly at the mechanical resonant frequency, where the nanowire mechanical response is maximal. This dynamical aspect of the hybrid interaction certainly opens an even larger panel of experimental investigations and among others, the above-mentioned possibility to detect the Mollow triplet sidebands directly in the vibrations of the nanowire is certainly an attracting perspective to pursue the analogy between quantum electrodynamics and spin-nanomechanics. Then, in analogy with cavity optomechanics physics, dynamical back action should be exploited in the parametrically coupled hybrid system. Associated signatures will be the modification of the mechanical frequency and damping rate, when pumping the spin-qubit with a detuned microwave tone, possibly leading to a qubit assisted cooling of the nanowire if an active spin re-polarisation could be ensured to accumulate cooling cycles, as routinely employed in trapped ion experiments and investigated in the original papers by I. Wilson Rae [3] and P. Rabl [119]. In that view, we point out the elegant experiments realized in the group of G. Hétet [120] where dynamical backaction from a levitating ensemble of NV spin could be investigated. However these are truly challenging experiments, but once again the orders of magnitude and

the depth of the accessible physics are encouraging.

## 4.2 Quantum dots

This section is dedicated to the second class of hybrid system we investigated, in collaboration with the *Equipe Mixte* of the Institute. The experiments were realized in the lab of Jean-Philippe Poizat, during the PhD theses of Inah Yeo [121] and Nitika Vaish [122] with the assistance of Pierre Louis de Assis and Jan Kettler as postdocs, and several colleagues specialists in semiconductor/quantum dot physics (Maxime Richard, Julien Claudon, Alexia Auffeves, Jean-Michel Gerard, ..). The central devices are photonic trumpets grown and micro-fabricated at CEA, see Fig.4.6a hosting quantum dots at their base, which were initially developed to efficiently pump and collect photons in and out of the quantum emitters [22]. They are made of epitaxial GaAs, presenting an inverted cone geometry of approx. 18 $\mu$m in height with a 2 $\mu$m top facet. A layer of self assembled InAs quantum dots is located 800 nm above the pyramidal pedestal of the trumpet whose top facets are also covered with a $Si_3N_4$ antireflection coating, while their side walls are passivated with the same material. When the trumpets vibrate, they generate a dynamical stress on the quantum dots which get deformed and in turn see their optical transition frequency being modulated by the mechanical motion. The strength of the parametric coupling depends on the precise trumpet geometry and in particular on how it transforms a deformation of its vibrating extremity into a stress applied on the quantum dots. It also depends on the position of the quantum dots within their growth plane and on the specific geometry of the dots. In turn, the excited quantum dot will apply an internal strain change in the trumpet, putting the oscillator into motion.
Compared to the hybrid systems based on NV spin qubits, this quantum-dot-based system presents an optically cycling transition, which rapidly decays into its fundamental ground state and does not need an artificial qubit initialization (granted by the optical pumping scheme in the NV case). Other differences are that the rapid evolution of its dipole cannot be resolved (using traditional optical methods) contrary to the spin qubit, that it operates in the strong adiabatic regime so that the oscillator will essentially be sensitive to its time-averaged mean population, which can be adjusted using non-resonant or resonant optical pumping. Furthermore, the parametric coupling strength is extremely large, sufficient to enter the regime where the spin dependent force displaces the oscillator by more than its zero-point fluctuations, which requires, as in single photon optomechanics, $g_0 > \Omega_\mathrm{m}$.

A first experiment [23, 121] allowed to quantify the oscillator characteristics and the strength of the parametric interaction. The mechanical properties of the nanowire were readout using a quadrant photodetector and the calibration methods similar to the ones employed for nanowires. The trumpets oscillate transversally with 2 fundamental transverse eigenmodes found around 400 -500 kHz, with mechanical quality factors of a few thousands at low temperatures and an effective mass of a few tens of pg. The photoluminescence of the quantum dots (around 920 nm) was excited by a non-resonant laser at 825 nm (1.503 eV) injected through a high numerical aperture objective. This creates free carriers in the wetting layer which subsequently decay, emitting photons around 920 nm (1.35 eV) collected in reflection and sent to a high resolution spectrometer (1.5 m focal length, 1200 grooves/mm), sufficient to resolve their intrinsic linewidth. The vibrations of the photonic wire, generate a parametric modulation of the QD energy, which can be visualized and quantified through the motional broadening of the photoluminescence spectra, as observed in the NV spin qubit experiment. If $\mathcal{L}_\kappa(\omega, \omega_0)$ represents the photoluminescence spectral shape measured in absence of mechanical excitation, then the broadened spectra can be adjusted with $L(\omega) = \frac{1}{T_m}\int_0^{T_m} \mathcal{L}_\kappa(\omega, \omega_0 + \delta\omega_0 \cos\Omega_\mathrm{m} t)dt$, where the integral is performed over an oscillation period $T_m$. It is also possible to investigate the time evolution of the parametric energy shift. To do so, we integrated an acousto-optic modulator on the pump laser allowing

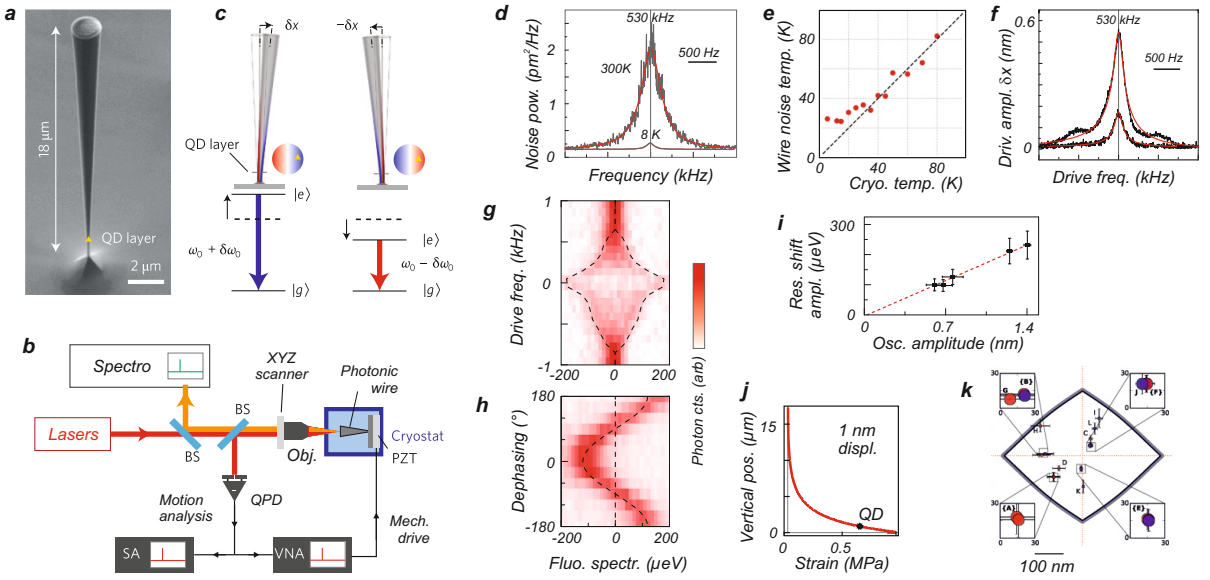


Figure 4.6: **Parametric coupling in a hybrid mechanical quantum-dot system.** **a** SEM image of a semi-conductor photonic trumpet hosting quantum dots at its base, which are strain-coupled to its mechanical deformations [23]. **b** Experimental setup: the device is operated in a liquid helium cryostat (4K). Its mechanical vibrations are readout in reflection, while the QD fluorescence properties are obtained using spectrometry techniques. **c** When the wire gets deformed, it generates a strain, which is parametrically modulating the quantum dot resonant energies. **d** Thermal noise spectra of one of the fundamental transverse eigenmode, obtained at room and cryogenic temperatures, which allow to determine the apparatus vibration temperature as reported in **e** for different cryostat temperatures. **f** A piezo element allows to resonantly drive the mode of interest (here for 3.16 and 7.94 mV drive amplitudes) that will in turn generate a coherent modulation of the QD energy as shown in **g** for different drive frequencies across the mechanical resonance. **h** The broadened QD fluorescence spectra can be analyzed in time to track the time evolution of the QD energy and correlate it to the mechanical deformations. **i** Dependence of the parametric modulation on the oscillation amplitude. **j** FEM simulation of the maximum strain $\sigma_{zz}$ measured at different $z$ elevations for a top deformation of 1 nm. **k** Since the parametric modulation strength increases linearly with the distance of the QD to the center of the wire, by reproducing the above analysis for both transverse mechanical modes, it is possible to determine the relative QD positions within the wire cross section, using the simulated strain field map [24] and assuming that they identically respond to an external strain.

to realize stroboscopic measurements of the photoluminescence spectra sampled for a given the wire deformation [23]. Such a measurement allows to measure the amplitude of the parametric modulation, see Fig.4.6, but also to infer the position of the quantum dot with respect to the neutral line of the eigenmode deformation profile: for a given deformation of the trumpet, the QD will see its resonant transition being positively or negatively shifted if it is subject to a positive or negative $\sigma_{zz}$ stress respectively. This observation also allows to identify the positions of the different quantum dots with respect to each other, assuming that they identically respond to the dynamical stress. Reproducing such a measurement when driving the nanowire along both perpendicular orientations, using the two transverse fundamental modes allows to determine the relative position of the QD within the wire cross-section [24].

The parametric energy modulation amplitude was verified to increase linearly with the oscillation amplitude, see Fig. 4.7b with a slope reaching up to 166 $\mu$eV/nm for the quantum

dots studied in [23], see Fig. 4.6. This slope (equivalent to $4 \times 10^{19}$ Hz/m) corresponds to a parametric coupling strength of $g_0/2\pi = 440$ kHz, when using the zero point fluctuation of the wire $\delta x_{\mathrm{zpf}} = 11$ fm derived from thermal noise spectra measurements. This value is close to the mechanical frequency of the wire, meaning that the system approaches the regime where a single photonic excitation is capable of displacing the wire, statically, by more than its zero point fluctuations: $\delta x^{(1)} = \chi[0]\, F^{(1)} = \hbar g_0/\delta x_{\mathrm{zpf}}/M\Omega_{\mathrm{m}}^2 = \delta x^{\mathrm{zpf}} 2g_0/\Omega_{\mathrm{m}}$, an expression in direct analogy to one introduced in the single photon regime of cavity optomechanics.

After this first experiment, the collaboration investigated the possibility to detect the reverse side of the hybrid interaction, aiming at observing a mechanical actuation of the nanowire via a manipulation of the state of the quantum dot. The strategy employed consisted in pumping the QD with a quasi-resonant laser, whose intensity was time-modulated at the mechanical resonance frequency, and measuring the driven mechanical motion while sweeping the laser-quantum dot detuning. When the laser is out of resonance, it does not interact with the QD, so that it only exerts its direct optical force of photonic or photothermal origin. On the contrary when it is brought at resonance, the laser modulates the quantum dot population thus exerting a mechanically resonant time-modulated "spin" dependent force. The power of the pump laser was chosen close to optical saturation so that the quantum dot population changes (and thus the hybrid force) are maximized during the optical modulation cycle.
The experiment was rather complex to implement since one had to stabilize many sources of drifts to reach a proper measurement configuration: a laser was added to spatially track the trumpet top facet and compensate for thermal and mechanical perturbations. Another non-resonant laser was intensity modulated to apply a reference force used to track the frequency shifts of the wire using a PLL exploiting the signals emerging from the mechanical readout realized with a separate probe laser, so that the intensity modulation of the quasi-resonant laser pump beam could be adjusted over time to follow the slow mechanical resonance drifts that occurred during the long acquisition sequences (tens of hours). All lasers were intensity stabilized using active feedback loops, which was in particular necessary for the pump laser since it presented important intensity changes across the frequency sweeps. One also had to cope with the drifts of the quantum dot transition, which was difficult to actively track due to mode jumps in the resonant laser source employed. Furthermore, one had to realize the measurements once the cryostat and the quantum dot resonant drifts were stabilized, which required a significant preparation before launching a measurement sequence. To compensate for the residual QD resonant frequency shifts, we chose to realize multiple laser frequency sweeps across the resonance, record all the necessary signals: photo-luminescence and mechanical information, and implement a post-analysis of the data to compensate for those residual spectral drifts.
The results of the measurements [99] are shown in Fig. 4.7. The photoluminescence signal (recorded on the phonon sidebands) presents a characteristic resonant shape as a function of the laser-QD detuning. Also measured are the driven oscillation amplitude and its dephasing measured with respect to the intensity modulation, as well as the driving frequency. The non-resonant laser generates an optical force of photothermal origin, which is delayed with respect to the intensity modulation due to the time it takes to the thermal wave to propagate across the wire. This resonant phase, is the one on which is locked the PLL. When the pump laser hits the quantum dot transition, the hybrid force is activated and respond instantaneously to the intensity modulation. However since the PLL is locked on the non-resonant photothermal phase, it will change the driving frequency to stay at the phase set point. This frequency shift remains small compared to the mechanical linewidth since the hybrid force is small compared to the photothermal force (at the percent level). The data recorded from the PLL thus needs to be processed in order to reconstruct the resonantly driven oscillation amplitude and dephasing, as shown in Fig. 4.7.

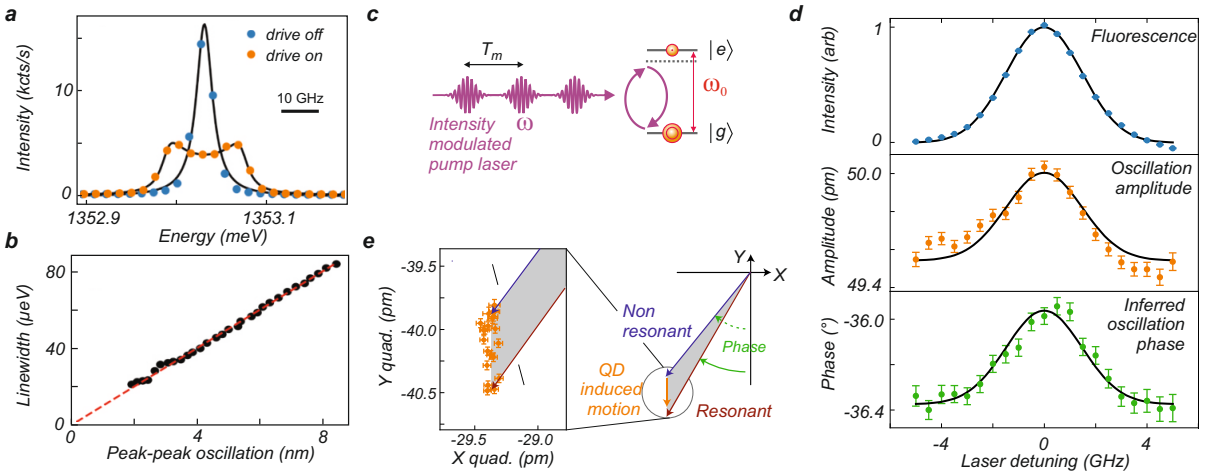


Figure 4.7: **Mechanical actuation of the photonic trumpet with a single quantum dot.** **a** Fluorescence spectra of the quantum dot used for actuating the wire, measured in presence and absence of a mechanical actuation. **b** QD resonance broadening measured for increasing resonantly driven oscillation amplitudes providing a $10\,\mu$eV/nm ($2.4 \times 10^{18}$ Hz/m) coupling strength. **c** Principle of the measurement: an intensity-modulated laser, quasi-resonant with the QD transition, modulates the QD population $\sigma_z(t)$ at a frequency chosen close to the mechanical resonance, thus causing a hybrid mechanical actuation via the "spin"-dependent force. Tuning the laser frequency $\omega/2\pi$ across the quantum dot transition $\omega_0/2\pi$ allows to discriminate spurious actuation effects such as photothermal or radiation pressure forces. **d** Measurement results averaged over many laser frequency sweeps across the QD resonance. The QD fluorescence (measured on the phonon sidebands), the oscillation amplitude and the inferred phase response are shown for varying laser detunings. **e** Principle of the measurement: when the pump laser is non-resonant with the QD, the photothermal force resonantly drives the nanowire in motion, presenting a non-instantaneous (-90 degrees phase delay with respect to the intensity modulation) response due to the non-instantaneous heat propagation in the device. The PLL used to maintain the drive at resonance is thus locked on this resonant phase value. When the pump laser becomes resonant with the QD transition, the hybrid force appears, which instantaneously follows the optical modulation and adds up to the photothermal response of the wire. The PLL compensates this shift of the resonance phase by slightly changing the modulation frequency. By recording the amplitude and frequency shifts, it is possible to reconstruct the amplitude and the phase of the total optical response.

As a conclusion, we could detect the mechanical actuation of the wire via the laser-induced modulation of the quantum dot population. This demonstration represented a true experimental tour de force, probably at the limit of what can be achieved with the current system. Future developments in the domain, along the same lines as the ones envisioned with the hybrid spin-qubit nanowire system will probably require novel geometries and strategies to enhance the force sensitivity of the oscillators and mitigate the parasitic mechanisms in competition with the hybrid interaction.

# Chapter 5
# Final words

We have thus presented the interest of silicon carbide nanowires for detecting weak forces and analyzing different force fields. The phenomenology emerging from their 2D character, once properly understood represents a significant asset for detecting weak forces, which is the objective of the future developments in the group. The different perspectives which were exposed in the manuscript will aim at observing and exploiting the spin-dependent forces in the hybrid experiments, at exploring the single photon regime of cavity nano-optomechanics, and to further investigate proximity forces, such as the Casimir and electro-optical forces. In parallel to those fundamental investigations, the developments towards scanning probe measurements of surface forces, of magnetic or electrostatic origins represent interesting avenues for diffusing the exceptional force sensing capacities of the nanowires towards other research areas.

All past developments would have not been possible without the daily help of many administrative, technicians, engineers and researchers from the Institute. I warmly thank them for all their help, and hope these fruitful interactions will continue in the future. Then, I should not finish this manuscript without acknowledging all the efforts realized by the students and postdocs who worked in the group, as well as thanking Benjamin Pigeau for these nice (nine already...) years spent working together and with other colleagues, without which we could have not reached the current state of art.

# Bibliography


[1] Enss, C. & Hunklinger, S. *Low-Temperature Physics* (Springer-Verlag Berlin Heidelberg, 2005).

[2] Rivière, R. *Cavity optomechanics with silica toroidal microresonators down to low phonon occupancy.* Ph.D. thesis, University Ludwig Maximilian (2011).

[3] Wilson-Rae, I., Zoller, P. & Imamoglu, A. Laser cooling of a nanomechanical resonator mode to its quantum ground state. *Phys. Rev. Lett.* **92**, 075507 (2004).

[4] Arcizet, O. *et al.* A single nitrogen-vacancy defect coupled to a nanomechanical oscillator. *Nature Phys.* **7**, 879–883 (2011).

[5] Rohr, S. *Hybrid spin-nanomechanical systems in parametric interaction.* Ph.D. thesis, Université de Grenoble (2014).

[6] Rohr, S. *et al.* Synchronizing the dynamics of a single nitrogen vacancy spin qubit on a parametrically coupled radio-frequency field through microwave dressing. *Phys. Rev. Lett.* **112**, 010502 (2014).

[7] Pigeau, B. *et al.* Observation of a phononic mollow triplet in a multimode hybrid spin-nanomechanical system. *Nat. Commun.* **6**, 8603 (2015).

[8] Gloppe, A. *Nano-optomécanique au coeur dun faisceau laser focalisé: cartographie du champ de force optique et action en retour bidimensionnelle.* Ph.D. thesis, Université de Grenoble (2014).

[9] Gloppe, A. *et al.* Bidimensional nano-optomechanics and topological backaction in a non-conservative radiation force field. *Nature Nano.* **9**, 920–926 (2014).

[10] Mercier de Lépinay, L. *Habillage mécanique d'un nanofil par un champ de force : de la mesure vectorielle ultrasensible aux systèmes quantiques hybrides.* Ph.D. thesis, Université Grenoble Alpes (2017).

[11] Mercier de Lépinay, L. *et al.* A universal and ultrasensitive vectorial nanomechanical sensor for imaging 2D force field. *Nat. Nanotechnol.* **12**, 156 (2017).

[12] Mercier de Lépinay, L., Pigeau, B., Besga, B. & Arcizet, O. Eigenmode orthogonality breaking and anomalous dynamics in multimode nano-optomechanical systems under non-reciprocal coupling. *Nat. Commun.* **9**, 1401 (2018).

[13] Heringlake, P. *Realtime imaging of force fields at the nanoscale with a 2D nano-optomechanical probe: Exploration of electrostatic, proximity and synthetic force fields.* Ph.D. thesis, Université Grenoble Alpes (2021).

[14] Berry, M. V. & Shukla, P. Curl force dynamics: symmetries, chaos and constants of motion. *New Journal of Physics* **18**, 063018 (2016).

[15] Heringlake, P. *et al.*. Exploring electrostatic forces above metalic nanostructures with an ultrasensitive vibrating nanowire. (2021).

[16] Levin, M., McCauley, A. P., Rodriguez, A. W., Reid, M. T. H. & Johnson, S. G. Casimir repulsion between metallic objects in vacuum. *Phys. Rev. Lett.* **105**, 090403 (2010).

[17] Fogliano, F. *Ultrasensitive nanowire force sensors in extreme conditions: from dilution temperature to ultra-strong coupling in cavity nano-optomechanics.* Ph.D. thesis, Université Grenoble Alpes (2019).

[18] Fogliano, F. *et al.* Ultrasensitive nano-optomechanical force sensor operated at dilution temperatures. *Nature Communications* **12**, 4124– (2021).

[19] Fogliano, F. *et al.* Mapping the cavity optomechanical interaction with subwavelength-sized ultrasensitive nanomechanical force sensors. *Phys. Rev. X* **11**, 021009 (2021).

[20] Reigue, A. *et al.*. Cavity nano-ptomechanics with suspended nanowires. *in preparation* (2021).

[21] Reigue, A. *et al.*. Observation of anomalous cavity shift in cavity nano-optomechanics. *in preparation* (2022).

[22] Claudon, J. *et al.* A highly efficient single-photon source based on a quantum dot in a photonic nanowire. *Nature Photonics* **4**, 174–177 (2010).

[23] Yeo, I. *et al.* Strain-mediated coupling in a quantum dot-mechanical oscillator hybrid system. *Nature Nano.* **9**, 106–110 (2014).

[24] de Assis, P.-L. *et al.* Strain-gradient position mapping of semiconductor quantum dots. *Phys. Rev. Lett.* **118**, 117401 (2017).

[25] Reserbat-Plantey, A. *Nanosystèmes graphitiques : cavités optiques ajustables et détection spectrale des contraintes dans un nanorésonateur mécanique.* Ph.D. thesis, Université de Grenoble (2012).

[26] Schwarz, C. *Optomechanical, vibrational and thermal properties of suspended graphene membranes.* Ph.D. thesis, Université Grenoble Alpes (2016).

[27] Reserbat-Plantey, A., Marty, L., Arcizet, O., Bendiab, N. & Bouchiat, V. A local optical probe for measuring motion and stress in a nanoelectromechanical system. *Nat Nano* **7**, 151–155 (2012).

[28] Schwarz, C. *et al.* Deviation from the normal mode expansion in a coupled graphene-nanomechanical system. *Phys. Rev. Applied* **6**, 064021 (2016).

[29] Binnig, G., Quate, C. & Gerber, C. Atomic force microscope. *Physical Review Letters* **56**, 930–933 (1986).

[30] Moser, J., Eichler, A., Gttinger, J., Dykman, M. I. & Bachtold, A. Nanotube mechanical resonators with quality factors of up to 5 million. *Nat. Nanotechnol.* **9**, 1007 (2014).

[31] Rugar *et al.*, D. Single spin detection by magnetic resonance force microscopy. *Nature* **430**, 329–32 (2004).

[32] Degen *et al.*, C. L. Nanoscale magnetic resonance imaging. *PNAS* **106**, 1313–7 (2009).

[33] Nichol, J., Hemesath, E., Lauhon, L. & Budakian, R. Nanomechanical detection of nuclear magnetic resonance using a silicon nanowire oscillator. *Physical Review B* **85**, 054414 (2012).

[34] Behunin, R. O., Zeng, Y., Dalvit, D. A. R. & Reynaud, S. Electrostatic patch effects in casimir-force experiments performed in the sphere-plane geometry. *Phys. Rev. A* **86**, 052509 (2012).

[35] Braginsky, V. B., Khalili, F. Y. & Thorne, K. S. *Quantum measurement* (Cambridge University Press, 1995).

[36] Caves, C. M. Quantum-mechanical radiation-pressure fluctuations in an interferometer. *Phys. Rev. Lett.* **45**, 75–79 (1980).

[37] Jaekel, M. T. & Reynaud, S. Quantum limits in interferometric measurements. *EPL* **13**, 301 (1990).

[38] Fabre, C. *et al.* Quantum-noise reduction using a cavity with a movable mirror. *Phys. Rev. A* **49**, 1337 (1994).

[39] Reynaud, S., Fabre, C., Giacobino, E. & Heidmann, A. Photon noise reduction by passive optical bistable systems. *Phys. Rev. A* **40**, 1440 (1989).

[40] Chan, J. *et al.* Laser cooling of a nanomechanical oscillator into its quantum ground state. *Nature* **478**, 89 (2011).

[41] Teufel, J. D. *et al.* Sideband cooling of micromechanical motion to the quantum ground state. *Nature* **475**, 359–363 (2011).

[42] Purdy, T. P., Peterson, R. W. & Regal, C. A. Observation of Radiation Pressure Shot Noise on a Macroscopic Object. *Science* **339**, 801 (2013).

[43] Peterson, R. W. *et al.* Laser Cooling of a Micromechanical Membrane to the Quantum Backaction Limit. *Phys. Rev. Lett.* **116**, 063601 (2016).

[44] Kampel, N. S. *et al.* Improving broadband displacement detection with quantum correlations. *Phys. Rev. X* **7**, 021008 (2017).

[45] Rossi, M., Mason, D., Chen, J., Tsaturyan, Y. & Schliesser, A. Measurement-based quantum control of mechanical motion. *Nature* **563**, 53 (2018).

[46] Weis, S. *et al.* Optomechanically induced transparency. *Science* **330**, 1520–1523 (2010).

[47] Verhagen, E., Delglise, S., Weis, S., Schliesser, A. & Kippenberg, T. Quantum-coherent coupling of a mechanical oscillator to an optical cavity mode. *Nature* **482**, 63 (2012).

[48] Palomaki, T. A., Teufel, J. D., Simmonds, R. W. & Lehnert, K. W. Entangling mechanical motion with microwave fields. *Science* **342**, 710 (2013).

[49] Lecocq, F., Clark, J. B., Simmonds, R. W., Aumentado, J. & Teufel, J. D. Quantum nondemolition measurement of a nonclassical state of a massive object. *Phys. Rev. X* **5**, 041037 (2015).

[50] Riedinger, R. *et al.* Non-classical correlations between single photons and phonons from a mechanical oscillator. *Nature* **530**, 313 (2016).

[51] Sudhir, V. *et al.* Appearance and disappearance of quantum correlations in measurement-based feedback control of a mechanical oscillator. *Phys. Rev. X* **7**, 011001 (2017).

[52] Pirkkalainen, J.-M., Damskägg, E., Brandt, M., Massel, F. & Sillanpää, M. A. Squeezing of Quantum Noise of Motion in a Micromechanical Resonator. *Phys. Rev. Lett.* **115**, 243601 (2015).

[53] Peterson, G. A. *et al.* Ultrastrong parametric coupling between a superconducting cavity and a mechanical resonator. *Phys. Rev. Lett.* **123**, 247701 (2019).

[54] Aspelmeyer, M., Kippenberg, T. J. & Marquardt, F. Cavity optomechanics. *Rev. Mod. Phys.* **86**, 1391 (2014).

[55] Bose, S., Jacobs, K. & Knight, P. L. Preparation of nonclassical states in cavities with a moving mirror. *Phys. Rev. A* **56**, 4175 (1997).

[56] Mancini, S., Man'ko, V. & Tombesi, P. Ponderomotive control of quantum macroscopic coherence. *Phys. Rev. A* **55**, 3042 (1997).

[57] Ludwig, M., Kubala, B. & Marquardt, F. The optomechanical instability in the quantum regime. *New J. Phys.* **10**, 095013 (2008).

[58] Rabl, P. Photon blockade effect in optomechanical systems. *Phys. Rev. Lett.* **107**, 063601 (2011).

[59] Nunnenkamp, A., Borkje, K. & Girvin, S. M. Single-photon optomechanics. *Phys. Rev. Lett.* **107**, 063602 (2011).

[60] Nunnenkamp, A., Børkje, K. & Girvin, S. M. Cooling in the single-photon strong-coupling regime of cavity optomechanics. *Phys. Rev. A* **85**, 051803(R) (2012).

[61] He, B. Quantum optomechanics beyond linearization. *Phys. Rev. A* **85**, 063820 (2012).

[62] Hong, T., Yang, H., Miao, H. & Chen, Y. Open quantum dynamics of single-photon optomechanical devices. *Phys. Rev. A* **88**, 023812 (2013).

[63] Nation, P. D. Nonclassical mechanical states in an optomechanical micromaser analog. *Phys. Rev. A* **88**, 053828 (2013).

[64] Rimberg, A. J., Blencowe, M. P., Armour, A. D. & Nation, P. D. A cavity-Cooper pair transistor scheme for investigating quantum optomechanics in the ultra-strong coupling regime. *New J. Phys.* **16**, 055008 (2014).

[65] Frisk Kockum, A., Miranowicz, A., De Liberato, S., Savasta, S. & Nori, F. Ultrastrong coupling between light and matter. *Nature Reviews Physics* **1**, 19 (2019).

[66] Forn-Díaz, P., Lamata, L., Rico, E., Kono, J. & Solano, E. Ultrastrong coupling regimes of light-matter interaction. *Rev. Mod. Phys.* **91**, 025005 (2019).

[67] Murch, K. W., Moore, K. L., Gupta, S. & Stamper-kurn, D. Observation of quantum-measurement backaction with an ultracold atomic gas. *Nat. Phys.* **4**, 561 (2008).

[68] Brennecke, F., Ritter, S., Donner, T. & Esslinger, T. Cavity optomechanics with a bose-einstein condensate. *Science* **322**, 235 (2008).

[69] Leijssen, R. & Verhagen, E. Strong optomechanical interactions in a sliced photonic crystal nanobeam. *Sci. Rep.* **5**, 15974 (2015).

[70] Leijssen, R., La Gala, G. R., Freisem, L., Muhonen, J. T. & Verhagen, E. Nonlinear cavity optomechanics with nanomechanical thermal fluctuation. *Nat. Commun.* **8**, 16024 (2017).

[71] Reinhardt, C., Müller, T., Bourassa, A. & Sankey, J. C. Ultralow-noise sin trampoline resonators for sensing and optomechanics. *Phys. Rev. X* **6**, 021001 (2016).

[72] Bohren, C. F. & Huffman, D. *Absorption and Scattering of Light by Small Particles* (WileyVCH, Berlin, 1983).

[73] Mercier de Lépinay, L. *et al.* Nanomechanical thermal noise squeezing and circulation generated by curl forces. *in preparation* (2021).

[74] Neuhaus, L. *et al.* Pyrpl (python red pitaya lockbox) an open-source software package for fpga-controlled quantum optics experiments. In *2017 Conference on Lasers and Electro-Optics Europe European Quantum Electronics Conference (CLEO/Europe-EQEC)*, 1–1 (2017).

[75] Treutlein, P., Genes, C., Hammerer, K., Poggio, M. & Rabl, P. *Hybrid Mechanical Systems* (2014).

[76] Lee, D., Lee, K. W., Cady, J. V., Ovartchaiyapong, P. & Jayich, A. C. B. Topical review: spins and mechanics in diamond. *Journal of Optics* **19**, 033001 (2017).

[77] Blatt, R. & Wineland, D. J. Entangled states of trapped atomic ions. *Nature* **453**, 1008–1015 (2008).

[78] Leibfried, D., Blatt, R., Monroe, C. & Wineland, D. Quantum dynamics of single trapped ions. *Rev. Mod. Phys.* **75**, 281–324 (2003).

[79] Schwab, K. & Roukes, M. Putting mechanics into quantum mechanics. *Phys. Today* **58**, 36–42 (2005).

[80] Camerer, S. *et al.* Realization of an optomechanical interface between ultracold atoms and a membrane. *Phys. Rev. Lett.* **107**, 223001 (2011).

[81] Jöckel, A. *et al.* Sympathetic cooling of a membrane oscillator in a hybrid mechanicalatomic system. *Nat. Nanotechnol.* **10**, 55 (2015).

[82] Vochezer, A., Kampschulte, T., Hammerer, K. & Treutlein, P. Light-mediated collective atomic motion in an optical lattice coupled to a membrane. *Phys. Rev. Lett.* **120**, 073602 (2018).

[83] Karg, T. *et al.* Light-mediated strong coupling between a mechanical oscillator and atomic spins 1 meter apart. *Science* **369**, 174–179 (2020).

[84] LaHaye *et al.*, M. D. Nanomechanical measurements of a superconducting qubit. *Nature* **459**, 960 (2009).

[85] O'Connell, A. D. *et al.* Quantum ground state and single-phonon control of a mechanical resonator. *Nature* **464**, 697 (2010).

[86] Pirkkalainen *et al.*, J.-M. Hybrid circuit cavity quantum electrodynamics with a micromechanical resonator. *Nature* **494**, 211–215 (2013).

[87] Rabl *et al.*, P. Strong magnetic coupling between and electronic spin qubit and a mechanical oscillator. *Physical Review B* **79**, 041302 (2009).

[88] Kolkowitz, S. *et al.* Coherent sensing of a mechanical resonator with a single-spin qubit. *Science* **335**, 1603–1606 (2012).

[89] Bennett *et al.*, S. D. Measuring mechanical motion with a single spin. *New Journal of Physics* **14**, 125004 (2012).

[90] Hong *et al.*, S. Coherent, mechanical control of a single electronic spin. *Nano letters* **12**, 3920–4 (2012).

[91] Ganzhorn *et al.*, M. Strong spin-phonon coupling between a single-molecule magnet and a carbon nanotube nanoelectromechanical system. *Nature Nanotech.* **8**, 165 (2013).

[92] Teissier, J., Barfuss, A., Appel, P., Neu, E. & Maletinsky, P. Strain coupling of a nitrogen-vacancy center spin to a diamond mechanical oscillator. *Phys. Rev. Lett.* **113**, 020503 (2014).

[93] Ovartchaiyapong, P., Lee, K. W., Myers, B. A. & Jayich, A. C. B. Dynamic strain-mediated coupling of a single diamond spin to a mechanical resonator. *Nat Commun* **5**, – (2014).

[94] Tian, Y., Navarro, P. & Orrit, M. Single molecule as a local acoustic detector for mechanical oscillators. *Phys. Rev. Lett.* **113**, 135505 (2014).

[95] Lassagne, B., Tarakanov, Y., Kinaret, J., Garcia-Sanchez, D. & Bachtold, A. Coupling mechanics to charge transport in carbon nanotube mechanical resonators. *Science (New York, N.Y.)* **325**, 1107–10 (2009).

[96] Steele, G. *et al.* Strong coupling between single-electron tunneling and nanomechanical motion. *Science (New York, N.Y.)* **325**, 1103–7 (2009).

[97] Sallen *et al.*, G. Exciton dynamics of a single quantum dot embedded in a nanowire. *Physical Review B* **80**, 085310 (2009).

[98] Bennett, S., Cockins, L., Miyahara, Y., Grutter, P. & Clerk, A. Strong electromechanical coupling of an atomic force microscope cantilever to a quantum dot. *Phys. Rev. Lett.* **104**, 017203 (2010).

[99] Kettler, J. *et al.* Inducing micromechanical motion by optical excitation of a single quantum dot. *Nature Nanotechnology* **16**, 283–287 (2021).

[100] Mollow, B. Power syectrum of light scattered by two-level systems. *Phys.Rev.* **188**, 1969 (1969).

[101] Autler, S. & Townes, C. *Phys. Rev.* **100**, 703 (1955).

[102] Haroche, S. & Raimond, J. M. *Exploring the quantum* (Oxford University Press, 2006).

[103] Wu, F. Y., Grove, R. E. & Ezekiel, S. Investigation of the spectrum of resonance fluorescence induced by a monochromatic field. *Phys. Rev. Let* **35**, 1426 (1975).

[104] Schabert, A., Keil, R. & Toschek, P. Dynamic stark effect of an optical line observed by cross-saturated absorption. *Applied physics* **6**, 181–184 (1975).

[105] Wrigge, G., Gerhardt, I., Hwang, J., Zumofen, G. & Sandoghdar, V. Efficient coupling of photons to a single molecule and the observation of its resonance fluorescence. *Nature Physics* **4**, 60–66 (2008).

[106] Tamarat, P. *et al.* Pump-probe experiments with a single molecule: ac-stark effect and nonlinear optical response. *Phys. Rev. Lett.* **75**, 1514–1517 (1995).

[107] Nick Vamivakas, A., Zhao, Y., Lu, C.-Y. & Atature, M. Spin-resolved quantum-dot resonance fluorescence. *Nat Phys* **5**, 198–202 (2009).

[108] Flagg, E. B. *et al.* Resonantly driven coherent oscillations in a solid-state quantum emitter. *Nat Phys* **5**, 203–207 (2009).

[109] Baur, M. *et al.* Measurement of autler-townes and mollow transitions in a strongly driven superconducting qubit. *Phys. Rev. Lett.* **102**, 243602 (2009).

[110] Beveratos, A. *et al.* Room temperature stable single-photon source. *EPJD* **18**, 191–196 (2002).

[111] Batalov, A. *et al.* Low Temperature Studies of the Excited-State Structure of Negatively Charged Nitrogen-Vacancy Color Centers in Diamond. *Physical Review Letters* **102**, 1–4 (2009).

[112] Lesik, M. *et al.* Magnetic measurements on micrometer-sized samples under high pressure using designed nv centers. *Science* **366**, 1359–1362 (2019).

[113] Jelezko, F., Gaebel, T., Popa, I., Gruber, A. & Wrachtrup, J. Observation of coherent oscillations in a single electron spin. *Phys. Rev. Lett.* **92**, 076401 (2004).

[114] Balasubramanian, G. *et al.* Nanoscale imaging magnetometry with diamond spins under ambient conditions. *Nature* **455**, 648 (2008).

[115] Rondin, L. *et al.* Magnetometry with nitrogen-vacancy defects in diamond. *Rep. Prog. Phys.* **77**, 056503 (2014).

[116] Staudacher, T. *et al.* Nuclear magnetic resonance spectroscopy on a (5-nanometer)3 sample volume. *Science* **339**, 561–563 (2013).

[117] Mamin, J. H. *et al.* Nanoscale nuclear magnetic resonance with a nitrogen-vacancy spin sensor. *Science* **339**, 557–560 (2013).

[118] Mercier de Lépinay, L. *et al.* Nano-optomechanical measurement in the photon counting regime. *arXiv:1503.03200* (2015).

[119] Rabl, P. Cooling of mechanical motion with a two-level system: The high-temperature regime. *Physical Review B* **82**, 165320 (2010).

[120] Delord, T., Huillery, P., Nicolas, L. & Htet, G. Spin-cooling of the motion of a trapped diamond. *Nature* **580**, 56–59 (2020).

[121] Yeo, I. *A quantum dot in a photonic wire: spectroscopy and optomechanics*. Ph.D. thesis, Université de Grenoble (2012).

[122] Vaish, N. *Optomechanical transducer based on a single quantum dot.* Ph.D. thesis, Université Grenoble Alpes (2019).